This is to certify that the

dissertation entitled

MANY-ELECTRON TUNNELING IN A MAGNETIC FIELD

presented by

TATYANA O. SHARPEE

has been accepted towards fulfillment
of the requirements for

PH.D. degree in PHYSICS

M. Dykman
Major professor

Date 05/17/01

MANY-ELECTRON TUNNELING IN A MAGNETIC FIELD

By

Tatyana Sharpee

A DISSERTATION

Submitted to
Michigan State University
in partial fulfillment of the requirements
for the degree of

DOCTOR OF PHILOSOPHY

Department of Physics and Astronomy

2001

Abstract

MANY-ELECTRON TUNNELING IN A MAGNETIC FIELD

By

Tatyana Sharpee

The dissertation is devoted to the study of tunneling decay in a magnetic field. In its standard form, the semiclassical solution of the decay problem relies on tunneling trajectories in real space with purely imaginary momenta and time. Because of the broken time-reversal symmetry, trajectories of such form do not exist in a magnetic field. A semiclassical solution is presented which is valid for an arbitrary magnetic field and a three-dimensional potential, so that there is no need to treat magnetic field or some part of a potential as a perturbation. The decay rate and the outcoming wave packet have been found from the analysis of the set of Hamiltonian trajectories and its singularities in the complex phase space. A path-integral formulation for the tunneling decay problem in a magnetic field is provided as well.

The developed semiclassical solution to the problem of tunneling decay in a magnetic field was used to analyze tunneling from a strongly correlated system of *interacting* electrons. We show that the electron-electron interaction in a low density two-dimensional system can affect the rate of out-of the layer tunneling exponentially. The strongest and most interesting effects arise in the presence of a magnetic field

parallel to the layer. The tunneling rate becomes exponentially larger than that in the single-electron approximation. The physical mechanism is a dynamical Mössbauer-type recoil, in which the in-plane Hall momentum of the tunneling electron is partly transferred to the electron system as a whole. The interrelation between the characteristic rate of momentum exchange between electrons (plasma frequency) and the imaginary time of motion under the barrier determines what portion of the total momentum is transferred in a recoil-free way. The remaining part of the Hall momentum of the tunneling electron corresponds to excitation of phonons. Explicit results are obtained assuming that the electrons form a 2D Wigner crystal.

We show that, at higher temperatures, there is a possibility that the magnetic field parallel to the layer will increase, rather than suppress the out-of-plane tunneling rate. The B-enhanced tunneling allows to control the tunneling rate over several orders of magnitude just by changing magnetic field and temperature, without altering parameters of the tunneling barrier. Magnetic field can also induce switching between tunneling from different intra-well states, as well as switching from escape via over-barrier activation to tunneling escape, and vice versa.

The results, obtained with no adjustable parameters, were compared with data on tunneling from a correlated electron system on liquid helium surface. They are in both qualitative and quantitative agreement with the experimental data in a broad range of magnetic fields and temperatures. Therefore, tunneling experiments in a magnetic field can be used as a relatively simple and direct way to reveal electron correlations in other 2D systems, such as those in semiconductor heterostructures. The range of parameters for the tunneling experiments in heterostructures was provided.

To Brian

ACKNOWLEDGMENTS

I write with the deepest gratitude to my teacher, Professor Mark Dykman, whose extreme patience and attention to my problems cannot be underestimated. I can only hope to be worthy of his efforts.

I greatly appreciate interesting conversations and much valuable advice given to me by Prof. Philip Platzman and Prof. Leonid Pryadko. It was a pleasure to be in one working group with Frank Kuehnel, Vadim Smelyanskiy, and Alex Zhukov. I am indebted to Professors R. Brock, P. Duxbury, S. D. Mahanti, M. Thorpe, and V. Zelevinsky for teaching interesting classes that helped me understand more of the physics around. I am very thankful for the time and effort of Professors N. Birge, P. Danielewicz, and W. Tung spent in serving on my guidance committee.

My life during the years spent in working on this dissertation was enlighten by attentive kindness of many people, all of whom I thank. Of course, all of this would not come to be without the support of my family.

Table of Contents

List of Figures

Chapter 1

Introduction

Tunneling is a basic quantum phenomenon. As soon as a particle is described by a wave function, there is a finite probability to find it in regions of space that are classically inaccessible to it, that is where the potential energy $U(\mathbf{r})$ is bigger than the total energy E of the particle. Moreover, if this classically forbidden region has a finite width, then there is a finite probability to classically observe the particle behind the barrier.

Tunneling lies at the core of many physical and chemical phenomena ranging from alpha-particle decay in nuclear physics [1, 2], field ionization of neutral atoms [3], to tunnel splitting of molecular spectra [4] and scanning tunneling microscopy in condensed matter physics. In particular, Fowler and Oppenheimer [5] showed that tunneling could explain cold emission of electrons from a metal, a phenomenon that remained unexplained since Lilienfeld [6] discovered it in 1922.

Over the course of time much progress has been made in solving various tunneling problems. The semiclassical approximation turned out to be particularly useful in

solving tunneling problems, because the general solution can be obtained for an arbitrary potential, as long as it is sufficiently smooth [7]. The semiclassical approximation was originally used by Wentzel, Kramers, Brillouin [8] to solve a one-dimensional Schrödinger equation, and since then the method is called the WKB approximation. In the classically allowed region, the motion of a particle is semiclassical if its de Broglie wavelength $\lambda_D = \hbar/p$ is much smaller than the characteristic length of the potential. A semiclassical approximation can also be applied to describe the wave function in a classical forbidden region. Here, the appropriate condition is that the decay length is much smaller than the characteristic length of the potential [the decay length can be thought of as an imaginary part of a de Broglie wave length, which becomes imaginary in the region where there are no classically propagating solutions]. In other words, the tunneling barrier should be much wider than the particle's decay length. Therefore, the tunneling rate obtained in the semiclassical approximation will be exponentially small. A semiclassical solution of a one-dimensional tunneling problem is discussed in Chapter 2.

Numerous physical applications, chemical reactions being one of them, stimulated the extension of the semiclassical method to finite temperatures and beyond the one-dimensional approximation [9]-[15]. It is also very important to understand how tunneling occurs in cases where the particle motion is coupled to the bath [16] and where the underlying classical dynamics used to construct the semiclassical solution becomes chaotic [17]-[21].

A magnetic field can have a strong effect on the tunneling rate of charged particles. The exponential increase of resistance in semiconductors with increasing mag-

netic field has been known for years [22]. The conductance mechanism there is that of electron hopping between sites localized on defects. The magnetic field **B** leads to an exponential suppression of tails of the wave functions in the direction perpendicular to **B**, thus leading to an exponentially smaller overlap, and ultimately, to the exponentially smaller conductance value. Recently, this effect was used to probe two-dimensional electron systems (2DESs) in semiconductor heterostructures [23]-[33] and on a helium surface [34]. In the case of electron tunneling from a 2DES, as we shall show the rate of tunneling transverse to the magnetic field is very sensitive not only to the value of magnetic field, but also to electron correlations and temperature.

However, despite its interest and generality, even the problem of single-particle decay in a magnetic field lacked a semiclassical solution. Existing results, although highly non-trivial, are limited to the cases where the potential has a special form [16, 35, 36, 37], e.g. parabolic [35], or a part of the potential or the magnetic field are in some sense weak [38]-[45]. Chapter 3 of this dissertation will contain a discussion of a semiclassical solution to the problem of single-particle decay in a magnetic field [46, 47]. The proposed method applies to a three-dimensional potential of a general form and arbitrary magnetic fields. We assume, however, that the intrawell wave function is known and use to obtain the initial conditions which parametrize the set of tunneling trajectories. One of the unexpected results is that the tunneling particle has a finite momentum and velocity when it escapes from the barrier (see Fig. 1.1). This is in contrast to what happens for $B = 0$ where the particle comes out of the barrier with zero momentum on the line $E = U(\mathbf{r})$. The magnetic field breaks the time-reversal symmetry of the classical equations of motion, which in turn leads to

complex momentum of the tunneling particle under the barrier. The imaginary part goes to zero at the escape point, but the real part stays finite. To calculate the tunneling probability it is therefore insufficient to just find the probability for the particle to reach the classically allowed region $E = U(\mathbf{r})$. The probability to reach the escape point can be exponentially smaller.

The physical situation to which the proposed method will be applied is tunneling transverse to the field from low density 2DESs. In the low density limit Coulomb interaction dominates the exchange interaction, and as a result, electrons in the layer form a strongly correlated liquid, or, for yet lower densities, a 2D Wigner crystal (WC) cf. Fig 1.2. Strong electron correlations show up dramatically in many unusual transport properties [48]-[53]. The out-of-plane tunneling can also be very sensitive to electron correlations [54]. In double layer heterostructures, for example, a giant increase of the interlayer tunneling was recently observed and was related to interlayer electron correlations in the quantum Hall regime [55]. In the case of 2DESs on a liquid helium surface, it was known experimentally since 1993 [34] that the tunneling rate at low temperatures is exponentially larger than predicted by the single-electron approximation. This fact, however, was unexplained until the present work [56, 57].

A magnetic field parallel to a 2DES usually exponentially suppresses the out-of-plane tunneling. This can be understood from the following arguments. Consider an isolated electron, which is separated from the continuum states by a 1D potential barrier $U(z)$, see Fig. 1.2, and is free to move in the plane. When the electron moves a distance z away from the layer, it acquires the in-plane Hall velocity $\mathbf{v}_H = (e/c)\mathbf{B} \times \mathbf{z}$. The corresponding kinetic energy $mv_H^2/2 \equiv m\omega_c^2 z^2/2$ is subtracted from the energy

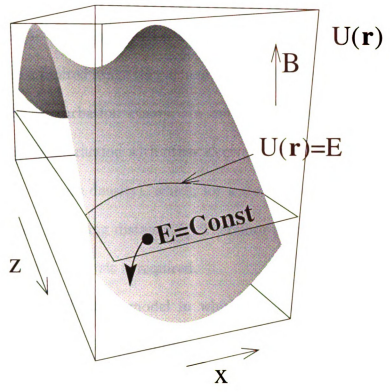

Figure 1.1: Tunneling in a two-dimensional potential $U(x, z)$ transverse to a magnetic field B pointing in the y direction. Initially the particle is localized in a metastable state behind the barrier, with energy E. In contrast to the case $B = 0$, a particle emerges from the barrier with a finite velocity, and therefore the exit point is located away from the line $U(\mathbf{r}) = E$.

of the out-of-plane tunneling motion ($\omega_c = |eB|/mc$ is the cyclotron frequency), or equivalently, there emerges a "magnetic barrier" $m\omega_c^2 z^2/2$. This leads to a sharp decrease of the decay rate.

For an electron that is confined in-plane, however, the in-plane force from the confinement can partly compensate the Lorentz force, thus reducing the suppression of the tunneling rate caused by **B**. In this way, the confining potential absorbs part of the in-plane Hall momentum of the tunneling electron. In a strongly correlated 2DES the in-plane confinement originates from Coulomb interactions with other electrons.

The idea that the momentum transfer may lead to strong increase of tunneling was first discussed in [38]-[40] in the context of scattering by defects. A confining potential from a defect has a limited range (in particular, in the tunneling direction), and could be considered by perturbation theory. In our problem, the confining potential is formed by Coulomb interaction with other electrons. It remains strong for distances $\sim n^{-1/2}$ (n is the electron density), which, for a strongly correlated electron system, are larger than the tunneling distance L. Therefore a perturbation theory may not be used, and an exact analysis is required.

If one adopts the Einstein model in which the in-plane electron motion is a harmonic vibration about an equilibrium position, with one frequency ω, then the problem is effectively reduced to a single-particle problem with in-plane potential $m\omega^2(x^2 + y^2)/2$ [directions $\hat{x}$ and $\hat{y}$ are in-plane, $\hat{z}$ is the out-of-plane direction]. Characteristic frequencies ω are of the order ofthe plasma frequency ω_p, which is related to the electron density n by $\omega_p = (2\pi e^2 n^{3/2}/m)^{1/2}$. As we will see below, modeling electron-electron interaction by such an effective single-particle potential results in an adequate explanation of experimental results.

The electron system accommodates the in-plane Hall momentum of the tunneling electron in a way similar to how it happens in the Mössbauer effect. In the latter effect the atom of a crystal emits the gamma quantum without recoil, if the momentum of the quantum is distributed to all atoms in the crystal. In the case of tunneling from a 2DES, however, the *dynamics* of the interelectron momentum exchange is very substantial [56]. The characteristic momentum exchange rate is also given by the zone-boundary plasma frequency ω_p. In the limit where ω_p exceeds the reciprocal

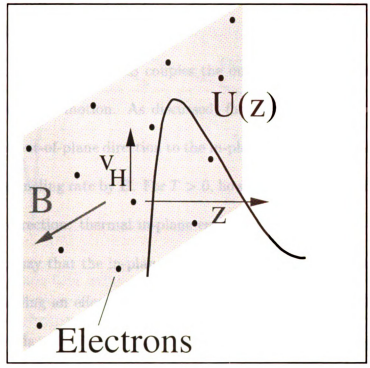

Figure 1.2: The geometry of tunneling from a correlated 2DES transverse to a magnetic field; electrons vibrate in the plane with frequencies of the order of the plasma frequency ω_p.

duration of under-barrier motion in imaginary time τ_f^{-1} and ω_c, other electrons in the WC adiabatically follow the momentum of the tunneling electron. As a result, the Hall velocity is the same for all electrons, and $v_H \propto 1/N \to 0$ (N is the number of electrons). The effect of the magnetic field on tunneling is then fully compensated. For $\omega_p \tau_f \sim 1$ the compensation is only partial, yet very substantial. One can say that tunneling is accompanied by creation of phonons of the WC, and the associated energy adds to the magnetic barrier[1]. However, the barrier turns out to be smaller

[1]The problem of tunneling between the lattice sites of WCs at the edges of a quantum Hall system was discussed by M.B. Hastings and L.S. Levitov, Phys. Rev. Lett. **77**, 4422 (1996). This problem is qualitatively different from that investigated in the present work, as are the results. In particular, opposite to the present case, the tunneling probability was determined by coupling to the low-frequency long-wavelength WC modes, it oscillated with B, and went to zero for $T \to 0$.

than for a free electron, and the tunneling rate is then exponentially larger. Still, for $T = 0$ it is much smaller than for $B = 0$.

The field **B** parallel to a 2DES couples the out-of-plane tunneling motion of an electron to its in-plane motion. As discussed, for $T = 0$ this results in the energy transfer from the out-of-plane direction to the in-plane one, and ultimately, in the suppression of the tunneling rate by **B**. For $T > 0$, however, the transfer of energy may go in the opposite direction: thermal in-plane energy is converted into the out-of-plane motion. One can say that the in-plane motion with a velocity **v** changes the tunneling barrier by adding an effective out-of-plane electric field $c^{-1}\mathbf{v} \times \mathbf{B}$, as illustrated schematically in Fig. 1.3. For an appropriate direction of **v** the field pulls an electron from the layer, and only these velocity directions contribute to the thermal-averaged tunneling rate. This result is rather unexpected, because it opens a possibility for an exponential increase of the tunneling rate with **B** [57]. The effect is analyzed in detail in Chapter 5, including specific calculations for some model potentials.

The crossover from suppression to enhancement of tunneling by the field occurs for a crossover temperature T_c. This temperature can be estimated by noticing that, for $B = 0$, the tunneling rate from the ground state $W_0 \propto \exp[-2S_0]$ exponentially depends on the energy E_g of the intrawell electron motion transverse to the layer [S_0 is the mechanical action for under-barrier motion; in what follows we use units where $\hbar = k_B = 1$]. The derivative $\tau_0 = \partial S_0/\partial E_g$ gives the imaginary duration of the under-barrier motion. The magnetic field effectively transfers the in plane electron energy E_{plane} into the out-of-plane energy E_g, at least in part. The probability to have an energy E_{plane} is $\propto \exp(-E_{\text{plane}}/T)$. Therefore the overall probability, which

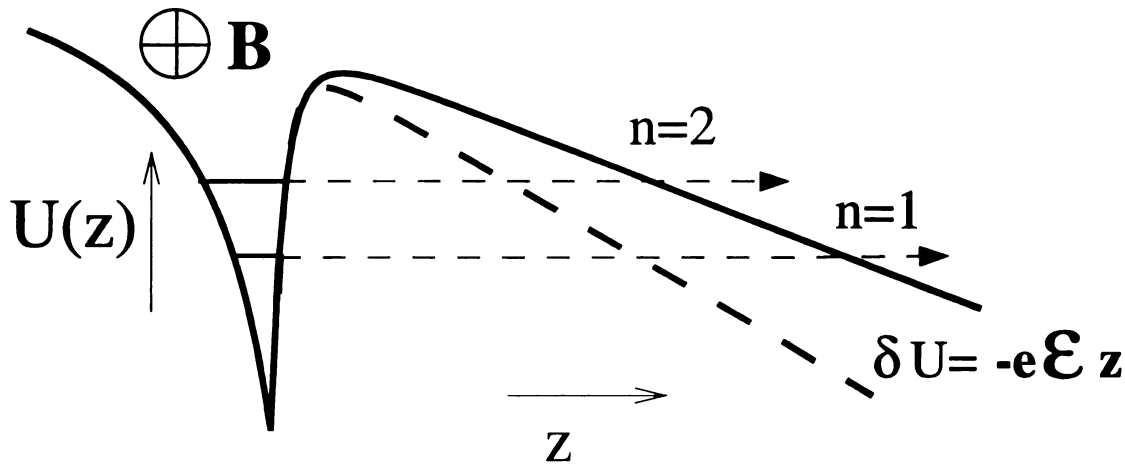

Figure 1.3: Magnetic field induced lowering of the tunneling barrier by thermal in-plane motion (schematically; the lowering is superimposed on the magnetic barrier for $T = 0$). The effective electric field $\mathcal{E}$ is determined by the T-dependent optimal in-plane velocity, $\mathcal{E} = \mathbf{v}_{\rm opt} \times \mathbf{B}/c$.

is determined by the product of the two exponentials, depends on the interrelation between T and τ_0, and one may expect that $T_c \sim \tau_0^{-1}$.

The time τ_0 also often determines the temperature T_a for which there occurs a crossover from tunneling decay to decay via activated over-barrier transitions for $B = 0$ [58, 59]. Therefore T_a and T_c are of the same order of magnitude. The interrelation between these temperatures is determined by the parameters of the system, and various interesting situations may occur depending on these parameters. For example, the logarithm of the escape rate may increase with B even for $T > T_a$, because in a certain B-range, the rate of tunneling from the ground state exceeds the activation rate, even though it is smaller than the activation rate for $B = 0$. Similarly, with increasing B there may occur switching from tunneling from the excited intrawell states (see Fig. 1.3) to tunneling from the ground state. Different switching processes

are considered in Chapter 5.

For $T < T_c$, on the other hand, the tunneling rate decreases with increasing B. For large enough B the tunneling rate becomes smaller than the rate of activated escape, which then determines the overall escape rate and generally weakly depends on B.

Although the thermal B-induced tunneling enhancement is generic, as we show it arises only in systems where intrawell motion transverse to the layer is not semiclassical. This is typical for 2DESs, where the confining potential $U(z)$ is usually non-parabolic near the minimum, and even non-analytic [2]. In contrast, the enhancement does not arise if the tunneling rate can be found using the instanton (bounce) technique [9], which is traditionally applied to describe tunneling for $B = 0$ [37]. The approach given in Chapter 4 allows one to calculate the tunneling rate from a potential well that is strongly non-parabolic both at finite and zero temperature. In addition to strong quantization of the intrawell motion, the instanton method has to be modified, because the magnetic field breaks time-reversal symmetry, and therefore, except for the case where the Hamiltonian of the system has a special form [16], there are no escape trajectories in real space and imaginary time, and the system comes out from the barrier with a finite velocity [46].

Explicit results on the effect of electron correlations on tunneling will be obtained assuming that the electrons form a Wigner crystal. Because of strong correlations, overlapping of the wave functions of individual electrons is small, and electrons can

[2] For example, in the case of a 2DES in heterostructures the potential has a step, and in the case of electrons on helium, the part of the potential which is due to image forces has a singularity on the surface.

be "identified". The problem is then reduced to the tunneling of an electron coupled to in-plane vibrations of the Wigner crystal. As discussed below, the results provide a good approximation also for a correlated electron liquid.

Comparison with experimental data on tunneling from a liquid helium surface is carried out in Chapter 6. The results, obtained with no adjustable parameters, provide full qualitative and quantitative explanation of the experimental data [34] in a broad rage of magnetic field and temperature. We show that the corresponding experiments on tunneling in heterostructures will be very sensitive to both electron correlations and in-plane electron dynamics. The range of parameters for such experiments is provided.

Part of the material presented in this dissertation has been published [46, 56, 77], submitted for publication [57], or is being prepared for publication [47].

Chapter 2

Semiclassical solution of a 1D tunneling problem

It is natural to suppose that the motion of a particle with a small de Broglie wave length $\lambda(x) = \hbar/p(x)$, i.e. much smaller than the characteristic length of a potential, should be similar to the motion described by classical equations of motion. We start with a Scrödinger equation

$$-\frac{\hbar^2}{2m}\frac{d^2\psi}{dx^2} + U(x)\psi = E\psi \tag{2.1}$$

In the limit where Plank's constant $\hbar \to 0$, one should recover the classical equations of motion. However, it would be inappropriate to set $\hbar = 0$ directly in the Eq. 2.1. Instead, similarly to how the limit of geometric optics is obtained through the eikonal equation, we look for the wave function in the form:

$$\psi(x) = \exp[iS(x)/\hbar], \tag{2.2}$$

and substitute (2.2) back into the Schrödinger equation. This gives us an equation for the function $S(x)$:

$$\frac{1}{2m}\left(\frac{dS}{dx}\right)^2 + U(x) - i\frac{\hbar}{2m}\frac{d^2S}{dx^2} = E \tag{2.3}$$

Now, we can use our assumption of small $\hbar$, and look for S as a power series in terms of $\hbar$:

$$S = S_0 + \frac{\hbar}{i}S_1 + \left(\frac{\hbar}{i}\right)^2 S_2. \tag{2.4}$$

In the lowest order, Eq. (2.3) becomes just the Hamilton-Jacobi equation of classical mechanics:

$$\frac{1}{2m}\left(\frac{dS_0}{dx}\right)^2 + U(x) = E \tag{2.5}$$

Therefore, it is the classical action S_0 that determines the exponent of the wave function (2.2). According to (2.5), for a 1D case we have:

$$S_0 = \pm\int p(x)dx, \quad p = \sqrt{2m[E - U(x)]}. \tag{2.6}$$

Here, $p(x) = dS_0/dx$ is the classical momentum of a particle. One can also calculate the next order in expansion (2.4) to find that $S_1 = -\frac{1}{2}\ln p(x)$. The semiclassical wave function consists then of two waves:

$$\psi(x) = \frac{C_1}{\sqrt{p(x)}}\exp\left[\frac{i}{\hbar}\int pdx\right] + \frac{C_2}{\sqrt{p(x)}}\exp\left[-\frac{i}{\hbar}\int pdx\right], \tag{2.7}$$

where the first term describes the wave propagating in the positive x-direction, while the second term corresponds to a wave propagating in the negative x-direction. Most of the essential physics is already present in (2.7). Taking higher order terms in $\hbar$ leads to changes of the first and higher orders of $\hbar$ in the prefactors.

The turning points where $p(x) = 0$ have to be treated with care in the semiclassical approximation. The prefactor diverges at a turning point, signaling the fact that the approximation becomes invalid. Indeed, the semiclassical approximation can be justified only if the zeroth order term in (2.3) is much larger than the one that we neglect:

$$\hbar \left| \frac{d^2S/dx^2}{(dS/dx)^2} \right| = \frac{1}{2\pi} \left| \frac{d\lambda}{dx} \right| \ll 1$$

Since the de Broglie wave length $\lambda = p^{-1}$, the approximation certainly does not work where $p(x) = 0$, i.e. at a turning point.

So far we have found the semiclassical wave function in a classically allowed region where $E > U(x)$. In a similar fashion to (2.2)-(2.6) the semiclassical approximation can be used to find the wave function in a classically forbidden region where $E < U(x)$. One of the first distinctions to be seen, is that momentum $p(x)$ from (2.6) is no longer real, but is purely imaginary. Because of the imaginary momentum, action S_0 also becomes imaginary:

$$S_0 = \pm i \int |p(x)| dx, \quad |p(x)| = \sqrt{2m[U(x) - E]}, \tag{2.8}$$

with the next order correction being $S_1 = -\frac{1}{2} \ln |p(x)|$. Therefore, deep under the barrier (far from the turning points $p(x) = 0$), the semiclassical wave function consists of an exponentially decaying and exponentially growing waves:

$$\psi(x) = \frac{C_1'}{\sqrt{|p(x)|}} \exp\left[\frac{1}{\hbar} \int |p| dx\right] + \frac{C_2'}{\sqrt{|p(x)|}} \exp\left[-\frac{1}{\hbar} \int |p| dx\right], \tag{2.9}$$

The semiclassical solutions (2.7) and (2.9) together describe the wave function everywhere except near the turning points. What one would like to have is a relation

between amplitudes $C_{1,2}$ of propagating waves in the classically allowed region and amplitudes $C'_{1,2}$ of evanescent waves in the classically forbidden region. There are two possibilities to achieve this. The first one is to solve the Schrödinger equation near a turning point using a linear function to approximate the potential. The solution can then be extended to regions far enough from from the turning point, where both the WKB and the linear approximation of the potential are valid.

Another method, which we will use below, is to analytically continue the semiclassical solutions (2.7) and (2.9) into the complex x plane [7]. Then it becomes possible to match the solutions continued from classically forbidden and allowed regions without going near the turning point where the WKB approximation breaks down.

Let us consider a specific example in which the two classically allowed regions are separated by a tunneling barrier for $x_1 < x < x_2$ [$x_{1,2}$ are the corresponding turning points]. The solution we would like to find is that of a tunneling problem: the particle wave packet is incident on the barrier from the left, part of it is reflected back, and an exponentially small part is emitted from the barrier on the other side. The boundary condition for this problem is the absence of a semiclassical wave incident on the barrier from the right. The wave function has the form:

$$\psi(x) = \begin{cases} \frac{A}{\sqrt{p}} \exp\left[\frac{i}{\hbar}\int_{x_1}^{x} dx p(x)\right] + \frac{B}{\sqrt{p}} \exp\left[-\frac{i}{\hbar}\int_{x_1}^{x} dx p(x)\right] & x < x_1 \\ \frac{C}{[2m(U(x)-E)]^{-1/4}} \exp\left[-\frac{1}{\hbar}\int_{x_1}^{x} dx \sqrt{2m[U(x)-E]}\right] & x_1 < x < x_2 \\ \frac{D}{\sqrt{p}} \exp\left[\frac{i}{\hbar}\int_{x_2}^{x} dx p(x)\right] & x_2 < x \end{cases} \tag{2.10}$$

where for $x < x_1$, the first term describes the wave incident on the barrier from the left, and the second describes the wave reflected back.

To find the relation between coefficients A, B, and C, let us track what happens to the exponentially decaying solution as we go around the turning point x_1 in the upper half plane. The phase of the difference $[U(x) - E] \propto (x - x_1)$ is incremented by π, so that the decaying solution transforms to the reflected wave

$$\frac{Ce^{-i\pi/4}}{\sqrt{p}} \exp\left[-\frac{i}{\hbar}\int_{x_1}^{x} dx p(x)\right] \tag{2.11}$$

As we go around the turning point in the lower half plane, the phase of $U(x) - E$ is incremented by $-\pi$, and the decaying solution goes over to the incident wave

$$\frac{Ce^{i\pi/4}}{\sqrt{p}} \exp\left[\frac{i}{\hbar}\int_{x_1}^{x} dx p(x)\right] \tag{2.12}$$

By comparing expressions (2.11) and (2.12) with the original one (2.10), we find that

$$B = -iA, \quad C = \exp[-i\pi/4]A. \tag{2.13}$$

To find the coefficient D, and the tunneling probability with it, let us rewrite the decaying under barrier solution as:

$$\psi_{\text{decaying}}(x) = \frac{C'}{[2m(U(x) - E)]^{-1/4}} \exp\left[-\frac{1}{\hbar}\int_{x_2}^{x} dx\sqrt{2m[U(x) - E]}\right],$$
$$C' = C\exp\left[-\frac{1}{\hbar}\int_{x_1}^{x_2} dx\sqrt{2m[U(x) - E]}\right] \tag{2.14}$$

The function $\psi_{\text{decaying}}(x)$ describes the wave with an amplitude that exponentially increases into the barrier (with increasing $|x - x_2|$). The tunneling current is described by the emitted wave in (2.10) for $x > x_2$. Let us analytically continue this wave into the upper half plane. As we go around the turning point x_2, the difference $U(x) - E$ acquires an extra phase of π, so that the emitted wave goes over into $\psi_{\text{decaying}}(x)$ with

$$C' = De^{-i\pi/4}. \tag{2.15}$$

We could also continue the emitted wave from (2.10) in the lower half plane, but this would result in a semiclassical solution that exponentially decreases in amplitude with increasing $x_2 - x$. We neglect this wave, because it is exponentially smaller than $\psi_{\text{decaying}}(x)$ everywhere in the tunneling barrier region.

By comparing (2.13), (2.15), we find the amplitude of the emitted wave D:

$$\frac{D}{A} = \exp[-\hbar^{-1}\text{Im}S(x_2, x_1)] = \exp\left[-\int_{x_1}^{x_2} \hbar^{-1}\sqrt{2m[U(x) - E]}dx\right]. \tag{2.16}$$

Therefore, we have constructed a semiclassical solution for all value of x by matching different semiclassical solutions across the turning points. An important feature of the final wave function is that the semiclassical wave valid on opposite sides of a turning point differ only by a phase factor, and have the same amplitudes. The decay of a wave function across the tunneling barrier is described by the imaginary part of a classical action S, as given by (2.16). The tunneling probability is given by $|D/A|^2$. Note that it does not depend on phase factors accumulated as a result of matching the semiclassical solution across the turning points (although in this case, the total phase is 0).

In preparation for the upcoming discussion of tunneling problems where the motion is not restricted to 1D, it is useful to write the action S_0 (2.6) in the classically allowed region as an integral along a classical trajectory $\mathbf{r}(t)$:

$$S_0 = \pm \int \mathbf{p}(\mathbf{r}) \cdot d\mathbf{r}, \quad \dot{\mathbf{r}} = \frac{\mathbf{p}}{m}, \quad \dot{\mathbf{p}} = -\nabla U. \tag{2.17}$$

Such a generalization becomes less straightforward in the classically forbidden region, where there is no real classical trajectory because momentum is imaginary under the barrier. Therefore we need to find some other trajectory (possibly in a different

potential) that would result in the action equal to the right hand side of (2.16). In order to achieve this, one could employ the following trick. Consider the usual Hamiltonian trajectory with $d\mathbf{r}/dt = \mathbf{P}/m$ and $d\mathbf{P}/dt = -\nabla U(\mathbf{r})$ and change $t \to -i\tau$. With $\mathbf{P}$ being imaginary, these equations can be solved! They have the form

$$\frac{d\mathbf{r}}{d\tau} = \frac{\mathbf{p}}{m}, \quad \frac{d\mathbf{p}}{d\tau} = +\nabla U(\mathbf{r}), \quad [\mathbf{P} = i\mathbf{p}] \tag{2.18}$$

which describes classical equations of motion in time τ in the potential $-U(\mathbf{r})$. The absolute value of momentum is given by $\sqrt{2m[U(\mathbf{r}) - E]}$. The corresponding classical action S_E evaluated along the trajectory

$$S_E(\mathbf{r}) = \int \mathbf{p}(\mathbf{r}) \cdot d\mathbf{r} \tag{2.19}$$

is related to that evaluated in real time by $S_E = iS$. Therefore, an appropriate generalization to the 1D answer (2.16) would be

$$\frac{D}{A} = \exp[-\hbar^{-1} S_E(\mathbf{r}_1, \mathbf{r}_2)],$$

with the tunneling probability given by

$$T = \left|\frac{D}{A}\right|^2 = \exp\left[-2\hbar^{-1} S_E(\mathbf{r}_1, \mathbf{r}_2)\right],$$

In summary, the 1D tunneling problem has a general solution in the semiclassical approximation. It uses the semiclassical solutions in regions that are separated by turning points, where the approximation breaks down. However, it is possible to relate the amplitudes of these semiclassical solutions by analytically continuing them into the complex plane, where they should match one another. The tunneling probability is given by the ratio of amplitudes of the wave incident on the barrier and the wave

emitted from the barrier on the other side. The method could also be extended to tunneling problems where the motion is not restricted to one dimension [15, 62].

Chapter 3

Multidimensional tunneling decay in a magnetic field

This chapter is devoted to the discussion of the problem of a single-particle tunneling decay in a magnetic field. The semiclassical solution applies to a smooth three-dimensional potential of a general form and for arbitrary magnetic fields that also have to be smooth (i.e., the characteristic lengths of the potential and the magnetic field should much larger than the particle's de Broglie wave length, if we discuss a classically allowed region, or the decrement of the semiclassical wave function, if we discuss a classically forbidden region. The method developed here will be used subsequently to analyze tunneling from a strongly correlated 2DES. In the semiclassical approximation we look for the wave function in the form:

$$\psi(\mathbf{r}) = D(\mathbf{r}) \exp[iS(\mathbf{r})] \ (\hbar = 1). \tag{3.1}$$

Here, $S(\mathbf{r})$ is the classical action. It satisfies the classical Hamilton-Jacobi equation with the Hamiltonian:

$$H = (\mathbf{p} + e\mathbf{A}(\mathbf{r}))^2/2m + U(\mathbf{r}), \tag{3.2}$$

where $\mathbf{A}(\mathbf{r})$ is the vector potential. The action S can be found from the corresponding Hamiltonian equations

$$\dot{S} = \mathbf{p} \cdot \dot{\mathbf{r}}, \quad \dot{\mathbf{r}} = \partial H/\partial \mathbf{p}, \ \dot{\mathbf{p}} = -\partial H/\partial \mathbf{r}. \tag{3.3}$$

The difficulty of solving the tunneling problem in a magnetic field lies in the absence of a time-reversal symmetry of the Hamiltonian equations (3.3). As discussed in the previous Chapter, this symmetry is essential for the standard approach to the problem of tunneling decay [11]-[13], [15] where after changing to imaginary time and momentum we have obtained the real Hamiltonian equations of motion. The equations then take the form of equations of classical motion in an inverted potential $-U(\mathbf{r})$, with energy $-E \geq -U(\mathbf{r})$. Such a procedure is appropriate in the absence of a magnetic field when the Hamiltonian (3.2) remains real. When the corresponding action $S(\mathbf{r})$ is purely imaginary, it describes a decay of wave function in the classically forbidden region ($E < U(\mathbf{r})$). The solution in this region then has to be matched to a wave function in the classically accessible region ($E > U(\mathbf{r})$) that is found from the classical Hamiltonian equations of motion with real time. The tunneling exponent is given by twice ImS at the end point of motion in imaginary time that lies on the boundary of the classically forbidden region $E = U(\mathbf{r})$. The tunneling particle "emerges" from under the barrier at this line with $\mathbf{p} = \mathbf{0}$.

The presence of a magnetic field breaks the time-reversal symmetry of trajectories

(3.3). For $B \neq 0$, we can no longer change $t \to -it$, $\mathbf{p} \to i\mathbf{p}$, $\mathbf{r} \to \mathbf{r}$, $U(\mathbf{r}) \to -U(\mathbf{r})$ and keep the Hamiltonian real. As a result it is impossible to match trajectories (and, therefore, wave functions) in the classically allowed and forbidden regions that have respectively real and complex E. It becomes clear that to solve the tunneling problem in the presence of a magnetic field, it is necessary to look for trajectories of a different kind.

Let me note in passing that there are some important cases where certain specific symmetry of a potential $U(\mathbf{r})$ allows us to use the standard method after some modifications. A particular case is when a canonical transformation of variables can be found that would restore the time-reversal symmetry of the Hamiltonian. This, for example, applies to tunneling of a particle coupled, for finite B, to a bath of harmonic oscillators [16], where the potential $U(\mathbf{r})$ is parabolic in the coordinates of the bath oscillators. We will encounter such coupling of the form $[\mathbf{z} \times \hat{\mathbf{B}}]\mathbf{p}_{\mathbf{k}j}$ in Chapter 4 in the discussion of tunneling from a Wigner crystal. Even though the time reversal symmetry may be broken by a magnetic field, it can be restored by a canonical transformation from coordinates $\mathbf{u}_{\mathbf{k}j}$ and momenta $\mathbf{p}_{\mathbf{k}j}$ to the new canonical coordinates and momenta $\mathbf{Q}_{\mathbf{k}j} = \mathbf{p}_{\mathbf{k}j}$ and $\mathbf{P}_{\mathbf{k}j} = -\mathbf{u}_{\mathbf{k}j}$. In the new representation, the tunneling trajectories can go with real coordinates $\mathbf{Q}_{\mathbf{k}j}$ and imaginary momenta $\mathbf{P}_{\mathbf{k}j}$.

In Sec. 3.1 we concentrate on the exponent of the tunneling rate in the presence of a magnetic field. The technique can be applied both in the case where the potential is parabolic near the intrawell minimum and in the case where the potential is singular, which is of relevance to tunneling from a 2DES. In a magnetic field the tunneling trajectories start to intersect, giving rise to a branching form of the action $S(\mathbf{r})$ and

corresponding singularities of the set of Hamiltonian trajectories. For the problem of tunneling decay, the most important among these singularities are caustics, or envelopes of trajectories. Section 3.2 deals with matching of different semiclassical solutions across caustics. We discuss generic features of the manifold of Im S near the branching point in complex space and its projection onto real space. In Sec. 3.3 we discuss the tunneling decay problem for $B \neq 0$ in the path-integral formulation. The corresponding "bounce" technique for tunneling out of a potential minimum is closely related to the instanton method for tunneling between two minima of a potential. The method applies in cases where the intrawell potential is parabolic near its minimum.

3.1 Tunneling exponent

The main idea is to consider Hamiltonian trajectories (3.3) that evolve in complex, rather than imaginary, time t in complex phase space $(\mathbf{p}, \mathbf{r})$. Motion along the trajectories occurs with real energy E equal to that of the metastable state. This corresponds to the analytical continuation of the WKB wave function (3.1) to complex variables. The action S will now have both real and imaginary parts, so that the wave function will be oscillating and decaying in space, which is natural in the presence of a magnetic field.

The tunneling trajectories (3.3) start in the vicinity of the localized metastable state at $t = 0$. The initial conditions can be obtained from the usually known form of the wave function near the potential well. This can be done both in the case where the potential is parabolic near its metastable minimum, so that $\psi(\mathbf{r})$ is semiclassical

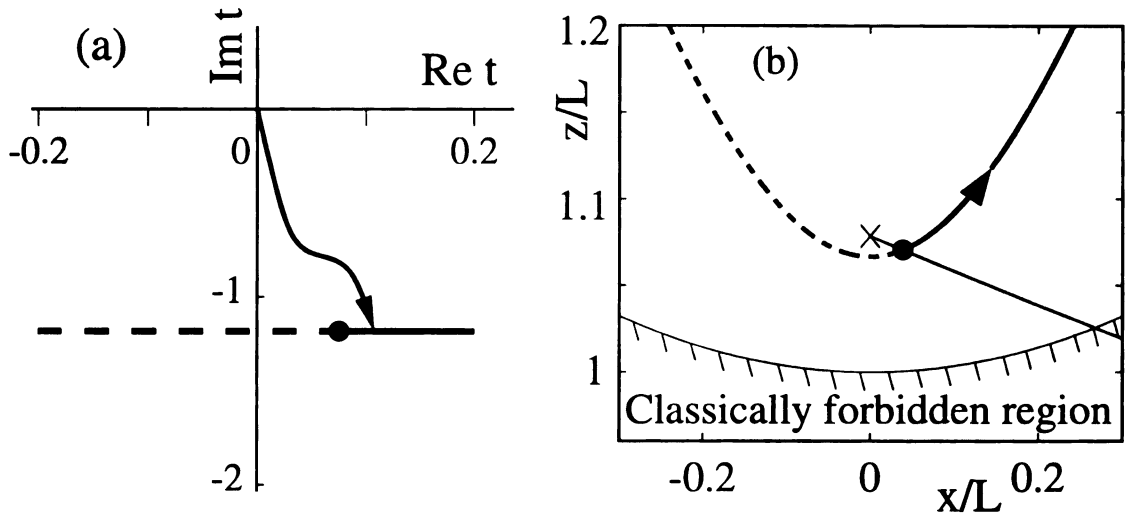

Figure 3.1: (a) Complex t plane for integrating the Hamiltonian equations (3.3) in the escape problem. The line Im t = const corresponds to the classical trajectory of outgoing electron. (b) The classical trajectory on the (x, z) plane. The solid lines in (a) and (b) show the range of Re t where the amplitude of the propagating wave exceeds the amplitude of the decaying underbarrier wave function, and the corresponding "visible" part of the trajectory. The escape occurs at the point where classical trajectory intersects the anti-Stokes line (thin solid line in (b)). Note that particle emerges from under the potential barrier with finite velocity and for $x \neq 0$. Thus the initial symmetry $x \to -x$ is broken by the magnetic field. The data refer to the potential (3.17) with $\omega_0\tau_0 = 1.2$ and $\omega_c\tau_0 = 1.2$, time in (a) is in the units of $\tau_0 = 2mL/\gamma$.

inside the well [9]-[14], and where the potential is nonanalytic, which is of interest for 2D electron systems. In either case the trajectories (3.3) can be parameterized by two complex parameters $x_{1,2}(0)$, e.g. the in-plane coordinates for a given out-of-plane coordinate, for tunneling from a 2DES. The in-plane momenta are then $p_{1,2}(0) = \partial S(0)/\partial x_{1,2}$.

With initial conditions at hand, the equations of motion (3.3) can be solved to find the action $S(t, x_{1,2}(0))$, together with $\mathbf{p}(t, x_{1,2}(0)))$ and $\mathbf{r}(t, x_{1,2}(0))$. The tunneling rate is determined by 2Im S at the point where the particle emerges from the barrier

as a semiclassical wave packet that propagates in real time along a *real* classical trajectory $\mathbf{r}_{cl}(t)$. This trajectory is yet another classical real-time solution of the Hamiltonian equations, the first one corresponding to the particle trapped in the well. To find the tunneling exponent we have to find such paths $\mathbf{r}(t), \mathbf{p}(t)$ (3.3) that would start in the vicinity of the well with some *complex* $x_{1,2}(0)$, then go in complex time and space to reach the classical trajectory $\mathbf{r}_{cl}(t)$. In other words, one has to find such $x_{1,2}(0)$ that, for some t, both $\mathbf{r}(t)$ and $\mathbf{p}(t)$ become *real*,

$$\text{Im } \mathbf{r}(t) = \text{Im } \mathbf{p}(t) = 0. \tag{3.4}$$

This is a set of equations for complex $x_{1,2}(0)$ and Im t. The number of equations is equal to the number of variables, taking into account that H is real. The Re t remains undetermined: a change in Re t in (3.4) results just in a shift of the particle along the classical trajectory $\mathbf{r}_{cl}(t)$, see Fig. 3.1. Such a shift does not change Im S. We note that $x_{1,2}(0)$ are real for $B = 0$.

The tunneling exponent $\mathcal{R}$ is given by the value of Im S at any point on the trajectory $\mathbf{r}_{cl}$,

$$\mathcal{R} = 2 \text{ Im } S(\mathbf{r}_{cl}), \tag{3.5}$$

For a physically meaningful solution, Im S should have a parabolic minimum at $\mathbf{r}_{cl}$ as a function of the coordinates transverse to the trajectory. Respectively, the outgoing beam will be Gaussian near the maximum.

From (3.4), the tunneling exponent can be obtained by solving the equations of motion (3.3) in imaginary time, with complex $\mathbf{r}$. However, that solution does **not** give the wave function for real $\mathbf{r}$ between the well and the classical trajectory $\mathbf{r}_{cl}$.

Neither does it tell us **where** the particle shows up on the classical trajectory.

To obtain a complete solution of the tunneling problem, we have to take into account that S is a multivalued function of $\mathbf{r}$ even though it is a single-valued function of t and $x_{1,2}(0)$. This means that several trajectories (3.3) with different t and $x_{1,2}(0)$ can go through one and the same point $\mathbf{r}$. The wave function $\psi(\mathbf{r})$ is determined by one of the branches of the action $S(\mathbf{r})$. How to match different branches to construct the wave function is discussed in the next section.

3.2 The action manifold

3.2.1 Branching lines - caustics

In multidimensional systems, branching generally occurs on caustics, or envelopes of trajectories [60, 62]. Their role in a multidimensional tunneling problem is analogous to that of turning points z_t in a 1D tunneling decay [see Chapter 2 for a discussion]. The common feature is the divergence of the prefactor $D(\mathbf{r})$ in the WKB wave function (3.1). In the case of a 1D tunneling, $D \propto p^{-1/2}$, leading to a branching action $S - S_t \propto (z - z_t)^{3/2}$ near the turning point z_t. The caustic is the line where the transformation between coordinates x_1, x_2 , z on the trajectory and parameters t, $x_1(0)$, $x_2(0)$ loses its uniqueness:

$$J(\mathbf{r}) = 0, \; J(\mathbf{r}) = \frac{\partial(x_1, x_2, z)}{\partial(x_1(0), x_2(0), t)}. \tag{3.6}$$

As we will now show, the prefactor in the WKB wave function is $D = \text{const} \times J^{-1/2}$. Indeed, the next-to leading order term in the expansion of action in powers of $\hbar$,

$S = S_0 + i\hbar S_1$ satisfies the equation:

$$2\mathbf{v}\nabla S_1 = -\mathrm{div}\mathbf{v}, \tag{3.7}$$

where $\mathbf{v} = \dot{\mathbf{r}}$ is the velocity along a trajectory, and the Coulomb gauge was used for the vector potential. The left-hand side of (3.7) is $2\dot{S}_1$. In the right-hand side, let us express the derivatives $\partial/\partial\mathbf{r}$ in terms of those with respect to t, $x_{1,2}(0)$:

$$\begin{aligned}
\frac{\partial}{\partial x_1} &= \frac{1}{J}\begin{vmatrix} \frac{\partial}{\partial t} & \frac{\partial x_2}{\partial t} & \frac{\partial z}{\partial t} \\ \frac{\partial}{\partial x_1(0)} & \frac{\partial x_2}{\partial x_1(0)} & \frac{\partial z}{\partial x_1(0)} \\ \frac{\partial}{\partial x_2(0)} & \frac{\partial x_2}{\partial x_2(0)} & \frac{\partial z}{\partial x_2(0)} \end{vmatrix} \\
\frac{\partial}{\partial x_2} &= \frac{1}{J}\begin{vmatrix} \frac{\partial x_1}{\partial t} & \frac{\partial}{\partial t} & \frac{\partial z}{\partial t} \\ \frac{\partial x_1}{\partial x_1(0)} & \frac{\partial}{\partial x_1(0)} & \frac{\partial z}{\partial x_1(0)} \\ \frac{\partial x_1}{\partial x_2(0)} & \frac{\partial}{\partial x_2(0)} & \frac{\partial z}{\partial x_2(0)} \end{vmatrix} \\
\frac{\partial}{\partial z} &= \frac{1}{J}\begin{vmatrix} \frac{\partial x_1}{\partial t} & \frac{\partial x_2}{\partial t} & \frac{\partial}{\partial t} \\ \frac{\partial x_1}{\partial x_1(0)} & \frac{\partial x_2}{\partial x_1(0)} & \frac{\partial}{\partial x_1(0)} \\ \frac{\partial x_1}{\partial x_2(0)} & \frac{\partial x_2}{\partial x_2(0)} & \frac{\partial}{\partial x_2(0)} \end{vmatrix}
\end{aligned} \tag{3.8}$$

Therefore,

$$\begin{aligned}
\mathrm{div}\mathbf{v} = \frac{1}{J}&\begin{vmatrix} \frac{\partial^2 x_1}{\partial^2 t} & \frac{\partial x_2}{\partial t} & \frac{\partial z}{\partial t} \\ \frac{\partial^2 x_1}{\partial t \partial x_1(0)} & \frac{\partial x_2}{\partial x_1(0)} & \frac{\partial z}{\partial x_1(0)} \\ \frac{\partial^2 x_1}{\partial t \partial x_2(0)} & \frac{\partial x_2}{\partial x_2(0)} & \frac{\partial z}{\partial x_2(0)} \end{vmatrix} + \frac{1}{J}\begin{vmatrix} \frac{\partial x_1}{\partial t} & \frac{\partial^2 x_2}{\partial^2 t} & \frac{\partial z}{\partial t} \\ \frac{\partial x_1}{\partial x_1(0)} & \frac{\partial^2 x_2}{\partial t \partial x_1(0)} & \frac{\partial z}{\partial x_1(0)} \\ \frac{\partial x_1}{\partial x_2(0)} & \frac{\partial^2 x_2}{\partial t \partial x_2(0)} & \frac{\partial z}{\partial x_2(0)} \end{vmatrix} \\
+\frac{1}{J}&\begin{vmatrix} \frac{\partial x_1}{\partial t} & \frac{\partial x_2}{\partial t} & \frac{\partial^2 z}{\partial^2 t} \\ \frac{\partial x_1}{\partial x_1(0)} & \frac{\partial x_2}{\partial x_1(0)} & \frac{\partial^2 z}{\partial t \partial x_1(0)} \\ \frac{\partial x_1}{\partial x_2(0)} & \frac{\partial x_2}{\partial x_2(0)} & \frac{\partial^2 z}{\partial t \partial x_2(0)} \end{vmatrix}
\end{aligned} \tag{3.9}$$

and we find that $\dot{S}_1 = -\dot{J}/2J$, so that the next correction is

$$S_1 \propto J^{-1/2},$$

and indeed diverges on the caustic. Therefore the WKB approximation does not apply close to it (cf. [60, 61]). Similarly to the 1D case, the different branches of action can be matched by going around the caustic line in complex space.

3.2.2 Local analysis near caustics

In our problem, in contrast to the usual case, the trajectories $\mathbf{r}(t)$ will be *complex*, as will also be the caustics. The caustic of interest is the one where the WKB wave function corresponding to the tail of the intrawell state is connected with the WKB wave function that describes the escaped particle [cf. Fig 3.2]. Both of the WKB solutions are analytically continued to complex $\mathbf{r}$, and merge on the caustic in the complex place.

Local analysis near the caustic will be similar to that in the 1D case [60, 61]. It is convenient to change to the variables x', y', and z' which are locally parallel and perpendicular to the caustic surface, respectively. We set $z' = 0$ on the caustic. Let us write the wave function near the caustic surface as:

$$\psi(\mathbf{r}_c + \mathbf{r}') = e^{i\mathbf{p}_c\mathbf{r}'}\phi(z'; \mathbf{r}_c). \tag{3.10}$$

Here, $\mathbf{p}_c$ is the momentum along a trajectory going through the point $\mathbf{r}_c$ of the caustic surface. For $B \neq 0$, the component of momentum perpendicular to the caustic surface is finite, but the velocity $\mathbf{p}_c + e\mathbf{A}(\mathbf{r}_c)$ should be tangent to the surface. As a

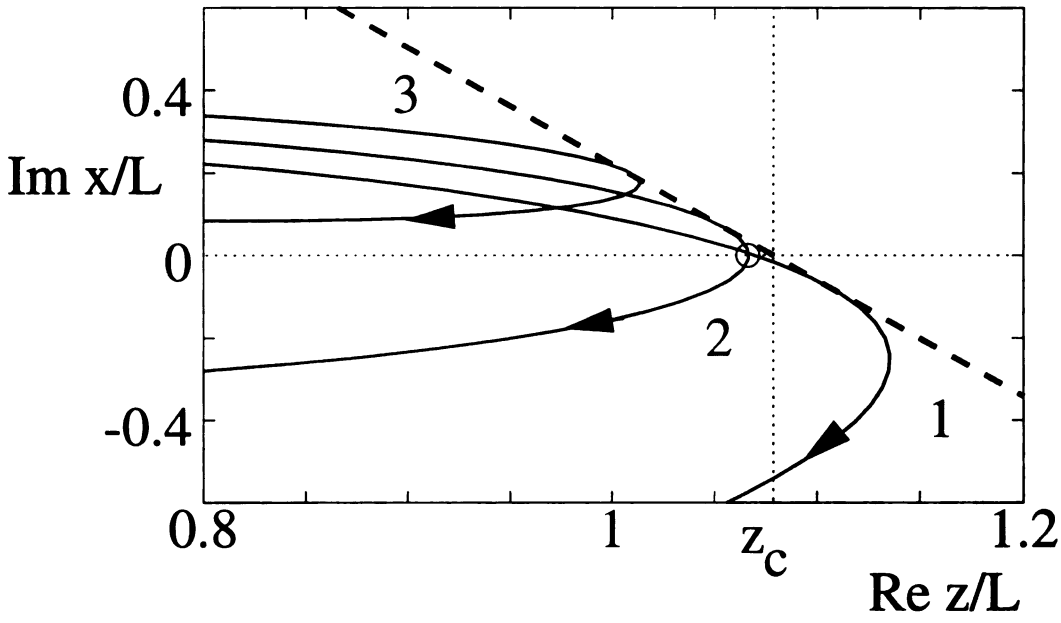

Figure 3.2: The complex tunneling trajectories (solid lines) and the complex caustic surface (dashed line) are shown in the (Re z, Im x) plane. The tunneling trajectory (2) reaches the clasical trajectory of an escaped particle for Im $x = 0$. At this point (shown by empty circle) the momentum is real along the trajectory (2). Even though other trajectories (1) and (3) cross the line of Im $x = 0$, it can be seen from the figure that Im $p_z \neq 0$ for Im $x = 0$. Therefore these trajectories do not touch the classical trajectory. Note that the point $z = z_c$ where the caustic goes through real space is *not* the point where the tunneling trajectory (2) becomes real.

result, in the Schrödinger equation for $\phi(z'; \mathbf{r}_c)$ motions along the caustic surface and perpendicular to it separate. In the perpendicular direction, the equation for $\phi(z'; \mathbf{r}_c)$ is identical to that near a 1D turning point in the absence of a magnetic field:

$$\left[\frac{\hbar^2}{2m}\frac{d^2}{dz'^2} + U'(\mathbf{r}_c)z'\right]\phi(z'; \mathbf{r}_c) = 0. \tag{3.11}$$

Therefore, we will be able to match semiclassical solutions of the wave function ψ across the caustic line, if we can find the proper asymptotes of the function $\phi(z', ; \mathbf{r}_c)$. As a solution of Eq. (3.11), $\phi(z')$ may be given in terms of a linear combination of Airy functions. Even though the function $\phi(z')$ is single-valued, its asymptotic behavior is

determined by one of the two branching functions:

$$w_{1,2} = [2mU'(\mathbf{r}_c)z']^{-1/4} \exp\left[\mp i \frac{2\sqrt{2mU'(\mathbf{r}_c)}}{3\hbar} z'^{3/2}\right] \tag{3.12}$$

Combining Eqs. (3.10) and (3.12), we find that the action for small $|z'|$ behaves as:

$$S(x', y', z') \approx S(x', y', 0) + a_1 z' + a_2 z'^{3/2} \tag{3.13}$$

The linear term reflects the fact that momentum perpendicular to the caustic remains *finite*, and, in general, complex (see Fig. 3.5). Therefore, the classical trajectory does not necessarily go through the caustic surface, contrary to the case without magnetic field.

Another way to understand the branching form (3.13) of the action S is to consider Hamiltonian trajectories near the caustic surface. Because of $v_{z'} = 0$, z' is quadratic in the increments $\delta x_{1,2}(0), \delta t$. Therefore $\delta x_{1,2}(0), \delta t$ are nonanalytic in z', as is also the action S. Taking into account cubic terms in $\delta x_{1,2}(0), \delta t$ we obtain (3.13), where the coefficients $a_{1,2} \equiv a_{1,2}(x', y')$ can be expressed in terms of the derivatives of $S, \mathbf{r}$ over $x_{1,2}(0), t$ on the caustic.

Having obtained the branching form for the action S (3.13), we now need to find out which of the branches describes the profile of the wave function $|\psi|$ in the global variables. The boundary conditions usually specify the asymptotic behavior at a particular value of $\theta = \arg z'$, the angle in the complex z'-plane. Our goal is then to find the asymptotic behavior throughout the complex z'-plane. When, and how, it can be done in the general case is discussed next.

Asymptotic analysis near a 1D turning point: the Stokes phenomenon.

The matching of asymptotes across a 1D turning point was extensively studied in the complex plane [7, 60, 61]. The difference with the analysis done in the context of 1D tunneling without magnetic field [7] is that now we need to know not only asymptotes for $\theta = 0, \pm\pi$ but for all values of θ [in a 1D tunneling problem, the classically allowed region may, for example, correspond to $\theta = 0$, and classically forbidden region to $\theta = \pm\pi$]. The asymptotic behavior at large $\rho = |z'|[2mU'(\mathbf{r}_c)/\hbar^2]^{1/3} \gg 1$ [a combination $[\hbar^2/2mU'(\mathbf{r}_c)]^{1/3}$ is appropriate to scale z', since it has the correct dimension of length] of the function ϕ is given by a linear combination $A(\theta)w_1 + B(\theta)w_2$. The functions $w_{1,2}$ are the first terms in the asymptotic expansion in $\hbar^{-1}$. In our case, the inherent error associated with an asymptotic expansion is of the order of $\hbar/\sqrt{2mU'(\mathbf{r}_c)|z'|^3}$. For some θ, the function w_1 is exponentially larger (dominant wave) than w_2 (subdominant wave). At other values of θ the asymptote w_2 becomes dominant, and w_1 becomes subdominant. The subdominant asymptote may, and should, be omitted, when it is smaller than the inherent error of an asymptotic expansion.

The branch cut from $z' = 0$ may be inserted arbitrarily. When going across the branch cut in the positive direction asymptotes interchange $w_1 \to -iw_2$ and $w_2 \to -iw_1$, with the property of dominance and subdominance preserved in the process. G.G. Stokes [63] was the first to notice that in order for the function $\phi(z')$ to be single-valued, the coefficients A and B should change with θ. Indeed, suppose the asymptotic behavior for $\theta = 0$ was described by $Aw_1 + Bw_2$. Then incrementing

θ by 2π leads to $-iBw_1 - iAw_2$, which can be satisfied only if both A and B are zero.

The coefficient A can change without causing a change in $\phi(z')$ only if the appropriate term is less than the error of the asymptotic expansion. In other words, the coefficients A (or B) can change only when (i) B (A) is non-zero, (ii) the asymptote w_1 (w_2) is subdominant. The change is concentrated in a narrow region around the so called Stokes line where the difference in amplitudes between the subdominant and dominant waves is maximal. In our problem the Stokes lines correspond to Re $z'^{3/2}$=0: $\theta = \pm\pi/3, \pi$. The width of the region where coefficients change is $\delta\theta \sim [\hbar|z'|^{3/2}/\sqrt{2mU'(\mathbf{r}_c)}]^{1/2} \sim \rho^{3/2}$ [60]. For our purposes, this change is equivalent to a jump [65], which is usually described in terms of a Stokes constant T. Upon crossing a Stokes line where w_1 is subdominant the coefficient changes as $A \to A+BT$.

One can find all three Stokes constants from the requirement that the function $\phi(z')$ should be single-valued. Indeed, let the asymptotic behavior at $\theta = 0$ be given by $Aw_1 + Bw_2$. The asymptotes w_1 and w_2 interchange the property of dominance and subdominance upon crossing lines where their amplitudes are equal. In our case, these so-called anti-Stokes lines are found from the condition Im $z'^{3/2} = 0$ ($\theta = 0, \pm 2\pi/3$). The branch cut, together with three Stokes and three anti-Stokes lines, divides complex plane into seven sectors, as shown in Fig. 3.3. The asymptotic

behavior in each sector is:

$$1: Aw_{1d} + Bw_{2s}; \quad 2: -iAw_{2d} - iBw_{1s}; \quad 3: -iAw_{1d} - i(B + AT_1)w_{1s};$$

$$4: -iAw_{2s} - i(B + AT_1)w_{1d}; \quad 5: -i[A + T_2(B + AT_1)]w_{2s} - i(B + AT_1)w_{1d};$$

$$6: -i[A + T_2(B + AT_1)]w_{2d} - i(B + AT_1)w_{1s};$$

$$7: -i[A + T_2(B + AT_1)]w_{2d} - i[B + AT_1 + AT_3 + T_2T_3(B + AT_1)]w_{1s} \qquad (3.14)$$

The single-valuedness for the function $\phi(z')$ is achieved if

$$A = -i[B + AT_1 + AT_3 + T_2T_3(B + AT_1)]; \quad B = -i[A + T_2(B + AT_1)], \qquad (3.15)$$

which gives equal Stokes constants on all three of the Stokes lines: $T_1 = T_2 = T_3 = i$. This calculation also shows that if we know the asymptotic behavior on one of the anti-Stokes lines, we can find it at all values of θ. In contrast, if the asymptotic behavior is specified on a Stokes line, then we have no knowledge about the coefficient in front of the subdominant wave, and therefore, are not able to uniquely specify the asymptotic behavior through out the complex plane.

Boundary conditions.

In the problem of tunneling decay the boundary condition that we need to satisfy is the absence of the wave incident on the barrier from large positive z. After transformation (3.10) to local variables x', y', z', the incident and outgoing waves in global variables become familiar 1D waves described by $\exp[\pm i \int_0^{z'} dz' p(z')/\hbar]$ with $\arg z' = \theta = 0$. Indeed, the coordinate-dependent amplitude is eliminated by a factor $\exp[i\mathbf{p}_c\mathbf{r}']$, which has complex $\mathbf{p}_c$. The direction of incident and outgoing classical waves is therefore

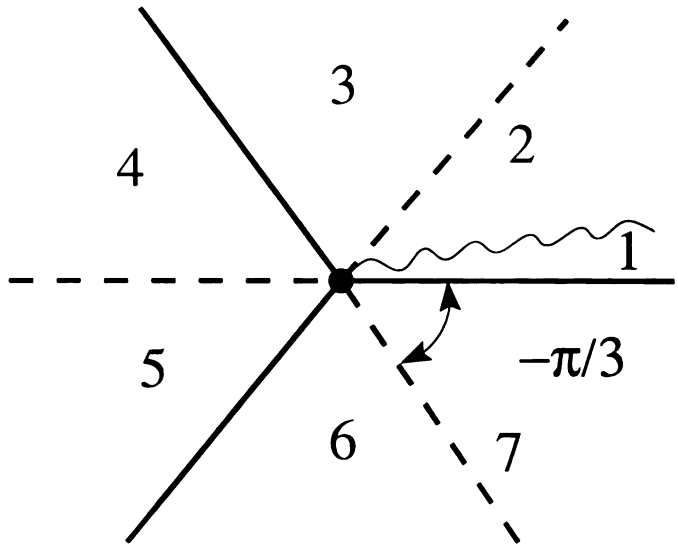

Figure 3.3: Sectors of complex z'-plane with different asymptotic behavior of the wave function around a 1D turning point with a first order zero. The anti-Stokes (solid) lines correspond to values of θ, where both asymptotes have equal amplitudes, $\theta = 0, 2\pi/3, 4\pi/3$.

projected onto one of the anti-Stokes lines, and we can always choose it to be the one with $\theta = 0$. As a result, the absence of the incident on the barrier wave in global variables eliminates the asymptote w_1 for $\theta = 0$.

To find the asymptotic behavior across the caustic line, we now can set coefficients $A = 0$ and $B = 1$ and use the previously calculated asymptotes (3.14) in complex space around a 1D turning point. The result is shown in Fig. 3.4. In the semiclassical approximation, we take into account only the exponentially larger, dominant wave. Therefore different waves will determine the profile of the wave function on different sides of an anti-Stokes line, where two waves have equal amplitude. It is interesting to note that because we have specified that there is only one solution w_2 at the anti-Stokes line for $\theta = 0$, there is also only one solution on the anti-Stokes line

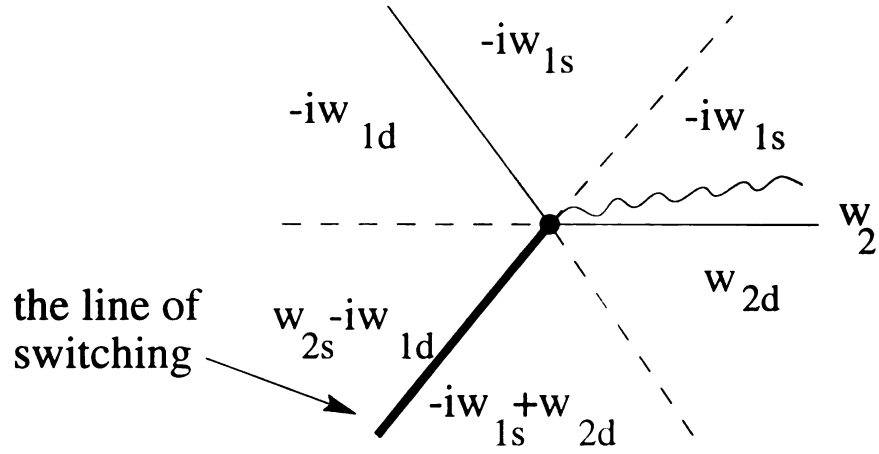

Figure 3.4: Complex z' plane perpendicular to the caustic surface at $z' = 0$. The anti-Stokes lines (solid) are located at $\arg z' = 0, 2\pi/3, 4\pi/3$. They divide regions where the solution is exponentially large and small. If there are two solutions on the anti-Stokes line, the one that was exponentially smaller in one region becomes exponentially larger after crossing the line. The subscripts s and d denote whether the solution is exponentially small or large, respectively, in a particular region. The dashed lines show Stokes lines, where the difference between the exponentially small and large solution is maximal. The wavy line shows the branch cut.

at $\theta = -4\pi/3$, and no switching occurs on it. The only anti-Stokes line where the switching between branches does take place is at $\theta = -2\pi/3$.

Switching between branches is accompanied by a change in phase by $\pi/2$. A useful check is that it is exactly the phase factor obtained in 1D tunneling between the incident and reflected wave [cf. Eq. 2.13], as well as between the outgoing and decaying wave[1] [cf. Eq. 2.15]. The amplitude remains unaffected. Therefore, the tunneling exponent (3.5) can be interpreted as a sum of the action Im $S(\mathbf{r}_c)$ for the tail of the intrawell wave function continued to a point $\mathbf{r}_c$ on the caustic, and the action Im $S(\mathbf{r}_{cl}|\mathbf{r}_c)$ for the outgoing wave from this point to a point on the classical

[1] An extra phase factor of $\pi/4$ is due to the difference between definitions of asymptotes $w_{1,2} \propto (z')^{-1/4}$ and $\psi_{\text{decaying}} \propto |z'|^{-1/4}$.

trajectory $\mathbf{r}_{cl}$:

$$\mathcal{R} = 2\mathrm{Im}\, S(\mathbf{r}_c|\mathbf{r}(0)) + 2\mathrm{Im}\, S(\mathbf{r}_{cl}|\mathbf{r}_c). \tag{3.16}$$

Since S is analytic in $x_{1,2}(0), t$, this sum is independent of the intermediate point $\mathbf{r}_c$. Notice that the two terms in (3.16) may have different signs.

3.2.3 Projection onto real space

According to (3.10), there is a one-to-one correspondence between asymptotes $w_{1,2}$ of the function $\phi(z';\mathbf{r}_c)$ in complex z'-plane and WKB solutions $D(\mathbf{r})\exp(iS_{1,2}(\mathbf{r}))$ for the wave function $\psi(\mathbf{r})$ in real space (the subscript in $S_{1,2}$ enumerates branches). After projection into real space $\mathbf{r}$ the caustic of interest, being a surface in complex space, will become a line (a point for a 2D potential). The relevant anti-Stokes surface after projection will remain a surface (a line in 2D). As in a complex space, it starts from the caustic line and separates the regions where Im S is smaller for one or the other of the solutions connected on the caustic. Only the solution with the smaller Im S should be held in the WKB approximation. Therefore across the anti-Stokes line there occurs switching between branches of action that describe physically different wave packets. The relevant example would be switching from the branch describing the tail of the intrawell state to the branch describing the wave packet of an escaped particle propagating along a real classical trajectory. The particle escapes from under the barrier at the point where the classical trajectory intersects the anti-Stokes surface (see Figs. 3.1, 3.7 in the case of a 2D potential). In other words, the probability to observe the tunneling particle at a point $\mathbf{r}_{cl}$ on the classical trajectory having real

momentum (branch S_2 on Figs. 3.6(a) and (b)) should be larger than that to observe it at that same point with a complex momentum (branch S_1 describing the tail of the intra well state).

We note that the position of the escape point is not generic: it is *not* located at the boundary of the classically allowed region $E = U(\mathbf{r})$, and not on the caustic surface. Interestingly, the tunneling particle is first observed with a non-zero kinetic energy, in contrast to the situation without magnetic field.

Let us consider, for example, tunneling through a potential:

$$U(\mathbf{r}) = \frac{m\omega_0^2}{2}(x^2 + y^2) + \frac{\gamma^2}{2m}\left(1 - \frac{z}{L}\right) \ (z > 0), \tag{3.17}$$

which is relevant for the problem of tunneling from a correlated 2DES on a helium surface. This system was experimentally investigated in Ref. [34], and showed an unexpected dependence of the tunneling rate on B, as addressed in a recent paper [46].

We specify initial conditions at the plane $z = 0$, neglecting the effect of the magnetic field on the wave function near the well. This can be justified if the characteristic intrawell localization length $1/\gamma$ is small compared to the tunneling length L. Then, even though the magnetic field has strong cumulative effect on the tunneling rate, it only weakly perturbs intrawell motion. The out-of-plane and in-plane motions are uncoupled, and we get:

$$z(0) = 0,\ p_z(0) = i\gamma,\ S(0) = im\omega_0(x(0)^2 + y(0)^2)/2,$$

$$p_x(0) = im\omega_0 x(0),\ p_y(0) = im\omega_0 y(0). \tag{3.18}$$

If we choose **B** along the y axis, then the motion in the y direction is decoupled and

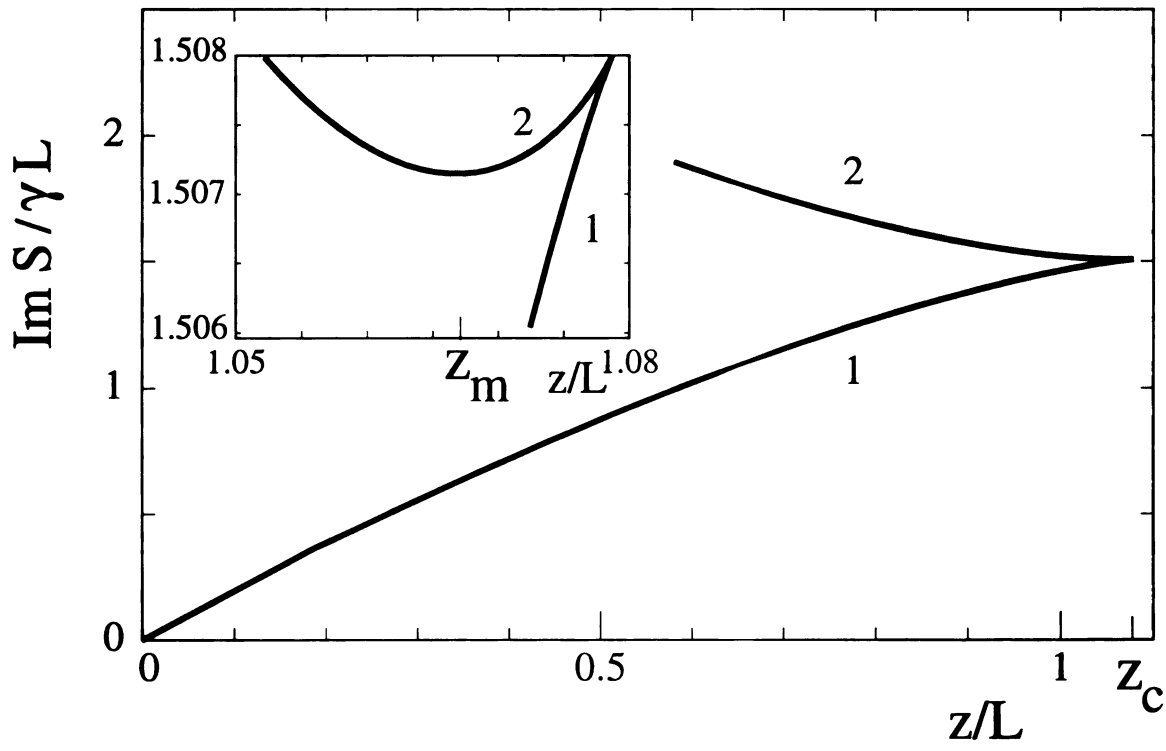

Figure 3.5: Two branches of the action on the symmetry axis $x = 0$ as a function of the tunneling coordinate z before the branching point, for the same parameter values as in Fig. 3.1. ImS is shown before the branching point z_c in the real space. The vicinity of the cusp z_c is zoomed in the inset to show that the upper branch is nonmonotonic. Its extremum at z_m lies on the classical trajectory of the escaping particle shown in Fig. 3.1(b). However, the particle emerge from the barrier for $z > z_m$ and $x \neq 0$.

the problem becomes two-dimensional. The Hamiltonian equations (3.3) are linear, and we can find trajectories explicitly. The symmetry $U(x, y, z) = U(\pm x, \pm y, z)$ gives rise to a specific symmetry of the set of the trajectories (3.3):

$$t \to t^*,\ x \to -x^*,\ y \to -y^*,\ z \to z^*, S \to -S^* \tag{3.19}$$

The caustic of interest goes through real space at the point $x = y = 0$, $z = z_c$ ($z_c = L$ for $B = 0$) on the symmetry axis. Knowing the momentum $\mathbf{p_c}$ at this point, we find that the complex plane perpendicular to the caustic is

$$z' = (z - z_c)\cosh\alpha - ix\sinh\alpha, \quad \alpha = \tanh^{-1}[\mathrm{Im}\, p_{cz}/(p_{cx} + \omega_c z_c)],$$

where the parameter α is positive for $B > 0$ in this problem. Therefore, positive x corresponds to the lower half-plane in the complex z'-plane. Near the caustic, the outgoing wave is described by asymptote w_2 from (3.12). From examination of Fig. 3.4, we find that only one branch of action is physically meaningful for negative x (the upper half of z' plane). For positive x however, both of the branches of Im S should be taken into account. The one with smaller Im S determines the profile of the wave function. Below we describe the resulting picture.

For $z \leq z_c$, the function Im S has two branches each of which is symmetrical in x. The branch 1 describes the tail of the intrawell wave function before branching. The branch 2 corresponds to the wave "reflected" from the caustic. Their cross-sections are shown in Fig. 3.5, 3.6. The branch 1 has a minimum at $x = 0$ and monotonically increases with x and z. As expected, the slope ∂ Im $S/\partial z$ is finite at the branching point z_c (see inset in Fig. 3.5). The branch 2 is nonmonotonic in z for $x = 0$, with a minimum at $z_m < z_c$. As it turns out momentum of the particle described by branch 2 is real at $z = z_m$. The point $z = z_m$, $x = 0$ belongs to the classical trajectory and is the point where the trajectory comes closest to the well ($z = 0$) as it approaches the barrier from large z and negative x, and goes away to large z and positive x (Fig. 3.1(b)). Note that the velocity of the particle is not equal to zero at any point on the classical trajectory. Although branch 2 describes a classical particle at $z = z_m$, $x = 0$, it is not the exit point for the tunneling particle, because the probability for it to have real momentum as described by branch 2 is smaller than that to have a complex momentum as described by branch 1 (Fig. 3.5). For $z_m < z \leq z_c$, the branch 2 is nonmonotonic in x, with local *maximum* at $x = 0$ and with two symmetrical

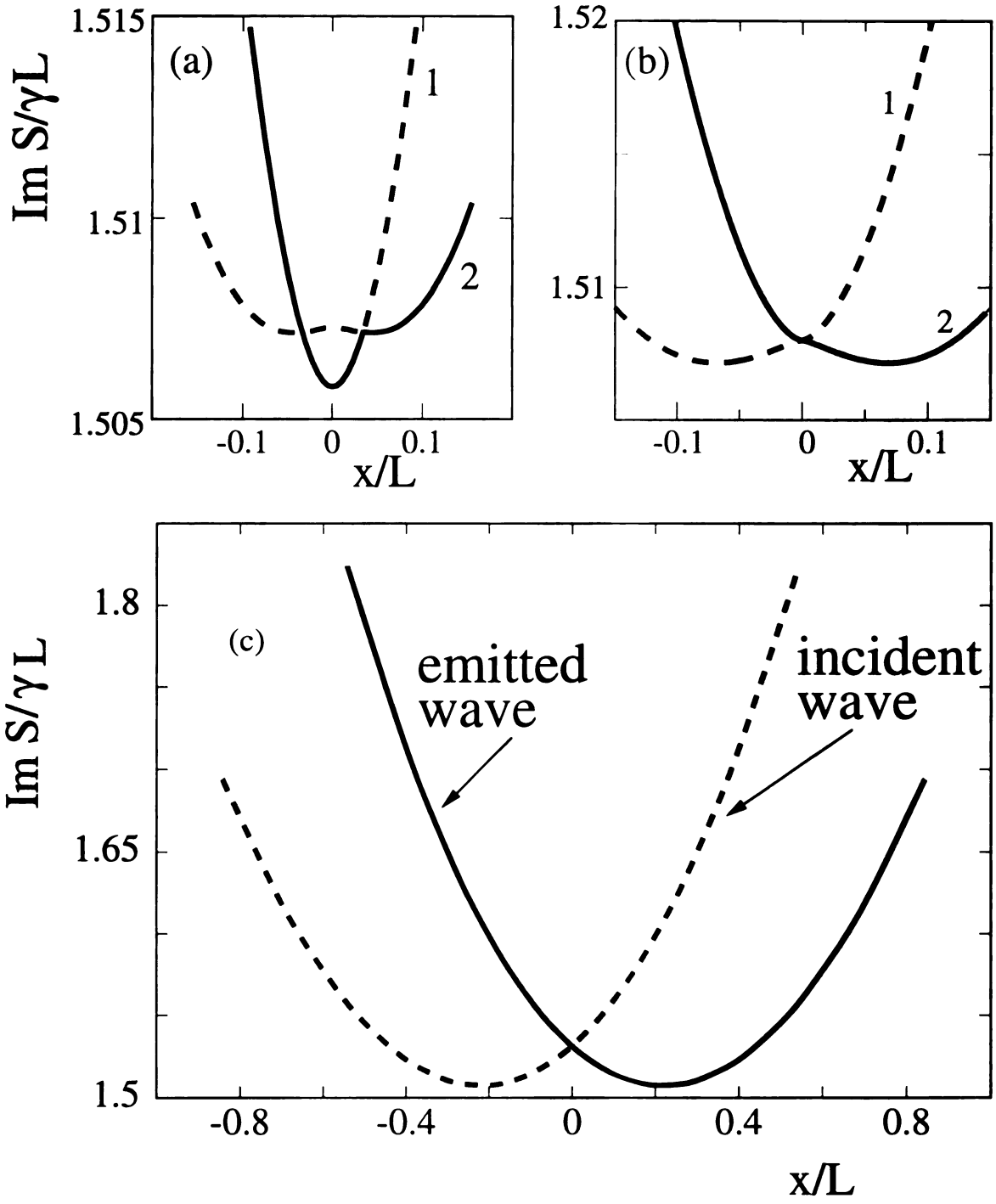

Figure 3.6: Cross sections of function ImS for constant z near the branching point z_c: (a) $z_m < z < z_c$; (b) $z = z_c$; (c) $z > z_c$. The parameter values are the same as in Figs. 3.1,3.5. The solid line shows the branches of Im S that determine the exponent of $|\psi|$. The minima of the branch 2 lie on the classical trajectory shown in Fig. 3.1(b).

minima. These minima lie on the classical trajectory shown in Fig. 3.1(b). For $z = z_m$, the maximum and the minima merge together.

For $z > z_c$, $S(x, z)$ on one of the two branches is equal to $-S^*(-x, z)$ on the other branch (cf. Fig. 3.6). The appropriate minima of Im $S(x, z)$ continue to follow the classical trajectory. As discussed above, ImS is constant on the classical trajectory. One may verify that the value of ImS at the minima of branch 2 have the same value for all cross-sections with different $z = \text{const}$. The exponent of $|\psi|$ is determined by either branch 1 or branch 2. It is plotted by solid line in Figs. 3.6. The switching takes place where $\text{Im}S_1(\mathbf{r}) = \text{Im}S_2(\mathbf{r})$, that is on the anti-Stokes line that starts from the caustic point $z = z_c$, $x = 0$ [compare to the anti-Stokes line for $\arg z' = 4\pi/3$ on Fig. 3.4]. The escaped particle can be seen moving along the classical trajectory, if $\mathcal{R}/2 = \text{Im}S_2(\mathbf{r}_{cl}) < \text{Im}S_1(\mathbf{r}_{cl})$. Therefore, it "shows up" at the point where the classical trajectory intersects the anti-Stokes line. The fact that the exit point is located for $x \neq 0$ even for a symmetric potential (3.17) demonstrates the symmetry-breaking induced by a magnetic field.

3.2.4 Exactly solvable non-symmetric model

The considered tunneling problem provides an insight into the dependence of the tunneling exponent on B and the electron density observed for electrons on helium [34], and can be applied to correlated electron systems in heterostructures [66]. Due to the specific symmetry (3.19) it can be also solved by a standard technique by considering (p_x, z) as coordinates of the tunneling particle instead of (x, z). In this

formulation, the kinetic energy $p_z^2/2m + m\omega^2 x^2/2$ does not include the magnetic field. The tunneling problem is therefore mapped onto the problem of multidimensional tunneling without magnetic field. To check that our approach works equally well in a case where there is no specific symmetry, we consider tunneling in a potential with a symmetry-breaking term αxz.

$$U(x,z) = \frac{1}{2}m\omega_0^2 x^2 + \alpha xz + \frac{\gamma^2}{2m}\left(1 - \frac{z}{L}\right) \ (z > 0). \tag{3.20}$$

Such a form of the tunneling potential accounts for the change in electron-electron interaction as the tunneling electron moves out of the 2D layer. The symmetry (3.19) is broken and there is no transformation of variables that would reduce the role of magnetic field to the potential energy only. We now show that the generic features of the solution remain unchanged.

The Hamiltonian equations (3.3) are linear even with the symmetry-breaking term, and can be solved exactly for the new potential (3.20). The same initial conditions (3.18) are used to construct the wave function $\psi(\mathbf{r}) = D(\mathbf{r})\exp[iS(\mathbf{r})]$. The caustic of interest crosses the real space at the point $x = x_c$, $z = z_c$ ($z_c = L$, $x_c = 0$ for $B = 0$) and is marked by a cross on Fig. 3.7. The escaped particle moves along the classical trajectory that comes from large z and negative x and goes to positive x and large z. Note that the classical trajectory does not cross the line $U(\mathbf{r}) = E$. The velocity of the escaped particle is not equal to zero at any point, including the exit point.

As before, the function ImS has two branches, which, however, are no longer symmetrical in x. The cross sections for constant z are shown in Fig. 3.8. Apart from the symmetry $x \to -x$, which is naturally no longer present, the main properties

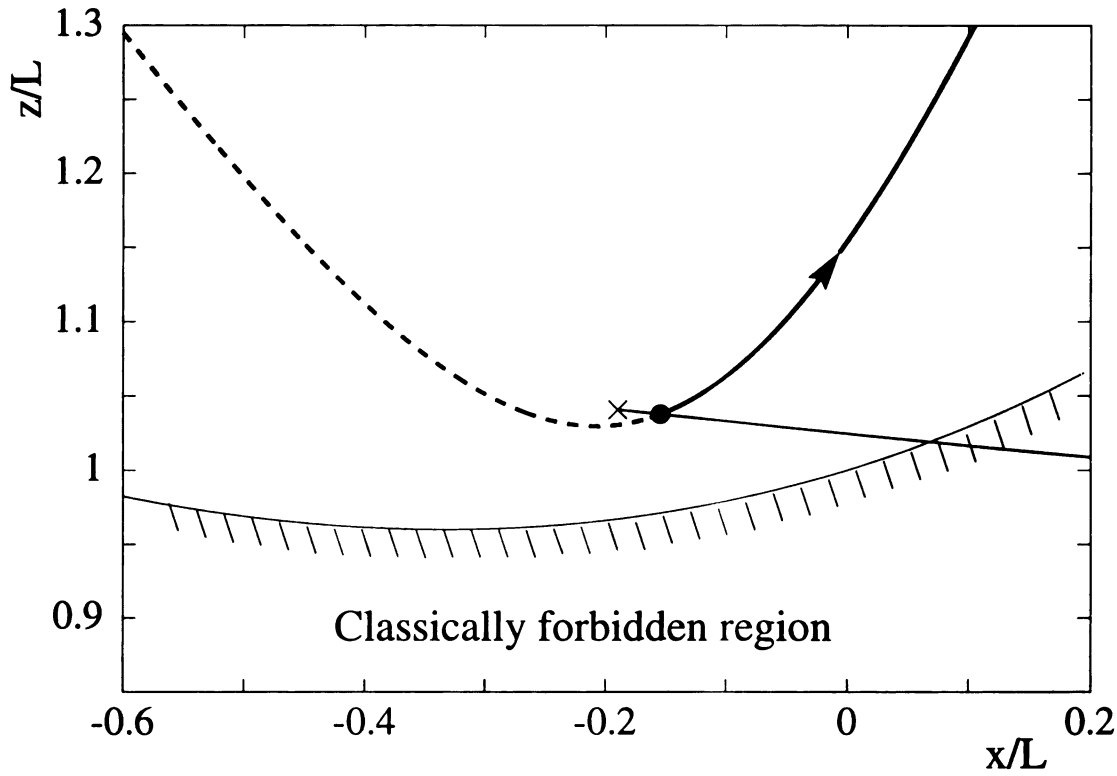

Figure 3.7: The classical trajectory of the escaping particle for potential (3.20) with $\alpha = 0.5$ and same values of parameters $\omega_c\tau_0$ and $\omega_0\tau_0$ as in Figs. 3.1, 3.5, 3.6. The cross marks the branching point for function ImS - the point where caustic goes through the real space. The anti-Stokes line starts from the branching point. The escape takes place at the point where classical trajectory intersects the anti-Stokes line. Note that the trajectory lies away from the line of zero velocity $U(x, z) = E$.

of the manifold remain unchanged (refer to Fig. 3.6). For $z < z_c$, the branch 1 describes the tail of the intrawell state. It has a minimum for $x \neq 0$ and monotonically increases with z. The branch 2 describes the wave "reflected" from the caustic and is nonmonotonic in both x and z. Let us denote by z_m the closest point on the classical trajectory to the well at $z = 0$. For $z_m < z < z_c$, the branch 2 of ImS as a function of x has two minima that correspond to the classical trajectory. For $z = z_m$ these two minima merge together. The value of ImS at the minima is independent of z, as it should be. For $z > z_c$, ImS is represented by two branches, one of them describing

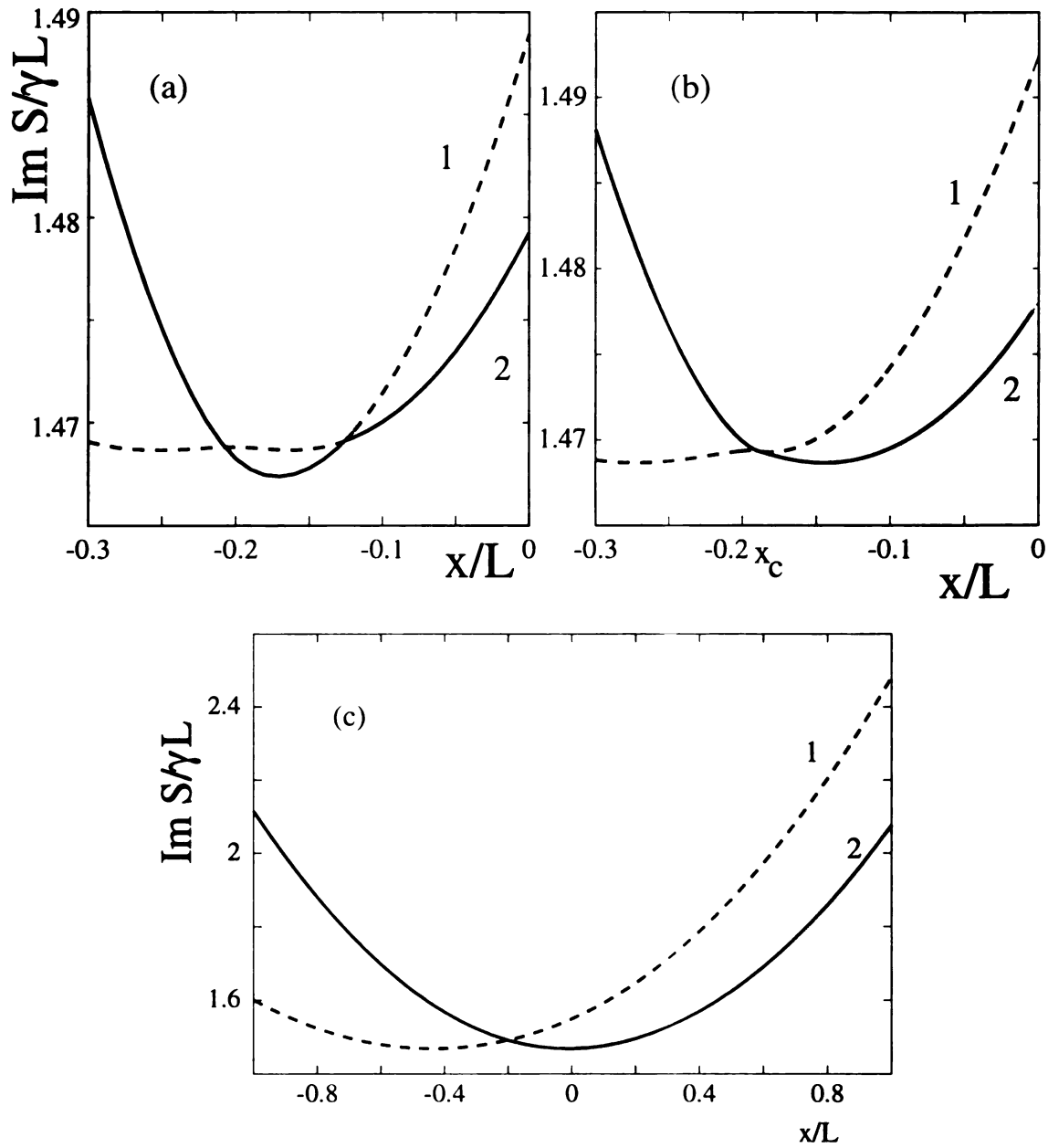

Figure 3.8: Cross-section of function Im S for constant z near a branching point (x_c, z_c): (a) $z_m < z < z_c$; (b) $z = z_c$; (c) $z > z_c$. The tunneling potential is (3.20) with the symmetry-breaking parameter $\alpha = 0.5$, and other parameters are the same as in Figs. 3.1, 3.5, 3.6, so that $\omega_c \tau_0 = 1.2$ and $\omega_0 \tau_0 = 1.2$. Although the symmetry $x \to -x$ is no longer present, all of the main features of the solution remain the same. The minima of the branch 2 lie on the classical trajectory shown in Fig. 3.7.

the wave coming from large z (unphysical) and the other describing the wave going to large z (escaped particle). The minima of the branches continue to follow the classical trajectory.

The wave function is determined by one of the branches of action $S(\mathbf{r})$. The switching between two branches takes place on the anti-Stokes line that starts form the caustic point $x = x_c$, $z = z_c$. The exit point is located where the classical trajectory intersects the anti-Stokes line (see Fig. 3.7). The exponent of the tunneling rate is $\mathcal{R} = 2\mathrm{Im}S(\mathbf{r}_{\mathrm{cl}})$. It can be found by solving the equations in imaginary time.

To summarize, the proposed solution to the tunneling problem in magnetic field does not rely on a special symmetry of the tunneling potential. The characteristic features of the action manifold, shown in Figs. 3.5, 3.6, remain unchanged.

3.3 The path-integral formulation in a magnetic field

In the absence of a magnetic field, the problem of tunneling decay has a very elegant solution in the path-integral formulation [9, 10, 16]. One of the main advantages of this method is that the escape rate can be calculated at finite temperatures, while the answer for $T = 0$ can be obtained by taking the appropriate limit[2]. Just like in the WKB approximation, the tunneling exponent is equal to the Euclidean action, which is calculated along a trajectory going in imaginary time with imaginary momentum

[2]However, the method heavily relies on the fact that the tunneling potential is parabolic near its minimum. Desire to calculate the tunneling rate from a 2DES, where the tunneling potential is strongly *non-parabolic* motivated the formulation of the WKB approximation presented in Sec. 4.2.

and real coordinates. The tunneling trajectory - "bounce"- starts from the well, reaches the boundary of classically allowed region and returns back to the well. In the presence of magnetic field, the time-reversal symmetry is broken, and it is therefore clear that not only regular WKB approximation, but also the "bounce" technique has to be significantly modified if it is ever to be used for $B \neq 0$. An attempt is provided in this section.

The general tunneling problem is formulated with non-Hermitian boundary conditions - current flowing from the well to infinity. Consequently, the energy E of a particle localized in the metastable state acquires a small imaginary part that describes exponentially small decrease of the probability to find a particle in the well as time goes. The tunneling probability is defined as a ratio of the current behind the well to the population of the well [64].

$$W = j\left[\int d\mathbf{r}|\psi|^2\right], \quad j = \frac{1}{2m}\left[\psi^*\left(\mathbf{p} - \frac{e}{c}\mathbf{A}\right)\psi + c.c\right].$$

On the other hand, from the Schrödinger equation, we know that

$$\begin{aligned} 2i\,\mathrm{Im}E\left[\int d\mathbf{r}|\psi|^2\right] = & \frac{1}{2m}\int d\mathbf{r}\left[-\psi^*\nabla^2\psi + \psi\nabla^2\psi^* + 2i\frac{e}{c}(\psi^*\mathbf{A}\nabla\psi + \psi\mathbf{A}\nabla\psi^*)\right] \\ & = \frac{-i}{2m}\left[\psi^*(-i\nabla - \frac{e}{c}\mathbf{A})\psi + \psi(i\nabla - \frac{e}{c}\mathbf{A})\psi^*\right] \\ & = -ij(\mathbf{r}). \end{aligned} \tag{3.21}$$

We have recovered the result valid in the absence of a magnetic field that the probability of tunneling from a state with energy E is given by

$$W(E) = -2\mathrm{Im}\,E.$$

The overall tunneling rate can be obtained by averaging over all states, $W =$

$-2\langle \mathrm{Im}E\rangle$. The fact that the tunneling rate is exponentially small implies that the imaginary part of energy Im E is exponentially smaller than its real part Re E. This is also true regarding the partition function Z, whose imaginary part is exponentially smaller than its real part. This results in a simple expression for the tunneling rate in terms of a partition function:

$$W = -2Z^{-1}\sum (\mathrm{Im}E)\, e^{-E/T} \approx 2TZ^{-1}\mathrm{Im}\left[\sum e^{-E/T}\right] \approx 2T\mathrm{Im}\ln Z, \qquad (3.22)$$

which coincides with the answer known to be valid for $B = 0$.

In the path-integral formulation, we represent the partition function as an integral over all closed paths that return to the well in time T^{-1} [9, 10, 16]:

$$Z = \int d\mathbf{r}(0) \int_{\mathbf{r}(0)=\mathbf{r}(\beta)} \mathcal{D}\mathbf{r}(\tau) \exp\left[-S_E[\mathbf{r}(\tau)]\right] \quad (\beta = T^{-1}), \qquad (3.23)$$

where the path-integral is taken over various real paths $\mathbf{r}(\tau)$ that satisfy periodic boundary conditions. The exponent is given by the classical Euclidean action in a magnetic field

$$S_E = \int_0^\beta d\tau \left[\frac{m}{2}\left(\frac{d\mathbf{r}}{d\tau}\right)^2 + U(\mathbf{r}) - i\frac{e}{c}\mathbf{A}(\mathbf{r})\dot{\mathbf{r}}\right] \qquad (3.24)$$

The path-integral (3.23) is dominated by paths that provide extremum to the Euclidean action, so that $\delta S_E = 0$. The extremal paths $\bar{\mathbf{r}}(\tau)$ therefore satisfy:

$$m\frac{d^2\bar{\mathbf{r}}}{d\tau^2} = \nabla U(\mathbf{r}) + i\frac{e}{c}\left[\frac{d\bar{\mathbf{r}}}{d\tau} \times \mathrm{B}\right]. \qquad (3.25)$$

Without a magnetic field, Eq. 3.25 describes classical trajectories $\bar{\mathbf{r}}(\tau)$ in the inverted potential $-U(\mathbf{r})$, which are real. For finite magnetic field both coordinate $\mathbf{r}$ and momentum $\mathbf{p}$ along the extremal trajectory become complex. The complex value

of dynamical coordinates present no difficulties, even though the integral (3.23) is evaluated over real paths $\mathbf{r}(\tau)$. This is because we can always shift the integration contour into complex value of $\mathbf{r}$ in the spirit of the steepest descent method.

The extremal path $\bar{\mathbf{r}}(\tau)$ is also called "bounce" because it starts close to the top of the inverted potential $-U(\mathbf{r})$ (minimum of the potential $U(\mathbf{r})$), then goes far away across the of $-U(\mathbf{r})$, and returns back to the top. Along this trajectory, most of the time is spent near the starting and ending points, where the velocity exponentially decreases. The fast oscillation occurs over time $\Omega^{-1} \sim |U''_{\max}|$ (curvature near the top of the real potential barrier, or equivalently near the bottom of the inverted potential). The actual instant of imaginary time τ_0 where this fast oscillation occurs becomes arbitrary in the limit $T \to 0$. We will use this idea when discussing the prefactor of the tunneling rate in Appendix A.

The fact that the dynamical coordinates take complex values along the bounce is a consequence of a broken time-reversal symmetry. However the equations of motion (3.25) preserve a symmetry under a simultaneous action of complex conjugation and time inversion. Periodic boundary conditions $\bar{\mathbf{r}}(0) = \bar{\mathbf{r}}(\beta)$ guarantee that this symmetry is valid for the extremal trajectory as well:

$$\bar{\mathbf{r}}(\tau) = \bar{\mathbf{r}}^*(\beta - \tau), \; \bar{\mathbf{p}}(\tau) = -\bar{\mathbf{p}}^*(\beta - \tau), \tag{3.26}$$

Due to the property (3.26), the maximum value of exponent given by the Euclidean action $S_E[\bar{\mathbf{r}}]$ along the extremal trajectory is real.

An interesting feature of the "bounce" trajectory in a magnetic field, is that momentum, and generally velocity, does not become zero at the turning point for

$\tau = \beta/2$. The symmetry (3.26) only requires that the real part of $d\bar{\mathbf{r}}/d\tau$ is zero for $\tau = \beta/2$. This is in accord with the results for WKB approximation in magnetic field [see Sec. 3.2], where the velocity is generally not equal to zero on the trajectory of an escaped particle in the classically allowed region. Real momentum of the escaped particle corresponds to purely imaginary momentum for the motion in the inverted potential. Therefore, if at the turning point of the "bounce", the momentum along $\bar{\mathbf{r}}$ matches that for the trajectory of classically propagating particle, it has to be purely imaginary. On the other hand, in the absence of a magnetic field the "bounce" trajectory is purely real. The velocity at the turning point is equal to zero, but so is that for a classically propagating particle.

In the path-integral (3.23), integration over fluctuations around the extremal trajectory $\bar{\mathbf{r}}(\tau)$ determines the prefactor. It is important that this prefactor is imaginary, since we are calculating the (exponentially small) imaginary part of the statistical sum. The detailed analysis of it is given in Appendix A.

3.4 Summary

In the semiclassical approximation, the problem of single particle tunneling in a magnetic field can be solved by analyzing the Hamiltonian trajectories of the particle in complex space and time. The connection of decaying and propagating waves occurs on caustics of the set of these trajectories. This approach does not require us to consider either any piece of the electron potential or magnetic field as a perturbation and can be applied to a three-dimensional potential of a general form. It gives an

escape rate which is generally *exponentially* smaller than the probability for a particle to reach the boundary of the classically accessible range $U(\mathbf{r}) = E$. The escaped particle "shows up" from the tunneling barrier with finite velocity and beyond the line $U(\mathbf{r}) = E$. Finally, it was shown that in cases where the intrawell potential is parabolic near its minimum, the escape rate in the presence of magnetic field can still be calculated using the "bounce" technique, if we allow the tunneling coordinates to take complex values. The "bounce", as well as instanton, technique is a thermodynamic method and gives the escape rate for both zero and finite temperature. Part of the next chapter is devoted to a finite-temperature calculation of the escape rate in cases where the intrawell potential is strongly *non*-parabolic near the minimum, as is certainly true for tunneling from 2D electron systems.

Chapter 4

Tunneling transverse to a magnetic field from correlated 2D electron systems.

A low-density 2DES is a very interesting system. Strong electron correlations that are present in it are very different from electron correlations found in the quantum Hall systems, in particular they are not necessarily imposed by the magnetic field. The unusual properties of in-plane transport characteristics [49]-[51] can be understood by taking many-electron effects into account [52]. Therefore it is natural to suppose that measuring the out-of-plane tunneling current can also be useful in revealing electron correlations. Such tunneling experiments deal with tunneling *from* the 2DES into the vacuum, not into the 2DES. In addition, magnetic field is applied *parallel*, not perpendicular to the layer.

The effect of electron correlations on the tunneling rate may not be described in terms of a phenomenological tunneling Hamiltonian: it is the tunneling matrix element itself that is sensitive to the electron correlations. Therefore we have to solve the coupled tunneling problem where the in-plane degrees of freedom change together with the tunneling coordinate. It is possible to do that using the approach developed in Chapter 3, where the multidimensional decay in a magnetic field was considered at zero temperature. During the escape, the tunneling electron transfers a part of its Hall momentum, which it acquired when moving out-of-plane perpendicular to **B**. The momentum transfer occurs dynamically. The overall effect is very similar to what happens in the Mössbauer effect, where the momentum of a gamma quantum is transfered to a whole crystal, and consequently there is no frequency shift in an absorption line.

The vibrations of electrons in the plane occur with frequencies of the order of the plasma frequency ω_p, which therefore characterizes the rate of inter-electron momentum exchange. The interrelation between the plasma frequency ω_p and the tunneling duration τ_f determines how much of the Hall momentum is transfered to the crystal. The remaining part goes into the excitation of phonons, and can be viewed as a remainder of the single-electron magnetic barrier. As a result, the tunneling matrix element depends strongly, and very specifically, on electron density, and also on temperature and the magnetic field. In particular, if $\omega_p \tau_f \gg 1$, then all of the Hall momentum is transfered to the crystal, and the suppression of the tunneling rate by B is completely eliminated. Because of such strong dependence, it is possible to study the electron correlations and in-plane dynamics for frequencies comparable to

the reciprocal imaginary tunneling time that an electron spends under the barrier.

Explicit results on the effect of electron correlations on tunneling will be obtained assuming that electrons form a Wigner crystal. Because of strong correlations, overlapping of the wave functions of individual electrons is small, and electrons can be "identified". The problem is then reduced to the tunneling of an electron coupled to in-plane vibrations of the Wigner crystal. As we will see, the results provide a good approximation also for a correlated electron liquid.

In Sec. 4.1 we formulate the model. In Sec. 4.2 we obtain the general expression for the tunneling rate in the WKB approximation for finite temperatures. In the analysis, the discreteness of the energy spectrum of electron motion transverse to the layer is taken into account. The result can be understood in terms of the tunneling trajectory where the duration of motion transverse to the layer (in imaginary time) is not fixed, it has to be found for given parameters of the tunneling barrier, temperature and the magnetic field. In Sec. 4.3 we derive the tunneling exponent. After the elimination of phonon variables, the tunneling exponent takes the form of a retarded action for 1D motion. The exponent depends on phonon frequencies and the form of the tunneling potential. The limits of $T = 0$ and the case of small phonon frequencies are analyzed in detail. As discussed in Sec. 4.4 the role of in-plane confinement in out-of-plane tunneling can be effectively described in terms of one characteristic phonon frequency. This corresponds to using the Einstein model of a crystal. For an Einstein solid, the many-electron problem is described by a single-particle potential. The transfer of in-plane Hall momentum from the tunneling electron to the electron system as a whole in a many-electron formulation corresponds to the momentum transfer to

the static confining potential in the effective single-electron problem. Two typical tunneling potentials are analyzed: (i) triangular barrier represents smooth tunneling potentials, where the tunneling length changes with the intra-well energy level; (ii) square barrier represents geometrically defined barriers, where the tunneling length is independent of the intra-well energy, at least in some broad range. It turns out that the tunneling rate has some qualitatively different features in these two cases.

4.1 The model: tunneling from a harmonic Wigner crystal

A 2D electron system displays strong correlations if the ratio Γ of characteristic Coulomb energy of the electron-electron interaction $e^2(\pi n)^{1/2}$ to the characteristic kinetic energy is large (here, n is the electron density). In degenerate systems the kinetic energy is the Fermi energy $\pi n/m$, whereas in nondegenerate systems it is the thermal energy T. An example of a strongly correlated nondegenerate 2DES is electrons on helium. The experimental data for this system refer to the range $\Gamma > 20$ [53]. A classical transition to a Wigner crystal (WC) was observed for $\Gamma \approx 130$ [67, 68]. Recently it became possible to achieve a strongly correlated regime with values of $\Gamma \sim 40$ in low-density electron and hole systems in semiconductors. This is expected to be sufficient for Wigner crystallization in a degenerate system [48, 66].

The effect on tunneling of the magnetic field B parallel to the electron layer is most pronounced if the tunneling length L is long, because the in-plane Hall momentum

due to tunneling $m\omega_c L$ is simply proportional to L. Respectively, of utmost interest to us are systems with broad and comparatively low barriers. Yet in experimental systems the barrier widths are most likely to be less than 10^3Å. Therefore, in order to somewhat simplify the analysis we will assume (although this is not substantial) that L is less than the average inter-electron distance $\sim n^{-1/2}$. In this case, since electrons in a strongly correlated system stay away from each other, the in-plane electron dynamics only weakly affects the tunneling potential [69] in the absence of a magnetic field. We will neglect the corresponding coupling that is present regardless of the presence of a magnetic field, and concentrate only on those effects of in-plane dynamics that are specific for finite B.

The major effect on tunneling comes from a few nearest neighbors, and the presence or absence of long-range order in the 2DES does not affect the tunneling rate. Therefore we will analyze tunneling assuming that the electron system is a Wigner crystal. As we will see, the results will indeed depend on the short-wavelength modes of the WC, as expected from the above arguments.

In a strongly correlated system where the characteristic energy of Coulomb interaction is much larger than the Fermi energy, exchange effects are not significant, and one can identify the tunneling electron. Its out-of-plane motion for $B = 0$ is described by the Hamiltonian

$$H_0 = \frac{p_z^2}{2m} + U(z). \tag{4.1}$$

The potential $U(z)$ has a well which is separated by a tunneling barrier from the extended states with a quasi-continuous spectrum, cf. Fig. 1.2. The well is non-

parabolic near the minimum, in the general case. The metastable intra well states are quantized. We will consider temperatures for which nearly all electrons are in the lowest level, with energy E_g.

The magnetic field **B** parallel to the layer mixes the out-of-plane motion of the tunneling electron with the in-plane vibrations of the Wigner crystal. The full Hamiltonian is of the form

$$H = H_0 + H_B + H_v. \tag{4.2}$$

with

$$H_v = \frac{1}{2}\sum_{\mathbf{k},j}\left[m^{-1}\mathbf{p}_{\mathbf{k}j}\mathbf{p}_{-\mathbf{k}j} + m\omega_{\mathbf{k}j}^2\mathbf{u}_{\mathbf{k}j}\mathbf{u}_{-\mathbf{k}j}\right] \tag{4.3}$$

and

$$H_B = \frac{1}{2}m\omega_c^2 z^2 - \omega_c z N^{-1/2}\sum_{\mathbf{k},j}[\mathrm{B}\times\mathbf{p}_{\mathbf{k}j}]_z. \tag{4.4}$$

Here, $\mathbf{p}_{\mathbf{k}j}$, $\mathbf{u}_{\mathbf{k}j}$, and $\omega_{\mathbf{k}j}$ are the 2D momentum, displacement, and frequency of the WC phonon of branch j ($j = 1, 2$) with a 2D wave vector $\mathbf{k}$. We chose the equilibrium in-plane position of the tunneling electron to be at the origin. Then its in-plane 2D momentum is $\mathbf{p} = N^{-1/2}\sum\mathbf{p}_{\mathbf{k}j}$ for $B = 0$.

The interaction Hamiltonian H_B (4.4) *does not* conserve the phonon quasimomentum $\mathbf{k}$. The Hall momentum of the tunneling electron, $p_H = (e/c)[\mathbf{B}\times\mathbf{z}]$, is transferred to the WC as a whole. The term H_B couples the out-of-plane motion to lattice vibrations. The problem of many-electron tunneling is thus mapped onto a familiar problem of a particle coupled to a bath of harmonic oscillators [70, 16], with the coupling strength controlled by the magnetic field. The distinctions from the standard situation stem from the non-parabolicity of the potential well near the

minimum and from the fact that coupled by H_B are the electron *coordinate* z and the in-plane *momenta* of the lattice. These quantities have different symmetry with respect to time inversion. In the general case [for example, where the potential energy of the system has odd-order terms in the displacements $u_{\mathbf{k}j}$], the broken time-reversal symmetry requires a special approach to the analysis of tunneling [46]. The results discussed below can be appropriately generalized using this approach.

For the model (4.2), the analysis is simplified by the structure of the Hamiltonian (cf. [16]). For vibrations with the Hamiltonian H_v (4.3), one can always make a canonical transformation from the canonical coordinates and momenta $\mathbf{u}_{\mathbf{k}j}$ and $\mathbf{p}_{\mathbf{k}j}$ to the new canonical coordinates and momenta $\mathbf{p}_{\mathbf{k}j}$ and $-\mathbf{u}_{\mathbf{k}j}$, respectively. This transformation interchanges the time-reversal symmetry of the in-plane dynamical variables, it makes $\mathbf{p}_{\mathbf{k}j}$ and $\mathbf{u}_{\mathbf{k}j}$ even and odd in time, respectively. Because H_B is independent of $\mathbf{u}_{\mathbf{k}j}$ and is linear in $\mathbf{p}_{\mathbf{k}j}$, in the new variables it takes on a more familiar form of a potential coupling which depends only on coordinates $z, \mathbf{p}_{\mathbf{k}j}$. In this representation the kinetic energy is given by $p_z^2/2m + \sum_{\mathbf{k}j} m\omega_{\mathbf{k}j}^2 \mathbf{u}_{\mathbf{k}j}\mathbf{u}_{-\mathbf{k}j}/2$ and does not depend on the magnetic field. The symmetry under time-inversion is therefore restored.

4.2 A many-body WKB approximation

4.2.1 General formulation

We will evaluate the tunneling rate W in the WKB approximation. The major emphasis will be placed on the tunneling exponent. We will assume that the escape rate is much less than the intrawell relaxation rate for relevant states, and there is an established thermal distribution over the intrawell states of the system. This is not necessarily true for 2D systems. Our results can be generalized to the case of slow intrawell relaxation, see Sec. 6.2.

We consider the decay of the metastable intrawell states $\alpha = [\{n, n_{\mathbf{k}j}\}]$, with decay rate rates W_α, where phonon states are enumerated by their occupation numbers $n_{\mathbf{k}j}$, and the index n enumerates states quantized in the out-of-plane direction. These rates sharply increase with state energies E_α, whereas the Boltzmann intrawell distribution exponentially decreases with E_α. As a result, there is a comparatively small group of states which mostly contribute to the escape from which the system is most likely to escape (for fast intrawell relaxation, the relative population of these states remains unchanged). This allows one to characterize escape by a single rate W. To logarithmic accuracy,

$$W = Z^{-1} \sum_\alpha W_\alpha \exp(-\beta E_\alpha), \tag{4.5}$$

$$W_\alpha = C_\alpha \exp\left[-2S_\alpha(\boldsymbol{\xi}_{\rm f}, \boldsymbol{\xi}_{\rm in})\right] \left|\psi_\alpha(\boldsymbol{\xi}_{\rm in})\right|^2 .$$

Here, we introduced a vector $\boldsymbol{\xi} = (z, \{\mathbf{p}_{\mathbf{k}j}\})$ with components which enumerate the z-coordinate of the tunneling electron and the "coordinates" $\mathbf{p}_{\mathbf{k}j}$ of the phonons,

$Z \approx \exp(-\beta E_1)$ is the partition function calculated neglecting escape, $\psi_\alpha(\boldsymbol{\xi})$ is the intrawell wave function, and C_α are the prefactors in the partial escape rates [although we will not discuss them here, they will be calculated for a particular tunneling problem in order to compare the theory with the experimental data [34] in Chapter 6].

The exponents in the rates W_α are determined [7] by the wave functions $\psi_\alpha(\boldsymbol{\xi})$ at the turning points $\boldsymbol{\xi}_\mathrm{f}$ on the boundary of the classically accessible ranges ($\boldsymbol{\xi}_\mathrm{f}$ depend on α, see below). It is convenient to evaluate $\psi_\alpha(\boldsymbol{\xi}_\mathrm{f})$ in two steps, each of which gives an exponential factor. The first factor, $\exp[-S_\alpha(\boldsymbol{\xi}_\mathrm{f}, \boldsymbol{\xi}_\mathrm{in})]$, describes the decay of the wave function under the barrier. Formally, it relates $\psi_\alpha(\boldsymbol{\xi}_\mathrm{f})$ to $\psi_\alpha(\boldsymbol{\xi}_\mathrm{in})$. The point $\boldsymbol{\xi}_\mathrm{in}$ is chosen close to the well, yet it lies under the barrier, so that S_α can be calculated in the WKB approximation. The second factor is $\psi_\alpha(\boldsymbol{\xi}_\mathrm{in})$ itself. The resulting rate should be independent of $\boldsymbol{\xi}_\mathrm{in}$.

We start with the function $S_\alpha(\boldsymbol{\xi}, \boldsymbol{\xi}_\mathrm{in})$. To the lowest order in $\hbar$, for systems with time-reversal symmetry (which we restored by the canonical transformation) it is the action for a classical underbarrier motion in imaginary time $\tau = it$ with purely imaginary momenta [9]

$$p_z = i\,\partial S/\partial z, \quad \mathbf{u}_{\mathbf{k}j} = -i\,\partial S/\partial \mathbf{p}_{\mathbf{k}j}. \tag{4.6}$$

As a function of the imaginary time τ, the action $S(\boldsymbol{\xi}, \boldsymbol{\xi}_\mathrm{in})$ is given by the integral of the Euclidean Lagrangian L_E,

$$S_\alpha(\boldsymbol{\xi}, \boldsymbol{\xi}_\mathrm{in}) = \int_0^\tau L_\mathrm{E} d\tau - E_\alpha \tau. \tag{4.7}$$

The Lagrangian L_E is obtained from the Hamiltonian (3.2) using the Legendre transformation $L = p_z(dz/dt) - \sum \mathbf{u}_{\mathbf{k}j}(d\mathbf{p}_{\mathbf{k}j}/dt) - H$, followed by the transition to imagi-

nary time, which gives

$$L_{\rm E} = L_0 + L_v + L_B. \tag{4.8}$$

Here,

$$L_0 = \frac{m}{2}\left(\frac{dz}{d\tau}\right)^2 + U(z), \quad L_B = H_B, \tag{4.9}$$

and L_v is the Lagrangian of the phonons, $L_v = \sum_{\mathbf{k}j} L_{\mathbf{k}j}$, with

$$L_{\mathbf{k}j} = \frac{1}{2m}\mathbf{p}_{\mathbf{k}j}\mathbf{p}_{-\mathbf{k}j} + \frac{1}{2m\omega_{\mathbf{k}j}^2}\frac{d\mathbf{p}_{\mathbf{k}j}}{d\tau}\frac{d\mathbf{p}_{-\mathbf{k}j}}{d\tau}. \tag{4.10}$$

The classical equations of motion in imaginary time have the standard form

$$\frac{d}{d\tau}\frac{\partial L_{\rm E}}{\partial \dot{\boldsymbol{\xi}}} - \frac{\partial L_{\rm E}}{\partial \boldsymbol{\xi}} = 0. \tag{4.11}$$

where overdot means differentiation over τ. To calculate the escape rate, one has to find the trajectory which goes from $\boldsymbol{\xi}(0) = \boldsymbol{\xi}_{\rm in}$ to the boundary of the classically accessible range $\boldsymbol{\xi}_{\rm f}$ at a certain time τ_f and calculate the action S_α along this trajectory.

If the potential barrier $U(z)$ is smooth, the wave function and its derivatives under the barrier have to match the WKB wave function in the classically allowed range behind the barrier. The matching occurs at a turning point of the classical motion (4.11) where the derivatives of the both wave functions become equal to zero [7], i.e. for $\partial S_\alpha/\partial z = \partial S_\alpha/\partial \mathbf{p}_{\mathbf{k}j} = 0$, i.e.

$$\dot{z}(\tau_f) = 0, \ \dot{\mathrm{p}}_{\mathbf{k}j}(\tau_f) = 0. \tag{4.12}$$

Eq. (4.12) is also the condition of the extremum of S_α with respect to the points $\boldsymbol{\xi}$ on the boundary of the classically accessible range: the escape rate is determined

by the minimum of S_α on this boundary. A detailed analysis of the behavior of multidimensional tunneling trajectories in imaginary time for systems with time-reversal symmetry is given in Ref. [15].

Time-reversal symmetry of the equations (4.11) in coordinates $(z, \mathbf{p}_{\mathbf{k}j})$, together with the condition (4.12), shows that if the equations of motion are extended beyond τ_f, the system will bounce off the turning point and then move under the barrier back to the starting point. The section of the trajectory for $\tau > \tau_f$ is mirror-symmetrical to that for $\tau < \tau_f$,

$$z(\tau_f + \tau) = z(\tau_f - \tau),\ \mathbf{p}_{\mathbf{k}j}(\tau_f + \tau) = \mathbf{p}_{\mathbf{k}j}(\tau_f - \tau), \tag{4.13}$$

where $0 \leq \tau \leq \tau_f$. As a result, the tunneling exponent $2S_\alpha$ can be calculated along the trajectory (4.11) that reaches the turning point at τ_f and returns to the well at $2\tau_f$.

The time τ_f is determined by the boundary conditions (4.12) and by the initial conditions on the trajectory, which are given by $\psi_\alpha(\boldsymbol{\xi}_{\text{in}})$. If the intrawell dynamics is semiclassical, the dominating contribution to the overall rate W (4.5) comes from the energies E_α for which the duration of the tunneling motion $\tau_f = \beta/2$ [9]. In the general case this is no longer true.

4.2.2 The initial conditions

We are consider the situation where, at least for low-lying intrawell states n, the characteristic lengths $1/\gamma_n$ of localization in the z-direction are much less the typical widths L of the tunneling barrier, so that $\gamma_n \ll L$. Then, even where the effect of

the magnetic field accumulates under the barrier and the tunneling rate is strongly changed, the field may still only weakly perturb the intrawell motion. In this case, inside the well and close to it, the out-of-plane electron motion is separated from the in-plane vibrations. Respectively, the states of the electron-phonon system can be enumerated by n and the phonon occupation numbers $n_{\mathbf{k}j}$, i.e. $\alpha = (n, \{n_{\mathbf{k}j}\})$, and the energies are

$$E_\alpha = E_n + \sum_{\mathbf{k}j} \varepsilon_{\mathbf{k}j}, \quad \varepsilon_{\mathbf{k}j} = \omega_{\mathbf{k}j} n_{\mathbf{k}j}. \tag{4.14}$$

Usually the interlevel distances $E_{n+1} - E_n \gg \omega_{\mathbf{k}j}$, for low-lying levels.

Because of the separation of motions, we can choose a plane $z = z_{\text{in}}$ under the barrier but close to the well, so that for $\boldsymbol{\xi} \approx \boldsymbol{\xi}_{\text{in}}$ the wave functions $\psi_\alpha(\boldsymbol{\xi})$ are semiclassical and at the same time can be factored,

$$\psi_{n,\{n_{\mathbf{k}j}\}}(\boldsymbol{\xi}) \propto e^{-\gamma_n z} \exp\left[-\sum_{\mathbf{k}j} S_{n_{\mathbf{k}j}}(\mathbf{p}_{\mathbf{k}j})\right]. \tag{4.15}$$

The action $S_{n_{\mathbf{k}j}}$ determines the dependence of the wave function on the phonon coordinates.

For $\boldsymbol{\xi} = \boldsymbol{\xi}_{\text{in}}$, Eq. (4.15) gives the initial values of the dynamical variables $\boldsymbol{\xi}(0) \equiv \boldsymbol{\xi}_{\text{in}}$ and $\dot{\boldsymbol{\xi}}(0)$ on the WKB trajectory (4.11). In particular if, for $z \approx z_{\text{in}}$, the potential $U(z)$ varies over the distance much bigger than $1/\gamma_n$, then

$$z(0) = z_{\text{in}}, \quad \dot{z}(0) = \frac{\gamma_n}{m} = \left[\frac{2[U(z_{\text{in}}) - E_n]}{m}\right]^{1/2}, \tag{4.16}$$

and γ_n (4.16) is independent of the exact position of the plane $z = z_{\text{in}}$.

It is convenient to write $S_{n_{\mathbf{k}j}}$ and $\mathbf{p}_{\mathbf{k}j}$ in Eq. (4.15) in the energy-phase representation, using the phonon energy $\varepsilon_{\mathbf{k}j}$ and the imaginary time $\tau_{\mathbf{k}j}$ it takes for a phonon

to move under the barrier from the boundary $(2m\varepsilon_{\mathbf{k}j})^{1/2}$ of the classically allowed region to the given $\mathbf{p}_{\mathbf{k}j}$. With the Euclidean Lagrangian of the phonons (4.10), we have for $\mathbf{p}_{\mathbf{k}j} = [\mathbf{p}_{\mathbf{k}j}]_{\text{in}} \equiv \mathbf{p}_{\mathbf{k}j}(0)$

$$S_{n_{\mathbf{k}j}}(\mathbf{p}_{\mathbf{k}j}(0)) = \int_{-\tau_{\mathbf{k}j}}^{0} d\tau L_{\mathbf{k}j}(\tau) - \varepsilon_{\mathbf{k}j}\tau_{\mathbf{k}j}, \tag{4.17}$$

and

$$\begin{aligned} \mathbf{p}_{\mathbf{k}j}(0) &= \mathbf{e}_{\mathbf{k}j}(2m\varepsilon_{\mathbf{k}j})^{1/2}\cosh\omega_{\mathbf{k}j}\tau_{\mathbf{k}j}, \\ \dot{\mathbf{p}}_{\mathbf{k}j}(0) &= \mathbf{e}_{-\mathbf{k}j}\left(2\varepsilon_{\mathbf{k}j}m\omega_{\mathbf{k}j}^2\right)^{1/2}\sinh\omega_{\mathbf{k}j}\tau_{\mathbf{k}j} \end{aligned} \tag{4.18}$$

[$\mathbf{e}_{\mathbf{k}j}$ is the polarization vector of the mode $(\mathbf{k}, j)$].

4.2.3 A three-segment optimal trajectory

To evaluate the escape rate W to logarithmic accuracy, one can, following Feynman's procedure, solve the equations of motion (4.11) for the vibration "coordinates" $\mathbf{p}_{\mathbf{k}j}(\tau)$ in terms of $z(\tau)$ and the initial energies $\varepsilon_{\mathbf{k}j}$ and phases $\omega_{\mathbf{k}j}\tau_{\mathbf{k}j}$. Then, from the boundary condition (4.12), one can express $\tau_{\mathbf{k}j}$ in terms of other variables, and then do thermal averaging by integrating the escape rate over $\varepsilon_{\mathbf{k}j}$ with the Boltzmann weighting factor. Here we reverse the order and give an alternative derivation, which provides a better insight into the structure of the tunneling trajectory. In this section we average over phonon energies $\epsilon_{\mathbf{k}j}$ to find times $\tau_{\mathbf{k}j}$. In the next section we eliminate the phonon variables to obtain the tunneling exponent. We note that, from Eqs. (4.5), (4.7), (4.15), and (4.17), the partial escape rate W_α can be written as $W_\alpha \propto \exp(-s_\alpha)$,

with

$$s_\alpha = \sum_{\mathbf{k}j} \int_{-\tau_{\mathbf{k}j}}^{0} d\tau\, L_{\mathbf{k}j}(\tau) + \int_0^{2\tau_f} d\tau\, L_{\mathrm{E}}(\tau) + \sum_{\mathbf{k}j} \int_{2\tau_f}^{2\tau_f+\tau_{\mathbf{k}j}} d\tau\, L_{\mathbf{k}j}(\tau) - 2E_n\tau_f$$
$$-2\sum_{\mathbf{k}j} \varepsilon_{\mathbf{k}j}(\tau_f + \tau_{\mathbf{k}j}). \tag{4.19}$$

(the term $\gamma_n z_{\mathrm{in}}$ in (4.15), which is small compared to $s_\alpha \sim \gamma_n L$, is incorporated into the prefactor, see Sec. 6.3.

Eq. (4.19) suggests that one can think of the optimal trajectory as consisting of 3 segments. In the first segment, from $-\tau_{\mathbf{k}j}$ to 0, the z-motion of the tunneling electron is disconnected from the vibrations. The electron stays at $z = 0$, while each vibrational mode moves for the time $\tau_{\mathbf{k}j}$, starting from the boundary $\mathbf{u}_{\mathbf{k}j} = \mathbf{0}$ [cf. Eq. (4.17)]. This motion is determined by the Lagrangian $L_{\mathbf{k}j}$. At $\tau = 0$ the interaction is turned on, and in the second segment the electron and the vibrations move together for the time $2\tau_f$, with the Lagrangian L_{E}. During this motion, the trajectory (4.11) bounces off the turning point (4.12), and the electron comes back to $z = z_{\mathrm{in}}$. After that, in the 3rd segment, the coupling is turned off again, the electron stays at z_{in}, while the vibrations continue to move for the times $\tau_{\mathbf{k}j}$ back to $\mathbf{u}_{\mathbf{k}j} = \mathbf{0}$. The three-segment vibration trajectory is continuous.

To logarithmic accuracy, the tunneling rate W is given by $\langle \exp(-2S_E) \rangle$. The averaging here should be performed over the intrawell vibration energies $\varepsilon_{\mathbf{k}j}$ [we note that τ_f and $\tau_{\mathbf{k}j}$ in S_E are determined by $\varepsilon_{\mathbf{k}j}$],

$$W \propto \sum_n \int \prod_{\mathbf{k}j} d\varepsilon_{\mathbf{k}j} \exp\left[(2\tau_f - \beta)E_n - 2\int_0^{\tau_f} d\tau L_{\mathrm{E}}(\tau)\right.$$
$$\left. -2\sum_{\mathbf{k}j} \int_{-\tau_{\mathbf{k}j}}^{0} d\tau L_{\mathbf{k}j}(\tau) + (2\tau_{\mathbf{k}j} + 2\tau_f - \beta)\varepsilon_{\mathbf{k}j}\right]. \tag{4.20}$$

The integral over $\varepsilon_{\mathbf{k}j}$ should be calculated by the steepest descent method. From Eqs. (4.12), (4.17) it follows that the partial derivatives of $S_{\rm E}$ over the times τ_f and $\tau_{\mathbf{k}j}$ (which depend on $\varepsilon_{\mathbf{k}j}$) are equal to zero. The condition of the extremum of $S_{\rm E}$ with respect to $\varepsilon_{\mathbf{k}j}$ then gives

$$\tau_{\mathbf{k}j} = \frac{1}{2}\beta - \tau_f, \tag{4.21}$$

This expression shows that the duration of motion $\tau_{\mathbf{k}j}$ is the same for all vibrational modes. Moreover, the overall duration of the three-segment optimal trajectory of each vibration is $2(\tau_{\mathbf{k}j} + \tau_f) = \beta$. Examples of the trajectories are shown in Fig. 4.1.

For low temperatures, $\beta > 2\tau_f$, the direction of time along the vibrational trajectory does not change. In this case the value of $\tau_{\mathbf{k}j}$ (4.21) which provides an extremum to the integral over $\varepsilon_{\mathbf{k}j}$ is positive. The corresponding branch of the intrawell vibrational wave function $\propto \exp[-S_E(0)]$ decays with the increasing $p_{\mathbf{k}j}$ in the classically forbidden region $p_{\mathbf{k}j} > (2m\varepsilon_{\mathbf{k}j})^{1/2}$. On the other hand for higher temperatures, $\beta < 2\tau_f$, we have $\tau_{\mathbf{k}j} < 0$. This shows that the extremum of the integrand in Eq. (4.20) is reached if the intrawell vibrational wave function is analytically continued from the decaying to the increasing branch.

For $\tau_{\mathbf{k}j} = (\beta/2) - \tau_f < 0$, the "free-vibrations" term $S_E(0)$ in the Euclidean action S_E is negative, it gives rise to the decrease of the tunneling exponent. This is the formal reason why an in-plane magnetic field can increase the tunneling rate compared to its $B = 0$ value by coupling thermally-excited in-plane vibrations to tunneling.

If the intrawell motion transverse to the layer were semiclassical, the sum over

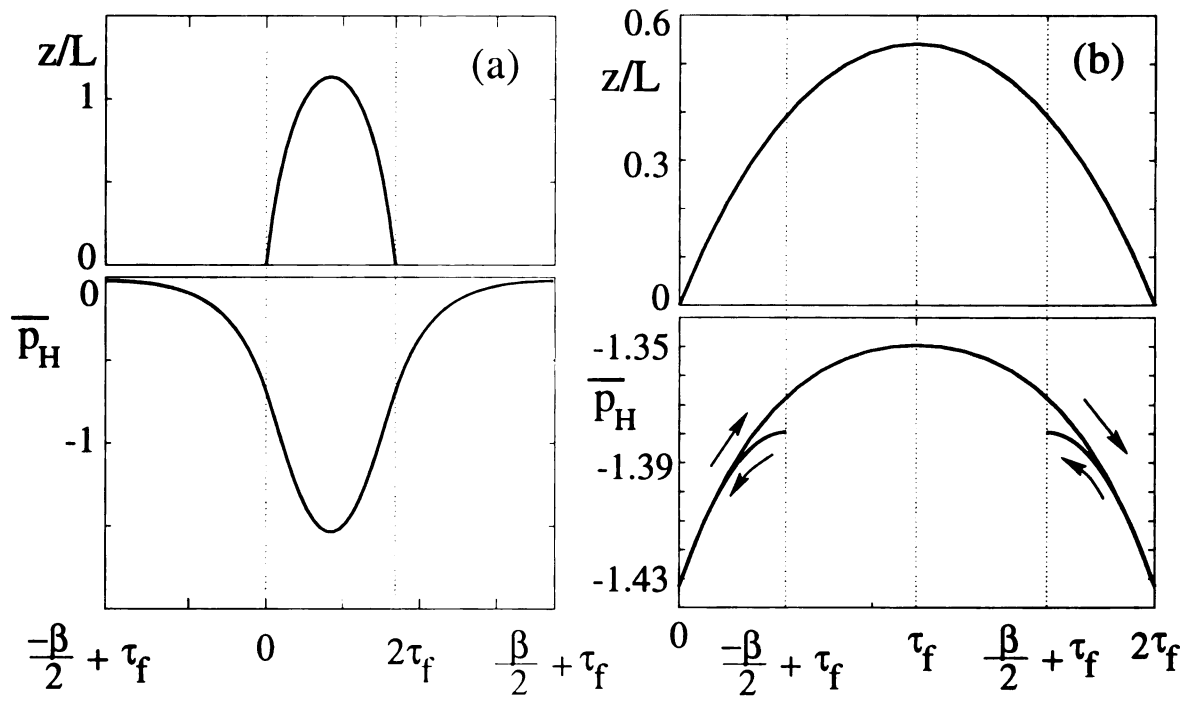

Figure 4.1: The optimal trajectories of the tunneling electron $z(\tau)$ and of one of the vibrational modes $p_H(\tau)$ for $\beta > 2\tau_f$ (a) and $\beta < 2\tau_f$ (b). The numerical data refer to the Einstein model of the Wigner crystal, p_H is the p-component of the vibrational momentum in the Hall direction $\hat{\mathbf{z}} \times \mathbf{B}$. The arrows show the direction of motion along the optimal trajectory when $\beta < 2\tau_f$. The tunneling potential is of the form (4.38), with dimensionless cyclotron frequency $\omega_c\tau_0 = 2.0$, where $\tau_0 = 2mL/\gamma$ is the imaginary transit time for $B = 0$. The phonon frequency is $\omega_p\tau_0 = 1.0$.

the energy levels of this motion E_n in Eq. (4.20) could be replaced by an integral. It could then be evaluated by the steepest descent method, as in the case of in-plane vibrations, with the result $\tau_f = \beta/2, \tau_{\mathbf{k}j} = 0$. This is the familiar result of the instanton theory, in which the whole system moves under the barrier from the well to the turning point and back over the imaginary time β [9]. Clearly, in this case one should not expect the tunneling rate to be enhanced by a magnetic field.

In the case of 2D electron systems, the potential well is *not* parabolic and the low-lying intrawell states are not semiclassical. Therefore the sum over E_n in (4.20)

may not be replaced by an integral, each term has to be considered separately, and the duration of motion τ_f for each energy level has to be found from the boundary condition (4.12).

4.3 The tunneling exponent

Eqs. (4.5) and (4.19) allow us to write the escape rate as a sum of the escape rates for different intrawell states n. To logarithmic accuracy, the overall escape rate is determined by the maximum of the escape rate with respect to the intrawell state n, with account taken of the thermal population of the state [here we assume that thermalization inside the well occurs faster than escape],

$$W \propto \max_n \exp(-R_n - \beta E_n), \quad R_n = \min_{z(\tau)} \mathcal{R}_n[z(\tau)], \tag{4.22}$$

The functional $\mathcal{R}_n[z]$ is a retarded action functional for a 1D motion normal to the electron layer. It is determined by the functional s_α for the nth state from which the the dynamical variables of the in-plane vibrations have been eliminated. The elimination can be done in a standard way [70] by solving the linear equations of motion (4.11) for $\mathbf{u}_{\mathbf{k}j}, \mathbf{p}_{\mathbf{k}j}$ with the boundary conditions (4.18), (4.12), and (4.21). This gives

$$\mathcal{R}_n[z] = \int_0^{2\tau_f} d\tau_1 \left[\frac{m}{2} \left(\frac{dz}{d\tau} \right)^2 + U(z) + \frac{1}{2} m\omega_c^2 z^2(\tau_1) \right] + \mathcal{R}_{\rm ee}[z] - 2\tau_f E_n \tag{4.23}$$

(we have set the energy of the intrawell ground state $E_g = 0$).

The term $\mathcal{R}_{\rm ee}$ is the retarded action describing the effects of electron-electron

interaction that we modeled by electron-phonon coupling [cf. 4.4],

$$\mathcal{R}_{\rm ee}[z] = -\frac{\omega_c^2}{2}\int_0^{2\tau_f}\int_0^{\tau_1} d\tau_1 d\tau_2 z(\tau_1)z(\tau_2)\chi(\tau_1-\tau_2) \tag{4.24}$$

Here, the $\chi(\tau) = \langle \mathbf{p}_{||}(\tau)\mathbf{p}_{||}(0)\rangle$ is the correlation function of the in-plane momentum $\mathbf{p}_{||}$ of an electron in the correlated 2DES. For electrons forming a Wigner crystal, it is simply related to the phonon Green's function,

$$\chi(\tau) = \frac{m}{2N}\sum_{\mathbf{k}j}\omega_{\mathbf{k}j}\left[\bar{n}_{\mathbf{k}j}e^{\omega_{\mathbf{k}j}\tau} + (\bar{n}_{\mathbf{k}j}+1)e^{-\omega_{\mathbf{k}j}\tau}\right] \tag{4.25}$$

($\bar{n}_{\mathbf{k}j} = [\exp(\beta\omega_{\mathbf{k}j}) - 1]^{-1}$ is the thermal occupation number).

The term $\mathcal{R}_{\rm ee}$ is negative. It means that the electron-electron interaction in a correlated 2DES always *increases* the tunneling rate in the presence of a magnetic field. Moreover, when this term exceeds $(m\omega_c^2/2)\int z^2 d\tau$, the tunneling exponent as a whole decreases with the increasing B.

Two physical phenomena are described by the term $\mathcal{R}_{\rm ee}$. One is the dynamical compensation of the Hall momentum of the tunneling electron by the WC as the electron moves under the barrier in the z-direction. The other is thermal "preparation" of the Hall momentum for the tunneling electron, which is then transformed by the magnetic field into the momentum of motion in the z-direction. These effects are analyzed in the following subsections.

4.3.1 Zero temperature limit

It would be natural to think that, since tunneling is accompanied by creation of phonons for $T = 0$, then the higher the phonon frequency the lower the tunneling rate. In fact just the opposite is true.

The effect of the electron-electron interaction on tunneling, as characterized by $\mathcal{R}_{ee}$, depends on the interrelation between the characteristic phonon frequency ω_p and the tunneling duration τ_f. The quantity ω_p also characterizes the rate of inter-electron in-plane momentum exchange. When the tunneling electron is "pushed" by the Lorentz force, it exchanges the in-plane momentum with other electrons. The parameter $\omega_p\tau_f$ determines what portion of the momentum goes to the crystal as a whole during the tunneling (note that the tunneling motion goes in imaginary time, and the quantity τ_f characterizes the time uncertainty rather than the actual duration of a real process, see Ref. [71]). In the adiabatic limit of large $\omega_p\tau_f$, all electrons have same in-plane velocity, with an accuracy to quantum fluctuations. Therefore the Lorentz force produces no acceleration, and *no phonons* are created during the tunneling. The effect of the magnetic field on tunneling should then be eliminated.

These arguments are confirmed by the analysis of Eq. (4.24). If the electron system is rigid enough, so that $\omega_{\mathbf{k}j}\tau_f \gg 1$, the major contribution to $\mathcal{R}_{ee}$ comes from $\tau_1 - \tau_2 \sim \omega_{\mathbf{k}j}^{-1} \ll \tau_f$. Therefore $z(\tau_2) \approx z(\tau_1)$, and we could use an expansion:

$$z(\tau_2) \approx z(\tau_1) + \dot{z}(\tau_1)(\tau_2 - \tau_1) + \frac{1}{2}\ddot{z}(\tau_1)(\tau_2 - \tau_1)^2 \tag{4.26}$$

in the functional $\mathcal{R}_{ee}$. The upper limit in the integration over τ_2 can be extended to infinity, since it introduces only an exponentially small error. Then the leading term in expansion (4.26) cancels the term $\propto z^2$ in (4.23), which represent the single-particle magnetic field barrier. The linear term in expansion (4.26) gives a zero contribution. The quadratic term leads to an effective renormalization $m \to m^*$ of the electron

mass in a magnetic field:

$$m^* \approx \; m\left[1+\frac{1}{2m}\int_0^{\tau_f} d\tau\tau^2\chi(\tau)\right] \approx m\left[1+(2N)^{-1}\sum_{\mathbf{k}j}\frac{\omega_c^2}{\omega_{\mathbf{k}j}^2}\right]. \qquad (4.27)$$

Tunneling occurs as if the electron were disconnected from the phonons, and did not experience a magnetic field. The only effect of the magnetic field is that the electron mass in Eq. (4.23) is effectively incremented by a B-dependent factor. This change is reflected in all of the tunneling characteristics, including the tunneling time $\tau_f = (m^*/m)^{1/2}\tau_0$, and most importantly, the tunneling exponent becomes appropriately renormalized:

$$R \to \sqrt{\frac{m^*}{m}} R_{B=0}. \qquad (4.28)$$

This analysis is quite general and applies for arbitrary form of potential $U(z)$. This includes potentials where the tunneling length is well defined by a jump in the potential, as it happens in semiconductor heterostructures. Expressions (4.23), (4.24) for the tunneling exponent still apply provided that the tunneling trajectory for $\tau > \tau_f$ is now *defined* through $z(\tau) = z(2\tau_f - \tau)$. In addition, because $\dot{z}(\tau_f) \neq 0$ expansion (4.26) has to be changed to:

$$z(\tau_2) \approx z(\tau_1) + \dot{z}(\tau_1) \times \begin{cases} (\tau_2 - \tau_1), & \text{for } \tau_1 < \tau_f \text{ or } \tau_f < \tau_2 \\ (2\tau_f - \tau_1 - \tau_2), & \text{for } \tau_2 < \tau_f < \tau_1 \end{cases} \qquad (4.29)$$

Details of the analysis for a square potential can be found in Appendix B. The scaling behavior of the tunneling time τ_f and the tunneling exponent $\mathcal{R}$ can be also checked using the explicit answers for a triangular barrier (4.41) and for a square barrier (5.6), (5.7).

In this derivation we assume that the major contribution to the integral over τ comes from times $\tau \sim 1/\omega_p \ll \tau_f$. Respectively, for a Wigner crystal, the major contribution to the sum over $(\mathbf{k}, j)$, comes from $\omega_{\mathbf{k}j} \sim \omega_p$. The integral only weakly depends on the upper limit τ_f, which also provides the inverse of the lower cutoff frequency in the sum over $(\mathbf{k}, j)$. For a Wigner crystal, the dependence of the mass renormalization on τ_f is logarithmic.

The tunneling rate approaches its value for $B = 0$ with increasing ω_p. On the other hand, the slope of the logarithm of the tunneling rate as a function of ω_c depends explicitly on ω_p, for $\omega_c \gtrsim \omega_p$. This provides a means for measuring ω_p.

For $\omega_p \tau_f \sim 1$, only a part of the Hall momentum can be taken by the electron crystal. The rest goes into the in-plane kinetic energy of the tunneling electron, and ultimately into creations of WC phonons. However, the major contribution to $\mathcal{R}_{\mathbf{ee}}$ still comes from high-frequency phonons. It can be shown from (4.24) that this contribution monotonically increases with increasing $\omega_{\mathbf{k}j}$ [see Appendix B for a derivation]. This is because the more rigid the electron system is, the more effectively it compensates the in-plane Hall momentum. An important consequence is that, since high-frequency vibrations have small wavelengths, the major effect on tunneling comes from the short-range order in the electron system.

On the whole, for $T = 0$, the magnetic-field induced term in the tunneling exponent is positive, i.e. the tunneling rate decreases with the magnetic field. This can be seen from Eqs. (4.23), (4.24) by replacing $z(\tau_1)z(\tau_2)$ in $\mathcal{R}_{\mathbf{ee}}$ with $(1/2)[z^2(\tau_1) + z^2(\tau_2)] \geq z(\tau_1)z(\tau_2)$ and then integrating the function $\chi(\tau_1 - \tau_2) =$

$\exp[-\omega_{\mathbf{k}j}(\tau_1 - \tau_2)]$ over τ_2 [for the term $z^2(\tau_1)$] and over τ_1 [for the term $z^2(\tau_2)$]:

$$-\mathcal{R}_{\rm ee}[z] < \frac{m\omega_c^2}{8N}\sum_{\mathbf{k}j}\omega_{\mathbf{k}j}\int_0^{2\tau_f}\int_0^{\tau_1} d\tau_1 d\tau_2 [z^2(\tau_1)+z^2(\tau_2)]e^{\omega_{\mathbf{k}j}(\tau_1-\tau_2)}$$
$$= \frac{m\omega_c^2}{8N}\sum_{\mathbf{k}j}\int_0^{2\tau_f} d\tau_1 z^2(\tau_1)\left(2-e^{-\omega_{\mathbf{k}j}\tau_1}-e^{-\omega_{\mathbf{k}j}(2\tau_f-\tau_2)}\right)$$

By dropping the exponentials in the integrand, we eliminate dependence on $\omega_{\mathbf{k}j}$, and the sum over phonons gives a factor $2N$. As a result, we get an upper bound for the many-electron term in the exponent:

$$-\mathcal{R}_{\rm ee}[z] < \frac{1}{2}m\omega_c^2\int_0^{2\tau_f} d\tau z^2(\tau), \tag{4.30}$$

The last expression describes the suppression of the tunneling rate by B for non-interacting electrons. Therefore, many-electron effects at $T = 0$ can lead at most to a compensation of the suppression introduced by the magnetic field. The tunneling rate cannot exceed its value for $B = 0$.

Electron correlations exponentially reduce the effect of the magnetic field on the tunneling rate in a magnetic field. For specific models, the dependence of the tunneling rate on B and the vibration frequencies will be illustrated in Sec. 4.4. The results will also be compared with the experiment in Chapter 6.

4.3.2 High temperatures and small phonon frequencies

The analysis of the tunneling rate somewhat simplifies in the case of comparatively high temperatures and small phonon frequencies, where the vibrations are classical and their frequencies are small compared to the reciprocal tunneling duration,

$\omega_{\mathbf{k}j}\beta, \omega_{\mathbf{k}j}\tau_f \ll 1$. In this case

$$\mathcal{R}_{\rm ee}[z] = -2mT\omega_c^2\tau_f^2\bar{z}^2, \quad \bar{z} = \tau_f^{-1}\int_0^{\tau_f} d\tau z(\tau). \tag{4.31}$$

Note that the origin of the z-axis has been chosen in Eq. (4.2) in such a way that $z = 0$ inside the potential well where the electrons are localized (or that the diagonal matrix element of z on the intrawell ground state wave function is equal to zero). Therefore in Eq. (4.31) $\bar{z} \neq 0$ for an optimal tunneling trajectory, and correspondingly the value of $\mathcal{R}_{\rm ee}$ on this trajectory is nonzero and negative.

Eqs. (4.23), (4.31) describe also the tunneling action of a single electron, with the Maxwell distribution of the in-plane momentum inside the well $\exp(-p^2/2mT)$. The coupling of the $\hat{\mathbf{z}} \times \mathbf{B}$ component of the momentum to the out-of-plane motion gives rise to the term $-2p\omega_c \int_0^{\tau_f} d\tau z(\tau)$ in the tunneling action [cf. Eqs. (4.4), (4.7)]. The extreme value of the sum of this term and $-p^2/2mT$ is just equal to $-\mathcal{R}_{\rm ee}[z]$ as given by (4.31).

The single-electron form of the tunneling exponent is to be expected in the limit of small $\omega_{\mathbf{k}j}$, because the distribution over in-plane momenta of electrons forming a Wigner crystal is Maxwellian, in the classical limit. For small $\omega_{\mathbf{k}j}\tau_f$ the momenta do not change over the tunneling duration, therefore only the momentum of the tunneling electron itself is important. The above derivation provides an independent test of the derivation used to obtain the general expression (4.23), (4.24).

Let us note that the action $\mathcal{R}_{\rm ee}[z]$ (4.31) is still retarded, it does not correspond to a local in time Lagrangian. The functional form of $\mathcal{R}_{\rm ee}$ remains the same even for temperatures $T \lesssim \omega_{\mathbf{k}j}$ provided the phonon frequencies are small compared to

τ_f^{-1} and ω_c. In this case T in Eq. (4.31) has to be replaced by $(4N)^{-1}\sum\omega_{\mathbf{k}j}(2\bar{n}_{\mathbf{k}j}+1)$. This factor explicitly depends on the phonon dispersion law, but again, the major contribution comes from short-wavelength high-frequency phonons, which are determined by the short-range order in the electron system.

4.4 Effect of in-plane confinement on the tunneling rate

4.4.1 The Einstein approximation for a Wigner crystal

The exchange of momentum between electron in the layer is realized more efficiently by higher frequency phonons, as was discussed in subsection 4.3.1. This is also reflected by the fact that high frequencies dominate the electron-electron interaction term $\mathcal{R}_{ee}$ in the exponent. Therefore it may be natural to use the Einstein model for a Wigner crystal and set all frequencies equal to a characteristic value: $\omega_{\mathbf{k}j}=\omega_p$. The plasma frequency for a 2D crystal is $\omega_p=(2\pi e^2 n^{3/2}/m)^{1/2}$, where n is the electron density.

In the Einstein approximation the Hamiltonian H_v of in-plane vibrations can be written as:

$$H_v=\frac{1}{2}\sum_n\left[m^{-1}\mathbf{p}_n^2+m\omega_p^2\mathbf{u}_n^2\right] \tag{4.32}$$

and the Hamiltonian coupling between out-of-plane and in-plane motions due to the

presence of magnetic field:

$$H_B = \frac{1}{2}m\omega_c^2 z^2 - \omega_c z[\hat{\mathbf{B}} \times \mathbf{p}], \tag{4.33}$$

where $\mathbf{p} \equiv \mathbf{p}_0$ is momentum of the tunneling electron. As one can see by examining Eqs. (4.32), (4.33), the motion of electrons in the crystal becomes uncoupled. The tunneling electron now moves in a static potential created by other electrons in the crystal. Its in-plane motion is a harmonic vibration about the equilibrium position with frequency ω_p. The problem is effectively reduced to a single-particle problem, which mimics the many-electron one.

The single-particle character of the solution in the Einstein approximation can be also traced from the equations of motion (4.11). Indeed, $\mathbf{p}_{\mathbf{k}j} \propto \mathbf{e}_{\mathbf{k}j}(\mathbf{e}_{\mathbf{k}j}[\hat{\mathbf{B}} \times \hat{z}])$, where factors independent of $\mathbf{k}j$ have been omitted. Consequently, $\mathbf{p}_n \propto \delta_{n0}[\hat{\mathbf{B}} \times \hat{z}]$, which shows that only the tunneling electron is moving in the plane.

If we choose $\mathbf{B}$ along the y axis, then the problem becomes effectively two-dimensional, with the Hamiltonian

$$H = \frac{(p_x + m\omega_p z)^2}{2m} + \frac{1}{2}m\omega_p^2 x^2 + \frac{p_z^2}{2m} + U(z). \tag{4.34}$$

The Coulomb interaction between electrons in the layer not only provides the in-plane confinement for the tunneling electron, which as discussed in the Introduction, is so important for tunneling transverse to $\mathbf{B}$, but also lowers the tunneling barrier $U(z)$. For $nL^2 \ll 1$, the change in potential energy for the tunneling electron to move a distance z out-of-plane is given by:

$$U_C(z) = \sum_n{}' \frac{e^2}{\sqrt{z^2 + \mathbf{r}_n^2}} - \sum_n{}' \frac{e^2}{r_n} \approx -z^2 \sum_n{}' \frac{e^2}{r_n^3} \tag{4.35}$$

Using the sum rule $\sum_{\mathbf{k}j} m\omega_{\mathbf{k}j}^2 = 2N\sum_{ns}{}' \Lambda_{ss}^n = 2N\sum_n{}' e^2/2r_n^3$, where the Λ_{ss}^n are diagonal elements of the dynamical matrix of the Wigner crystal. Therefore the "correlation-hole" potential [72, 34] may be written as

$$U_C(z) = -m\bar{\omega}^2 z^2 \tag{4.36}$$

where the mean square frequency $\bar{\omega}$ for a triangular lattice [73] is approximately:

$$\bar{\omega} = \left[\sum_{\mathbf{k}j} \omega_{\mathbf{k}j}^2/2N\right]^{1/2} \approx \left(4.45e^2 n^{3/2}/m\right)^{1/2} \tag{4.37}$$

We now illustrate the role of electron correlations on the tunneling rate for two model potentials. A triangular tunneling potential was chosen to represent a class of problems where the tunneling length varies with intrawell energy (we will refer to such potentials as smooth). Tunneling through a rectangular barrier represents the opposite case where the tunneling length L is geometrically defined and does not change with energy.

4.4.2 Triangular barrier

In many tunneling experiments, the escape is measured for a finite applied voltage. For electrons above helium surface and in certain types of semiconductor heterostructures, the potential $U(z)$ in the barrier region ($z \geq 0$) is then determined by the electric field which pulls electrons away from the intrawell states. Although the correlation-hole potential $U_c(z)$ (4.36) has strong effect on the tunneling rate, its role is similar whether or not the magnetic field is applied. Therefore, to illustrate purely the role of in-plane confinement on the rate of of tunneling transverse to **B** we do

not take $U_C(z)$ into account. The effect of the correlation-hole potential $U_C(z)$, as well as other corrections important for small z [cf. Eq. (6.4) below], will be studied in detail in Chapter 6, where the quantitative comparison with experimental data is made. Counting the energy from the ground intrawell state, so that $E_g = 0$, we have:

$$U(z) = \frac{\gamma^2}{2m}\left(1 - \frac{z}{L}\right) \quad (z \geq 0). \tag{4.38}$$

Here, $\gamma \equiv \gamma_1$ is the inverse localization length of the ground-state wave function $\psi_g \equiv \psi_1$ near the well, $\partial \ln \psi_1/\partial z = -\gamma$ for $z = 0$, cf. the discussion before Eq. (4.16); L is the tunneling length in the ground state for $B = 0$. We assume that $\gamma L \gg 1$.

In order to calculate the ground-state tunneling exponent, it is convenient to solve directly the equations of motion (4.11) with the boundary conditions (4.16), (4.18), (4.12), and (4.21). For a triangular potential, these equations are linear. This allows us to obtain for the tunneling exponent a simple expression

$$\begin{aligned}\tilde{\mathcal{R}} = \; & -\nu_p^2\tau_{\rm rd}^3 + 3\nu_p\tau_{\rm rd}(1-\tau_{\rm rd})\coth[\omega_p\beta/2 - \nu_p\tau_{\rm rd}] + 3 \\ & +3\tau_{\rm rd}(\nu^2 - 1), \quad R_g = 2\gamma L\tilde{\mathcal{R}}/3\nu^2.\end{aligned} \tag{4.39}$$

Here, $\nu_p = \omega_p\tau_0$ and $\nu_c = \omega_c\tau_0$ are the dimensionless in-plane and cyclotron frequencies scaled by the tunneling duration τ_0 for $B = 0$, and $\nu^2 = \nu_p^2 + \nu_c^2$.

The quantity $\tau_{\rm rd} = \tau_f/\tau_0$ in Eq. (4.39) is the reduced tunneling duration. It is given by the equation

$$\left[(1-\tau_{\rm rd})\nu_p\nu^2\coth[\omega_p\beta/2 - \nu_p\tau_{\rm rd}] - \nu_c^2\right]\tanh\nu\tau_{\rm rd} = \nu[\nu_p^2\tau_{\rm rd} - \nu^2] \tag{4.40}$$

The tunneling exponent in the limit $T \to 0$ can also be obtained by solving the equations of motion (4.11) in the (x, z) representation, according to the method of

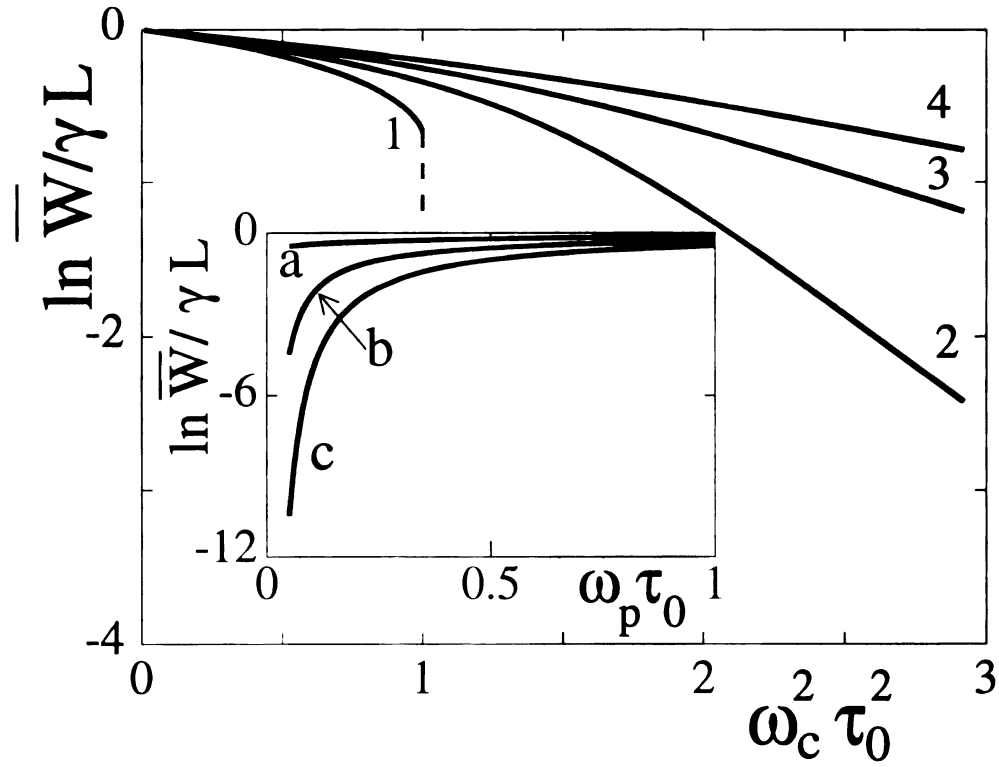

Figure 4.2: The dependence of the tunneling rate at zero temperature on magnetic field, $\bar{W} = W(B)/W(0)$. The curves 1 to 4 refer to $\omega_p\tau_0 = 0, 0.2, 0.4, 0.6$. Magnetic field eliminates single-electron tunneling for $\omega_c\tau_0 \geq 1$ (cf. curve 1). Inset: tunneling exponent vs in-plane frequency ω_p for $\omega_c^2\tau_0^2 = 1.0, 2.0, 3.0$ (curves a,b,c).

Chapter 3. Because of the symmetry $x \to -x$ of the potential on the tunneling trajectory with imaginary time $t = -i\tau$, variables p_x and z are real, meanwhile x and p_z are imaginary. The tunneling exponent is given by

$$\tilde{\mathcal{R}} = -\nu_p^2\tau_{\rm rd}^3 - 3\nu_p(1-\tau_{\rm rd})^2 + 3(1+\nu_p)(1-\tau_{\rm rd}) + 3\nu^2\tau_{\rm rd}, \qquad (4.41)$$

$$\left[\nu^2\nu_p(1-\tau_{\rm rd}) - \nu_c^2\right]\tanh\nu\tau_{\rm rd} = \nu(\nu_p^2\tau_{\rm rd} - \nu^2) \qquad (4.42)$$

Note that expressions (4.41,4.42) coincide with (4.39,4.40) for $T = 0$.

The role of the many-electron effects is particularly important in the limit $T \to 0$. From (4.41), (4.42), we have that without the magnetic field $\tau_{\rm rd} = 1$ and $R = 4/3$ (the "duration" of underbarrier motion in imaginary time is τ_0). In the single-electron

approximation ($\omega_p = 0$) the tunneling duration τ_f and the tunneling exponent R_g diverge for $\omega_c \to \tau_0^{-1}$ [34], as shown in Fig. 4.2 on curve 1. This happens because the effective single-electron potential $U(z) + (1/2)m\omega_c^2 z^2$, which takes into account the parabolic magnetic barrier, does not have classically allowed extended states with energy $E_g = 0$ behind the barrier. Formally, $\tau \to \infty$ for $\nu_p = 0, \nu_c \to 1^-$)

Even comparatively weak in-plane confinement eliminates this effect. The reduction of the tunneling suppression is significant already for small $\omega_p\tau_0$, and increases fast with increasing $\omega_p\tau_0$. For $\omega_c\tau_0 > 1$ and $T = 0$, the tunneling exponent is a steep function of the exchange rate ω_p in the limit of slow exchange, $\omega_p\tau_0 \ll 1$. In the opposite limit of the fast momentum exchange, $\omega_p \gg \tau_0^{-1}$, from Eqs. (4.39), (4.40) we obtain that $R_g = \frac{4}{3}\gamma L\sqrt{1 + \omega_c^2\omega_p^{-2}}$. Therefore, with increasing ω_p beyond ω_c, the exponent of the tunneling rate approaches the zero-magnetic-field value of $4\gamma L/3$. The tunneling time becomes $\tau_{\rm rd} \approx 1$ [i.e., $\tau_f \approx \tau_0$]. On the other hand, for large and but finite ω_p, the slope of the logarithm of the tunneling rate as a function of magnetic field provides a direct measurement of the characteristic frequencies of in-plane electron vibrations. The tunneling exponent for zero temperature as a function of ω_p, ω_c is shown in Fig. 4.2. The overall dependence of the tunneling exponent on ω_p is shown in the inset.

For a given magnetic field, the dependence of the tunneling exponent R_g on the frequency ω_p becomes much less steep with increasing temperature, as seen from Fig. 4.3. This happens because at finite temperatures the tunneling electron may transfer its in-plane Hall momentum not only in a recoil-free way to electron system as whole ("zero-phonon" process), but also compensate it with a thermal in-plane

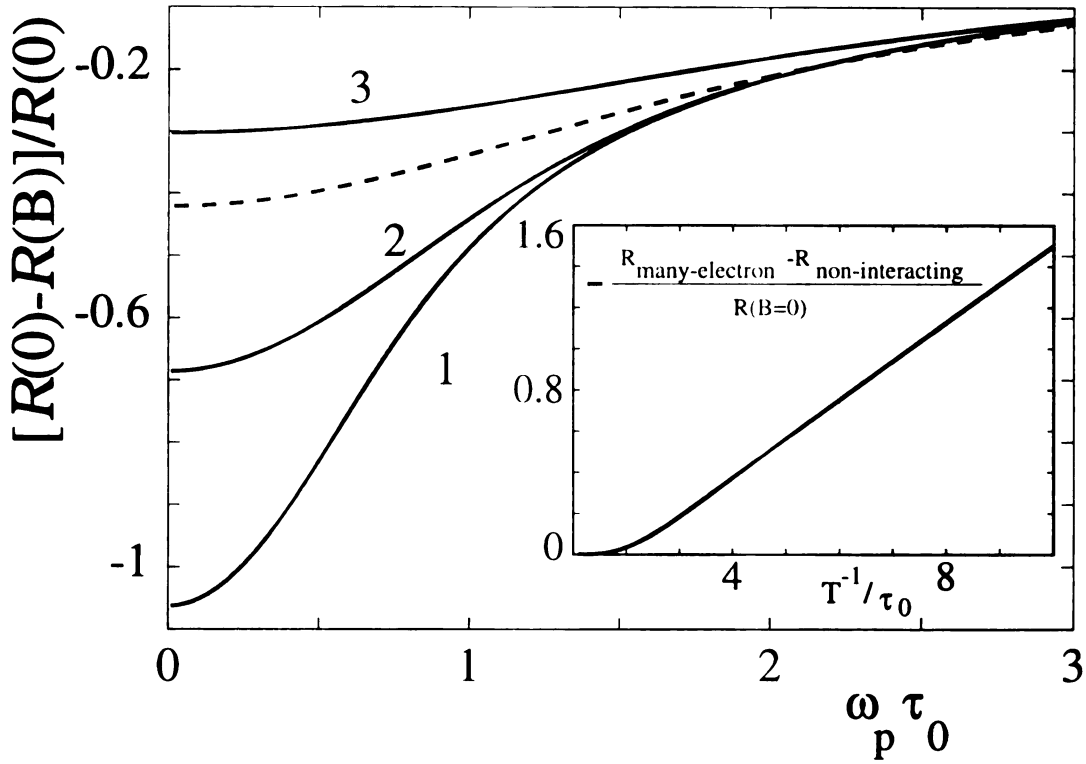

Figure 4.3: The tunneling exponent in the ground state for a triangular potential barrier (4.38) as a function of the phonon frequency ω_p in the Einstein model of the Wigner crystal for $\omega_c\tau_0 = 2$. The time $\tau_0 = mL/\gamma$ is the duration of tunneling for $B = 0$ and $T = 0$. The curves 1 to 3 refer to reciprocal temperatures $\beta/\tau_0 = 7, 5, 3$. The dashed line is the result of the direct variational method, with one variational parameter τ_f. The relative importance of many-electron effects is demonstrated in the inset. Here, the difference between the full many-electron tunneling exponent and that obtained in the single-electron approximation is plotted as a function of inverse temperature. The many-electron tunneling exponent was calculated for $\omega_p\tau_0 = 3.0$.

momentum. The recoil-free process depends very strongly on in-plane frequencies, because they determine how much of the Hall momentum will actually be compensated. Compensation by thermal momentum is present even in a non-interacting limit, does not have strong frequency dependence. This is again very similar to what happens in a Mössbauer effect, where the zero-phonon line disappears with increasing temperature. For large $\omega_p\tau_0$, $\omega_p\beta$, the curves for different temperatures merge

together and approach the $B = 0$ asymptote.

The value of R_g can be calculated independently from the functional $\mathcal{R}_n$ (4.23) using the direct variational method. Even a simple approximation where $z(\tau)$ is quadratic in τ, with the only variational parameter being the tunneling duration τ_f, gives a reasonably good result, which is shown in Fig. 4.3 by a dashed line for $\beta = 3\tau_0$. Such calculation gives a good approximation for higher temperatures, and also for lower temperatures but not too small $\omega_p\tau_0$. For low temperatures and small $\omega_p\tau_0$ the trajectory $z(\tau)$ is strongly nonparabolic, and more then one parameter is required in the variational calculation.

The above results provide an explanation of the magnetic field dependence of the tunneling exponent for electrons on helium, which was observed to be *much weaker* [34] than it would be expected from the single-electron theory. Detailed comparison with the data [34] will be discussed below in Chapter 6.

4.4.3 Square barrier

In many physically interesting systems, the tunneling barrier $U(z)$ is nearly rectangular. This is often the case for semiconductor heterostructures, where the barrier is formed by the insulating layer. If we count U off from the intrawell energy level E_g and set the boundaries at $z = 0$ and $z = L$, the barrier has the form

$$U(z) = \gamma^2/2m - m\bar{\omega}^2 z^2, \quad 0 < z < L \tag{4.43}$$

Here, $1/\gamma$ is the decay length under the barrier, cf. Eq. (4.16), and the mean square frequency $\bar{\omega}$ is given by (4.37).

We assume that, behind the barrier ($z > L$), an electron can move semiclassically with all energies. The picture of tunneling depends on the parameter $\Omega = \sqrt{2}\bar{\omega}\tau_0$ where $\tau_0 = mL/\gamma$ is the imaginary "time of flight" under the barrier for $\bar{\omega} = 0$. For $\Omega < 1$ the particle comes out from the barrier at the point $z = L$ where $U(z)$ is discontinuous, cf. Fig. 2b. Then the decaying underbarrier wave function has to be matched to an appropriate propagating wave behind the barrier at $z = L$. In contrast to the case of a smooth barrier, because the potential $U(z)$ is discontinuous at $z = L$, the z-component of the momentum should not be the same on the opposite sides of the boundary. However, the in-plane "momentum" components $\mathbf{u}_{\mathbf{k}j}$, which are imaginary under the barrier, still have to be continuous. Respectively, the boundary conditions (4.12) for the tunneling trajectory should be changed to

$$z(\tau_f) = L, \quad \mathbf{u}_{\mathbf{k}j}(\tau_f) = \mathbf{0}. \tag{4.44}$$

In fact, the condition $\mathbf{u}_{\mathbf{k}j} = \mathbf{0}$ gives the in-plane values of $\mathbf{p}_{\mathbf{k}j}$ for which the wave function is maximal for $z = L$.

With the boundary conditions (4.44), elimination of phonon variables from the Euclidean action S_E in the tunneling exponent is similar to what was done for a smooth barrier. The resulting expression for the retarded functional $\mathcal{R}_n[z]$ coincides with Eq. (4.23), provided $z(\tau_f + x)$ is defined as $z(\tau_f - x)$, for $0 \leq x \leq \tau_f$. In the Einstein approximation the boundary conditions (4.44) become:

$$z(\tau_f) = L, \; x(\tau_f) = 0. \tag{4.45}$$

For higher electron densities where $\Omega > 1$, potential $U(z)$ is no longer discontinu-

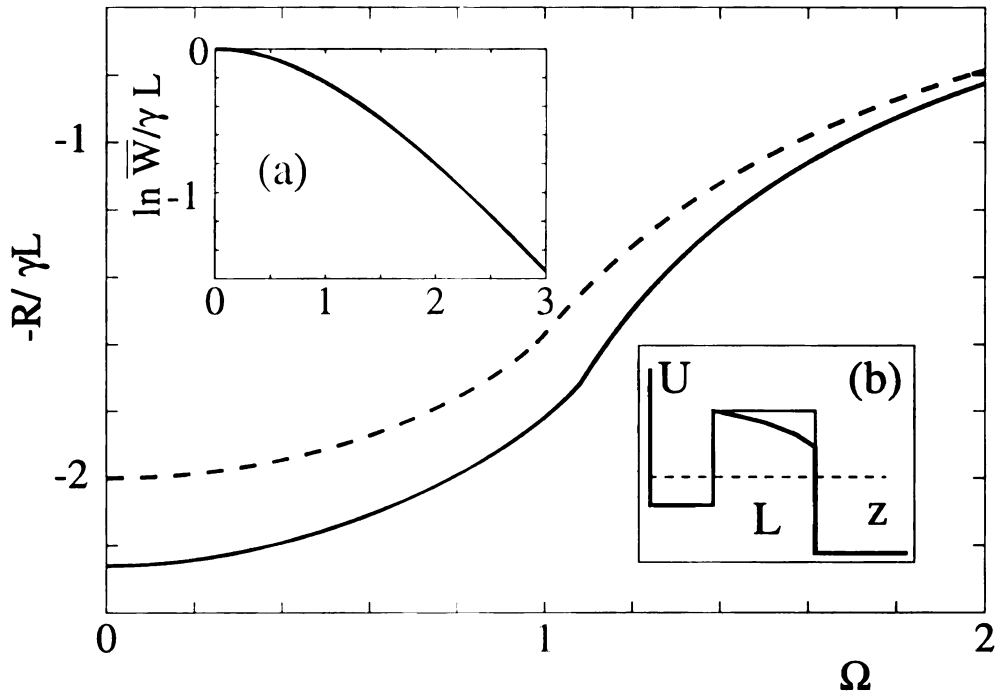

Figure 4.4: Exponent of the tunneling rate $-R$ from a 2D WC in a semiconductor heterostructure as a function of scaled electron density $\Omega = \sqrt{2}\bar{\omega}\tau_0$ ($\tau_0 = mL/\gamma$). Electron correlations increase the tunneling exponent both for $B = 0$ (dashed line) and in the presence of magnetic filed (solid line refers to $\omega_c\tau_0 = 1.0$). With increasing Ω the tunneling rate in the magnetic field approaches the zero-field line. Inset (a): relative tunneling rate $\bar{W} = W(B)/W(0)$ vs magnetic field for $\bar{\omega}\tau_0 = 0.5$. Inset (b): electron potential with (bold line) and without (thin line) the reduction of the tunneling barrier due to the effect of electron correlations.

ous and the usual boundary conditions apply

$$p_z(\tau_f) = 0, \; x(\tau_f) = 0. \tag{4.46}$$

The tunneling exponent is calculated along the tunneling trajectory satisfying that boundary condition out of two possible (4.45) and (4.46) which gives the smallest value. In the absence of a magnetic field, the transition from one boundary regime to another occurs for $\Omega = 1$. In the presence of a magnetic field, the transition shifts towards larger Ω. The detailed calculation is rather tedious, and is provided in

Appendix C. The result for the tunneling exponent in the Einstein approximation is plotted in Fig.4.4.

For $B = 0$ the tunneling exponent is $2S_E = \gamma L[\Omega^{-1} \arcsin\Omega + (1 - \Omega^2)^{1/2}]$ [$2S_E = \pi\gamma L/2\Omega$, for $\Omega > 1$]. Magnetic field causes S_E to increase and the tunneling rate to decrease, respectively. For weak fields, the increment of S_E is quadratic in B. Transfer of the Hall momentum of the tunneling electron to the WC strongly reduces suppression of tunneling by a magnetic field. Fig. 4.4 shows also how S_E is decreased by electron correlations even for $B = 0$, in the case of a broad barrier.

4.5 Summary

In the presence of a magnetic field parallel to a 2DES, the tunneling rate becomes exponentially sensitive to the presence of electron correlations in the system. These electron correlations are not imposed by the magnetic field, contrary to the case where magnetic field is applied perpendicular to the layer. Because the tunneling rate is exponentially small, one can consider tunneling of different electrons independently, and therefore single out the tunneling electron. Electron correlations affect the out-of-plane tunneling rate through an interelectron momentum exchange from the tunneling electron to the electron system as a whole. The mechanism is therefore similar to a Mössbauer effect. The tunneling electron usually transfers only part of its in-plane momentum to the electron system in a "recoil-free" way. The interrelation between the characteristic momentum exchange rate and the reciprocal duration of tunneling in imaginary time $1/\tau_f$ determines what portion of the in-plane momentum will be

transfered, so that the dynamics of electron motion under the barrier becomes very important.

With increasing temperature, the dependence of the tunneling rate on in-plane vibrational frequencies becomes less steep. This happens because at such temperatures the in-plane Hall momentum can be compensated by a thermal momentum, and not only through a recoil-free transfer to a whole electron system. This is again analogous to what happens in a Mössbauer effect, where the zero-phonon line disappears with increasing temperature. Therefore, tunneling experiments could probe the phonon spectrum of the 2D system, if they are done at sufficiently low temperatures. At higher temperatures, the tunneling rate can be described in the single-electron approximation. The dependence of the tunneling rate on temperature and magnetic field, however, is expected to be a very non-monotonic function and have interesting features, as discussed in the next chapter.

Correlated 2D electron systems in semiconductor heterostructures have been investigated by tunneling mostly for the magnetic field **B** perpendicular or nearly perpendicular to the electron layer, cf. [55]. The data on tunneling in a field parallel to the layer refer to high density 2DESs [21], where correlation effects are small.

It is expected that the effect of a parallel magnetic field will be most pronounced in systems with shallow and broad barriers $U(z)$. For example, in a GaAlAs structure with a square barrier of width $L = 0.1\,\mu$m and height $\gamma^2/2m = 0.02$ eV, for the electron density $n = 1.5 \times 10^{10}$ cm^{-2} and $B = 1.2$ T we have $\omega_p\tau_0 \approx 0.6$ and $\omega_c\tau_0 \approx 1$ ($\tau_0 = mL/\gamma$ is the tunneling duration for $n = B = 0$). The results of Sec. 4.4.3 for square barriers, where we have taken into account the correlation-hole potential

(4.36), show that the interelectron momentum exchange should significantly modify the tunneling rate in this parameter range, provided the 2DES is correlated [56]. One can therefore expect that tunneling experiments on low-density 2DESs in parallel fields will reveal electron correlations not imposed by the magnetic field, give insight into electron dynamics, and possibly even reveal a transition from an electron fluid to a pinned Wigner crystal with decreasing n.

Chapter 5

Magnetic-field-enhanced tunneling

This chapter is devoted to the theory of the enhancement of the tunneling rate by a magnetic field parallel to the electron layer. Its applications can be very useful, because it allows to increase the tunneling rate without changing the parameters of a tunneling barrier. A magnetic field parallel to the electron layer couples out-of-plane and in-plane degrees of freedom. For $T = 0$, this leads to the energy transfer from out-of-plane tunneling motion to the in-plane vibrational motion, which, in turn, results in the suppression of the tunneling rate by magnetic field. For finite temperatures, the direction of the energy transfer may be reversed, so that the energy of thermal in-plane motion can be used to assist the tunneling. Because coupling is proportional to the magnetic field, this is a qualitative reason why the magnetic field can enhance the tunneling rate. On the formal level, the B-enhanced tunneling is a consequence of the increase, with increasing temperature, of the absolute value of the term $\mathcal{R}_{ee}$ (4.24) in the tunneling action. Since this term gives a negative contribution to the tunneling exponent R, the whole B-dependent term in $\mathcal{R}$ becomes negative starting

with a certain crossover temperature T_c and then the tunneling rate increases with B.

The increase of the tunneling rate with magnetic field does not occur in all systems. In systems where it does occur, it happens in the range that is limited in both T and B. The range boundaries are not universal and depend on the potential $U(z)$ and the phonon spectrum. The main processes that limit this range are switching to tunneling from the next intrawell level or switching to the escape via thermal activation. The enhancement may start from $B = 0$ or have a finite threshold in B. The later variant occurs when escape for $B = 0$ occurs through tunneling from the next excited state or by over barrier activation. With increasing of magnetic field there occurs switching from one of these processes, which determined the escape rate for $B = 0$, to tunneling from the ground intrawell state, where the tunneling rate increases with B. However, very strong fields suppress rather than enhance escape.

In Sec. 5.1 the physical limits on the lower and upper temperature bounds for B-enhanced tunneling are discussed. The various switching processes that can take place with increasing of T or B are different in cases where the potential barrier is smooth (tunneling length is determined from $E = U(\mathbf{r})$) and discontinuous (the tunneling length is geometrically defined). Explicit results are obtained in Sec. 5.2 using the Einstein model of a Wigner crystal, in which all phonons are assumed to have the same frequency. As an example of a smooth tunneling barrier we take a triangular barrier, which is relevant for tunneling in the presence of applied electric field. Square barrier models the potential formed by the insulating layer in semiconductor heterostructures.

5.1 General properties of the transition

5.1.1 The temperature of crossover for small magnetic fields

The lower temperature bound of the enhancement domain is the crossover temperature T_c. It can be determined from the small-B expansion of the tunneling exponent for the ground state [$n = g$ in Eq. (4.22)],

$$R_g(\omega_c) \approx R_g(0) + A_g(T)\omega_c^2, \quad \omega_c\tau_0 \ll 1 \tag{5.1}$$

where τ_0 is the tunneling time in the ground state for $B = 0$. The role of the ground state is special in that the barrier width is bigger for the ground state energy than for the energies of the excited states. Therefore the effect of the magnetic field, which accumulates under the barrier, is most pronounced in the ground state.

The value of A_g is given by the terms $\propto \omega_c^2$ in the action R_g (4.23) calculated along the tunneling trajectory $z_0(\tau)$ for $B = 0$. From the analysis in subsection 4.3.1, it follows that $A_g > 0$ for $T \to 0$. The crossover temperature is given by

$$A_g(T_c) = 0. \tag{5.2}$$

For $T > T_c$ the tunneling exponent R_g decreases and the tunneling rate increases with B, for small B.

In the limit of low phonon frequencies, $\omega_{\mathbf{k}j} \ll 1/\tau_0, T_c$, from Eqs. (4.23), (4.31) it follows that $\beta_c \equiv 1/T_c = 2\tau_0\overline{z_0}^2/\overline{z_0^2}$, where $\overline{z_0}$ is the average coordinate $\bar{z}$ (4.31) for the $B = 0$ trajectory with energy E_g, and $\overline{z_0^2}$ is the mean square value of z on the same trajectory,

$$\overline{z_0^2} = \tau_0^{-1}\int_0^{\tau_0} d\tau z_0^2(\tau) \quad (E = E_g).$$

Clearly, in this case $\beta_c < 2\tau_0$. It follows from Eq. (4.24) that $2\tau_0$ is also the limiting value of β_c in the opposite case of high phonon frequencies, $\omega_{\mathbf{k}j} \gg 1/\tau_0$. On the whole, we have the bounds on temperature for the tunneling enhancement in the ground intrawell state

$$2\tau_0 \frac{\overline{z_0}^2}{\overline{z_0^2}} < \beta_c < 2\tau_0. \tag{5.3}$$

As noted above, $\overline{z_0}$ is nonzero, and generally $\overline{z_0}^2/\overline{z_0^2} \sim 1$.

It follows from the above arguments that the value of the crossover temperature $T_c = 1/\beta_c$ decreases with increasing phonon frequencies, that is the crossover is determined by high-frequency phonons which, in the case of 2D electron systems, have large wave numbers and are determined by the short-range order. Note that there is no threshold in B for tunneling enhancement for $T > T_c$ from the range (5.3), provided the system is tunneling from the ground state.

5.1.2 Upper temperature limit for enhancement for small magnetic fields

A threshold-less tunneling enhancement starting from $B = 0$ occurs for temperatures bounded from above by the condition that the system tunnels from the ground state rather than from excited intrawell states or via thermal activation over the barrier. In principle, even for excited states, the tunneling rate may increase with B, but this does not happen for simple model potentials investigated below.

If the tunneling is enhanced only in the ground state, the upper temperature bound is often the temperature $T_{1\to 2}$ where the probability of tunneling from the first

excited state, weighted with the occupation factor, exceeds that from the ground state, for $B = 0$. It can be estimated for smooth tunneling barriers, where the tunneling duration $\tau_0(E)$ for $B = 0$ often decreases with the increasing energy E. In fact, the function $\tau_0(E)$ may be nonmonotonic even for simple potentials $U(z)$; a detailed analysis of this function lies outside the scope of this work, but generalization of the results to appropriate cases is straightforward. From (4.23), for decreasing $\tau_0(E)$, switching from tunneling from the ground state ($n = 1$) to that from the first excited state ($n = 2$) occurs for the reciprocal temperature

$$\beta_{1\to 2} = 2\frac{\int_{E_1}^{E_2} \tau_0(E)dE}{E_2 - E_1} \quad (E_1 \equiv E_g).$$

This value lies between $2\tau_0(E_2)$ and $2\tau_0(E_1)$. Depending on the tunneling potential, $\beta_{1\to 2}$ can be smaller or larger than β_c (5.3). If a magnetic field does not increase the rate of tunneling from the state $n = 2$, threshold-less tunneling enhancement occurs for $T_c < T < T_{1\to 2}$.

Alternatively, for $B = 0$ the system may switch to activated escape over the barrier with increasing temperature for $T = T_a < T_c$. The threshold-less tunneling enhancement by the magnetic field does not occur in this case. However, both for $T_c > T_a$ and $T_c > T_{1\to 2}$ there may still occur a B-induced enhancement of the escape rate starting with some nonzero B. We note that in the above arguments, it was assumed that thermalization [1] inside the well occurs before the electron escapes.

[1]The Boltzmann distribution over in-plane energies is established very rapidly, on times of the order of ω_p^{-1}. In Chapters 4, 5 we assume that the Boltzmann distribution over out-of-plane intrawell states also occurs much faster than the process of the tunneling escape. It is not always true, since the thermalization proceeds through scattering on defects inside the quantum well (for a 2DES in heterostructures), or on ripplons (for a 2DES on a surface of liquid helium). Extension of the results to account for slow intrawell thermalization is straightforward, and will be done for electrons on helium in order to compare the theory with the experimental data [cf. Eq. 6.9].

5.1.3 Field-induced switching between tunneling from the ground state, excited states, and over-barrier activation

Even in the temperature range $T > T_{1\to 2}$ a sufficiently strong magnetic field can increase the tunneling rate, provided $T > T_c$. This happens if the tunneling exponent for the ground state $R_g(\omega_c) \equiv R_{n=1}(\omega_c)$ exceeds that in the first excited state $R_{n=2}(\omega_c)$ and its zero-field value $R_{n=2}(0)$. In a certain temperature range where $T > T_{1\to 2}$, the tunneling rate for $B = 0$ is determined by tunneling from the excited state $n = 2$. This rate decreases with increasing B (the tunneling exponent $R_{n=2}$ increases with B). For some B the exponents $R_{n=2}(\omega_c)$ and $R_{n=1}(\omega_c)$ become equal to each other. For larger B the system tunnels from the ground state, and the tunneling rate increases with B.

Similarly, since the activation rate is only weakly affected by B, in a certain temperature range where escape already occurs via activation for $B = 0$, starting with some B it may again go through tunneling from the ground state. This happens if the tunneling rate for the ground state becomes bigger than the activation rate and only happens in a limited range of B, see Sec. 5.2.1. For a special model the switching is illustrated in Fig. 5.2 below.

5.2 Tunneling enhancement for the Einstein model of a Wigner crystal

In what follows we will illustrate the general results and apply them to specific 2D systems using the Einstein approximation for the phonon spectrum, $\omega_{\mathbf{k}j} = \omega_p$. This is motivated by the fact that tunneling is determined primarily by short-wavelength vibrations, which have a comparatively weak dispersion. The magnetic-field-enhanced tunneling can be observed in experiments with smooth tunneling potentials. As before, we take a triangular barrier as a representative for such potentials. The case of tunneling through potentials where the tunneling length that does not change with intrawell energy is qualitatively different: tunneling enhancement is not expected to occur there [again, assuming that the intrawell relaxation is fast enough, with an approximate rule that the cleaner the sample is, the slower is the intrawell relaxation]. However, switching from tunneling to thermal activation can occur with increasing of magnetic field for such tunneling barriers.

5.2.1 Smooth potentials: field-induced tunneling enhancement and switching from activation to tunneling

Below we use the explicit expression for the tunneling exponent obtained earlier (4.39), (4.40) to analyze the effects of tunneling enhancement and magnetic field induced switching to tunneling. In the small-B limit, where $\omega_c \ll \omega_p, \tau_0^{-1}$, the tunneling exponent $R_g(B)$ is seen from Eq. (4.39) to be quadratic in B. The coefficient A_g in

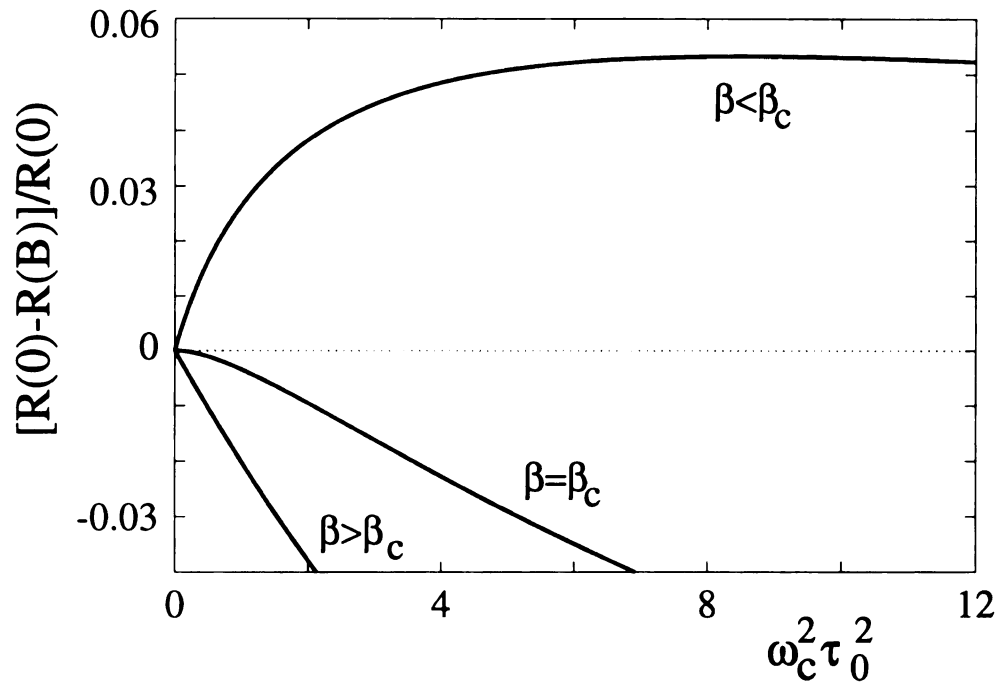

Figure 5.1: The dependence of the tunneling exponent $R(B) \equiv R_g(B)$ on the magnetic field (4.39) for $\omega_p\tau_0 = 1/3$ near the crossover temperature $\beta_c \approx 1.67\tau_0$ (5.4). The curves 1 to 3 correspond to $(\beta - \beta_c)/\tau_0 = 0.2, 0, -0.3$

Eq. (5.1) can be easily calculated. From the condition $A_g = 0$ we obtain the value of the reciprocal temperature β_c which corresponds to the crossover from decrease to increase of the tunneling rate due to a magnetic field,

$$\beta_c = 2\tau_0 + \frac{2}{\omega_p} \tanh^{-1}\left[\frac{\nu_p[3\nu_p - (3+\nu_p^2)\tanh\nu_p]}{\nu_p^3 - 3\nu_p + 3\tanh\nu_p}\right]. \tag{5.4}$$

In agreement with (5.3), β_c monotonically increases with ω_p from $5\tau_0/3$ at $\omega_p = 0$ to $2\tau_0$ for $\omega_p \to \infty$.

The dependence of the tunneling exponent (4.39) on the magnetic field for different temperatures is shown in Fig. 5.1. Above the crossover temperature ($\beta < \beta_c$), $R(B)$ *decreases* with B. Then $R(0) - R(B)$, and the tunneling probability with it, *increase* with the increasing field, for small B. The slope $dR/BdB \propto \beta - \beta_c$ for $B \to 0$.

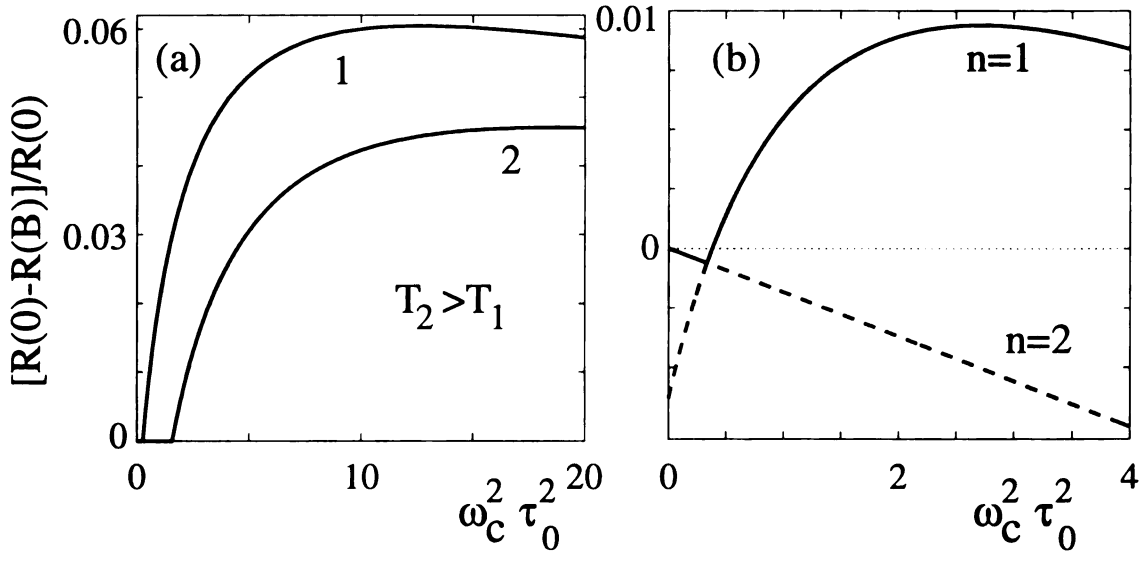

Figure 5.2: Magnetic field induced switching from activation (a) and from tunneling from the excited state (b) to tunneling from the ground state, for $\omega_p \tau_0 = 1/3$. In (a), there is only one intrawell state in the potential well $U(z)$, and the transition to activation for $B = 0$ occurs for $\beta/\tau_0 = 4/3$. The curves 1, 2 correspond to $(\beta - \beta_c)/\tau_0 = -0.35, -0.4$. In (b), the position E_2 of the excited level ($n = 2$) is chosen at $0.2\gamma^2/2m$ below the barrier top ($E_1 = 0$). The temperature is chosen at $(\beta - \beta_c)/\tau_0 = -0.16$, so that for $B = 0$ the system tunnels from the excited state. The observable (smaller) tunneling exponents for a given B are shown with bold lines, whereas dashed lines show the bigger exponents, which correspond to smaller tunneling rates.

However, for strong fields the tunneling rate decreases with the increasing B, because the Hall momentum can no longer be compensated by thermal fluctuations.

It is clear from the data in Fig. 5.1 that, for the barrier chosen, the magnetic field induced increase of the tunneling exponent R is numerically small. However, for typical $R \gtrsim 50$ it can still be noticeable, although strictly speaking it is on the border of applicability of the approximation in which only the exponent is taken into account.

The expression (4.39) gives the tunneling exponent only for low enough temper-

atures where the system escapes from the ground state. For higher temperatures, one should take into account the possibility of escape from excited states and via an activated transition over a potential barrier. The positions of the excited levels depend not only on the barrier shape, but also on the shape of the potential $U(z)$ inside the well. The analysis for a realistic system, electrons on the surface of liquid helium, is done in the next section. Here, in order to illustrate different options, we discuss two cases: a narrow well, in which case the ground state is essentially the only intrawell state, and a well with a comparatively shallow excited state for which still the intrawell relaxation rate is higher than the tunneling rate, so that its occupation is given by the Boltzmann factor.

We start with the discussion of the case of a single-state potential well. For $B = 0$ and a triangular barrier $U(z)$ (4.38), switching from tunneling to activation occurs here for the temperature $T_a \equiv 1/\beta_a = (4\tau_0/3)^{-1}$. This temperature is higher than the crossover temperature $1/\beta_c$ (5.4), and therefore there is a region where the enhancement of tunneling by a magnetic field can be observed, as discussed above (cf. Fig. 5.1). However, even though for $T > T_a$ the $B = 0$-escape occurs via over-barrier transitions, the increase of the tunneling rate with the increasing B can make tunneling more probable for sufficiently strong B. If the activation rate is independent of B, the overall dependence of the exponent of the escape rate $R(B) = \min_n[R_n(B) + \beta(E_n - E_1)] \propto \ln W(B)$ on B is shown in Fig. 5.2a. In this case, $R(0) = \gamma^2/2mT$ is the barrier height over temperature. Switching to tunneling and to the increase of the escape rate with B occurs where the tunneling exponent $R_g(B)$ as given by Eq. (4.39) becomes less than $R(0)$.

A similar switching occurs in the temperature range where tunneling from the first excited level is more probable than from the ground state, for $B = 0$. Since with increasing B the tunneling rate in the ground state increases, the system switches to tunneling from the ground state starting with a certain value of B. This is illustrated in Fig. 5.2b.

In narrow-well potentials, a magnetic field may strongly affect the wave functions with energies close to the barrier top. As a result, new bound metastable states may appear in a strong field. The field also shifts the energy levels of the existing states. The rate of interlevel transitions may also change, since the field mixes together the in-plane and out-of-plane motions. The related effects may become important with increasing temperature.

5.2.2 Square barrier: field-induced crossover to thermal activation

Tunneling through a rectangular barrier is special in that respect that the tunneling length L does not decrease with increasing of intrawell energy. As a result, the tunneling time $\tau_0(E) = -dS_0/dE$ for $B = 0$ monotonically increases with energy E, and correspondingly the energy level found from the condition $\beta = 2\tau(E)$ gives not a maximum of the function $-\beta E - 2S_0(E)$, but a minimum. The maximum value, which gives the probability of tunneling with energy E with account taken of the occupation factor, corresponds either to the transition from the ground state or to activation over the barrier.

Consider, for example, the simplest case of a square barrier with boundaries at $z = 0$ and $z = L$, which mimics the tunneling barrier formed by a insulating layer in semiconductor heterostructures.

$$U(z) = \gamma^2/2m, \quad 0 < z < L. \tag{5.5}$$

Here, we count U off from the intrawell energy level E_g; $1/\gamma$ is the decay length under the barrier, cf. Eq. (4.16), and we have neglected the lowering of the barrier due to the electrostatic field from other electrons at their lattice sites, which is a good approximation for $nL^2 \ll 1$.

Switching to activation occurs for the temperature $T_a = \gamma^2/4mS_0(E_g) \equiv \gamma/4mL = (4\tau_0)^{-1}$. It is lower than the temperature T_c of the crossover from B-suppressed to B-enhanced tunneling as given by Eq. (5.3), and therefore we do not expect the crossover to occur in systems with a square barrier.

If the temperature $T < T_a$, escape for $B = 0$ occurs via tunneling, and its probability decreases with the increasing B. Starting with some B, where the tunneling exponent becomes bigger than the activation exponent $\gamma^2/2mT$, it becomes more probable to escape by activated transition than by tunneling. To a good approximation, the escape rate becomes independent of the magnetic field.

The tunneling exponent that describes the escape rate for $T < T_a$ can be obtained directly from the [linear, in this case] equations of motion (3.3) with the boundary conditions (4.16), (4.18), (4.44). It has the form:

$$R = \gamma L \left[\tau_{\rm rd} + \nu_c \kappa(\tau_{\rm rd})\right]. \tag{5.6}$$

where the function $\kappa(\tau_{\rm rd})$ and the reduced tunneling time $\tau_{\rm rd} = \tau_f/\tau_0$ in Eq. 5.6 is

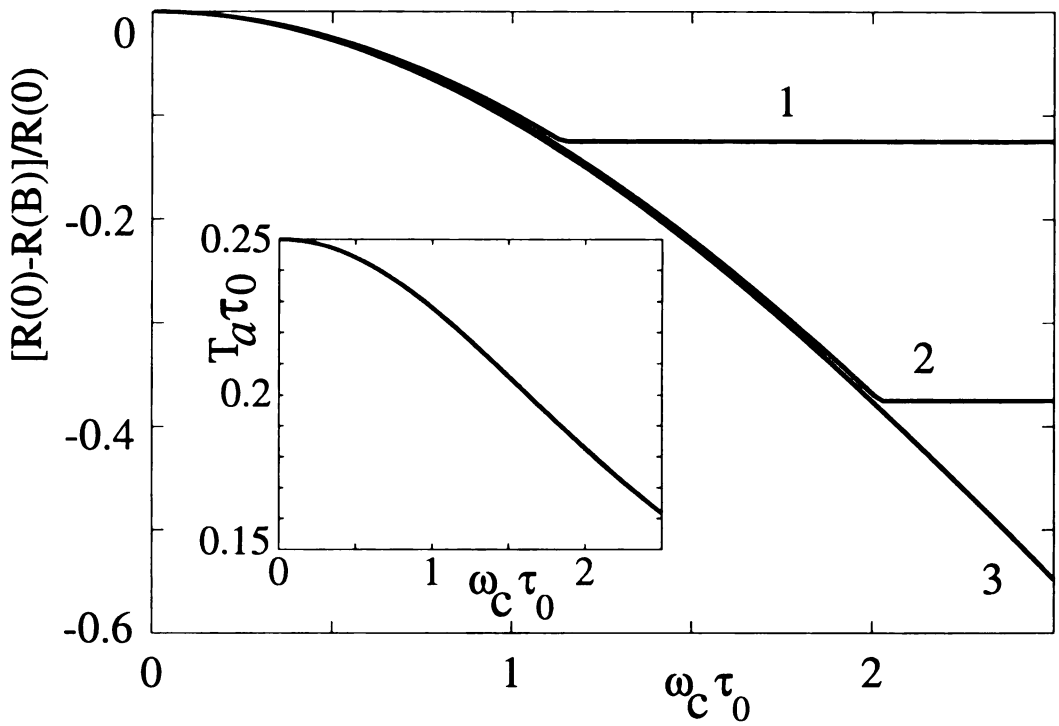

Figure 5.3: The logarithm of the escape rate $R(B)$ compared to its $B = 0$ value $R(0) = 2S_0(E_g) \equiv 2\gamma L$, which is determined by tunneling through the square barrier (5.5). Curves 1-4 correspond to $(\beta - \beta_c)/\tau_0 = 3, 4, 5$, with $\tau_0 = mL/\gamma$, and $\beta_c =$ for chosen $\omega_p = 1/2\tau_0$. As $\omega_c\tau_0$ increases, there occurs a transition from tunneling to thermal activation.

found from the following equations:

$$\begin{aligned}\kappa(\tau_{\rm rd}) &\equiv \frac{\nu_c(\cosh\nu\tau_{\rm rd} - 1)}{\nu_c^2 + \nu_p^2\cosh\nu\tau_{\rm rd} + \nu\nu_p\coth[\omega_p\beta/2 - \nu_p\tau_{\rm rd}]\sinh\nu_p\tau_{\rm rd}} \\ &= \frac{1}{\nu_c\nu_p^2}\frac{\nu_c^2(2 - 2\cosh\nu\tau_{\rm rd} + \nu\tau_{\rm rd}\sinh\nu\tau_{\rm rd}) - \nu^3(\tau_{\rm rd} - 1)\sinh\nu\tau_{\rm rd}}{(1 - \cosh\nu\tau_{\rm rd})(1 - \nu_c^2/\nu_p^2) + \nu\tau_{\rm rd}\sinh\nu\tau_{\rm rd}} \end{aligned} \quad (5.7)$$

Here, as before, the dimensionless in-plane and cyclotron frequencies $\nu_p = \omega_p\tau_0$ and $\nu_c = \omega_c\tau_0$ are scaled by the inverse tunneling duration for $B = 0$, $\tau_0^{-1} = \gamma/mL$, and $\nu^2 = \nu_p^2 + \nu_c^2$.

The B-dependence of the escape rate for different temperatures is illustrated in Fig. 5.3. With increasing of either temperature or magnetic field, the tunneling

exponent (5.6) becomes bigger than the activation exponent $\gamma^2/2mT = \gamma L\beta/2\tau_0$. Then it becomes more probable to escape by activated transition than by tunneling.

The temperature of switching to activation is given by the equation $T_a = \gamma^2/2mR_g$. From (5.6), (5.7), R_g increases with the magnetic field, and therefore the switching temperature T_a decreases with B. However, it follows from the analysis of the above equations that T_a remains lower than $1/(4\tau_0)$.

The effect of saturation of the escape rate with increasing B is not limited to square barriers, of course. For strong enough B and nonzero temperatures, the tunneling rate becomes less than the activation rate, and the system switches to activation; the switching may go in steps with increasing B, via tunneling from excited intrawell states.

5.3 Summary

Coupling between out-of-plane and in-plane degrees of freedom that is realized by magnetic field parallel to the layer leads at low temperatures to the suppression of the tunneling rate, and to the enhancement of it with B at higher temperatures. Because coupling strength is proportional to the magnetic field, one may be able therefore to control the tunneling rate in a broad range, just by changing temperature and magnetic field, without changing parameters of the tunneling barrier.

The overall escape rate as a function of B and T is expected to display a number of other unusual features. These include switching from activated escape to tunneling and vice versa, and switching between tunneling from the ground and excited states.

These switchings have been analyzed for simple but realistic models of the tunneling barrier.

Sufficiently strong magnetic fields will always suppress the tunneling rate. Therefore, the enhancement of tunneling occurs in a limited range of magnetic field. Other competing processes, such as tunneling from higher intra-well states, and over-barrier escape, limit the range of temperatures for B-enhanced tunneling. For a given geometry of the tunneling barrier, this effectively sets the limits on how fast the escape rate can be enhanced. However, in some cases, such as for high mobility samples, low in-plane scattering rate probability results in the suppression the rate of tunneling from higher intra-well levels and the rate of over-barrier escape. This happens because the occupation of higher levels depends on a scattering amplitude into these states and no in-plane momentum from the ground state and large in-plane momentum. In other words, there is no equilibrium distribution of states inside the well[2]. Because the competing escape processes are suppressed, the B-enhanced tunneling occurs for higher temperatures, where the effect is bigger. In particular this happens, for electrons on helium, where the electron mobility is $\sim 10^8$ $\mathrm{Vs}^{-1}\mathrm{cm}^{-2}$. If there were equilibrium distribution inside the well, then the over-barrier activation would be a dominated process even for $T < T_c$, and the enhancement of tunneling would not occur at all. Contrary to this, B-enhanced tunneling is indeed observed.

[2]This can also happen in classical systems, if they are highly underdamped.

Chapter 6

Comparison with experimental data on tunneling from helium surface

In this Chapter tunneling experiments are discussed. The only tunneling experiment known to me, where tunneling occurrs from a strongly correlated 2DES in the presence of magnetic field parallel to the electron layer was done for electrons on helium. Such systems are advantageous from the point of view that several major parameters that control tunneling can be easily varied. In addition, the electron mobility is very high. The tunneling rate, obtained from the model with no adjustable parameters, is in qualitative and quantitative agreement with the experiment [34] in a broad range of fields, electron densities, and temperatures. In particular, the results explain an exponentially strong deviation at low temperatures of the tunneling rate from the

predictions of the single-electron theory.

6.1 The tunneling potential for electrons on helium

The formation of an electron layer on a liquid helium surface occurs because of two forces. On one hand, there is an attractive image force on electrons because they polarize the dielectric. The effective charge is $\Lambda e = \frac{e^3(\epsilon-1)}{4(\epsilon+1)}$, where $\epsilon \approx 1.057$ is the dielectric constant of helium. On the other hand, a very high affinity potential for helium ($\approx 1ev$) prevents electrons from penetrating into the dielectric. The corresponding Schrödinger equation for a model potential

$$U_{\text{im}} = \begin{cases} -\frac{\Lambda}{z}, & z > 0 \\ \infty, & z = 0 \end{cases} \tag{6.1}$$

with the appropriate boundary condition $\psi(0) = 0$ can be solved exactly. This solution [74, 75] gives the energy levels $E_n = \gamma_n^2/2m$, where the intrawell localization length of the n-th level is $\gamma_n = \gamma_1/n = \Lambda m/n$, ($\gamma \equiv \gamma_1$). The ground state is described by a wave function $\psi_1(z) = 2\gamma^{3/2} z \exp(-\gamma z)$, with $\gamma^{-1} = 76$Åand energy $E_g \approx 7.5$K. The smallness of E_1 justifies the use of the infinite barrier approximation. The average distance to the surface for an electron is $\langle z \rangle = 3/2\gamma \approx 114$Å. This problem was analyzed more precisely in Ref. [74], taking into account the finite value for the affinity potential, but the results yield only small corrections to the above expression.

In experiment [34], electrons were injected from above into a cylindrical cell of height 2.5 ± 0.05 mm that is half filled with liquid helium. A negatively biased guard

ring of diameter 18 ± 0.05 mm prevents electrons from escaping to the sides. The helium surface was kept close to the middle of the cell: $d = \epsilon h$ (with the uncertainty of ± 0.025 mm), where d and h are distances from the layer to top and bottom electrodes.

A voltage V_t applied between the top plate and the grounded bottom plate creates the external electric field $-V_t/(d + h/\epsilon)$ that can either additionally confine electrons or extract them from the layer. The tunneling rate is measured as the difference in the number of electrons before and after the extracting pulse of the electric field. In addition to the applied electric field, there is an electric field from charges induced in the top and bottom electrodes by electrons of the 2DES. As a result, the total electric field becomes density-dependent [76]:

$$|\mathcal{E}_\perp| = \frac{V_t}{d + h/\epsilon} - 4\pi n \mid e \mid \frac{d - h}{(\epsilon + 1)(d + h/\epsilon)} \tag{6.2}$$

In the presence of electric field, the ground state energy changes. This change can be found by the first-order perturbation theory in electric field. The ground state energy becomes:

$$E_1 = -\frac{\gamma^2}{2m} - |e\mathcal{E}_\perp|\langle z\rangle = -\frac{\gamma^2}{2m}\left(1 + \frac{3}{2\gamma L}\right), \tag{6.3}$$

where the tunneling length $L = \gamma^2/(2m|e\mathcal{E}_\perp|)$. The energy shift is small as an inverse of γL, which is a large parameter of the theory. Large γL is also necessary for the adiabatic approximation to be valid. For electrons on helium this condition is well satisfied with $\gamma L \sim 30$.

The tunneling potential is also affected by the Coulomb interaction between electrons. The corresponding "correlation-hole" potential [69, 72] can be obtained by keeping only the lowest-order terms in the ratio of the tunneling length L to the

inter-electron distance $n^{-1/2}$, as discussed in paragraph 4.4.1, and has the form $-m\bar{\omega}^2 z^2$, where $\bar{\omega} \propto n^{3/2}$. The conditions $\gamma^{-1} \ll L \ll n^{-1/2}$ are typically very well satisfied in experiment, with the decay length $1/\gamma = 1/\Lambda m \approx 0.7 \times 10^{-6}$ cm, $L \sim |E_g/e\mathcal{E}_\perp| \approx \gamma^2/2m|e\mathcal{E}_\perp| \sim 2 \times 10^{-5}$ cm, and $n^{-1/2} \sim 10^{-4}$ cm [in the estimate of L we used that $|E_g| \gg |e\mathcal{E}_\perp|/\gamma, m\bar{\omega}^2/\gamma^2$, and that $|e\mathcal{E}_\perp|/\gamma \gtrsim \bar{\omega}$].

We can now write the total tunneling potential and separate terms that are small as $(\gamma L)^{-1}$:

$$U(z) = \frac{\gamma^2}{2m}\left[U_0(z) + \frac{1}{\gamma L}U_1(z)\right], \quad z > 0 \tag{6.4}$$

$$U_0(z) = 1 - \frac{z}{L} - \frac{1}{2}\bar{\omega}^2\tau_0^2\left(\frac{z}{L}\right)^2 \tag{6.5}$$

$$U_1(z) = -\frac{2}{(z/L)} + \frac{3}{2} + \frac{3}{2}\bar{\omega}^2\tau_0^2\frac{z}{L} \tag{6.6}$$

Here, the energy is counted from the ground state energy. The linear term in Eq. (6.4) describes the electric field that pulls electrons out of the layer. The parameter $\tau_0 = 2mL/\gamma$ is the imaginary tunneling time in the limit $n \to 0$. Although the image potential $\propto 1/z$ provides the major contribution for $z \sim \gamma^{-1}$, it becomes small deep under the barrier.

6.2 Exponent of the tunneling rate

To compare the predicted dynamical effect of the electron-electron interaction with the experimental data [34], we use the Einstein model of the WC, and set all the phonon frequencies $\omega_{\mathbf{k}j}$ to be equal to the characteristic plasma frequency $\omega_p = (2\pi e^2 n^{3/2}/m)^{1/2}$. The numerical results change only slightly when this fre-

quency is varied within reasonable limits, e.g., is replaced by the root mean square frequency $\bar{\omega}$. Note that the correlation-hole potential is determined by the mean square frequency $\bar{\omega} = (4.45e^2n^{3/2}/m)^{1/2}$.

The magnetic field dependence of the tunneling rate for different T is calculated from Eqs. (4.11). The actual calculation is largely simplified by the fact that, deep under the barrier, the image potential $-\Lambda/z$ in (6.4) can be neglected. The equations of motion (4.11) become then linear, and can be explicitly solved. In what follows we will use dimensionless frequencies $\nu_c = \omega_c\tau_0$, $\nu_p = \omega_p\tau_0$, $\bar{\nu} = \bar{\omega}\tau_0$, and $\nu^2 = \nu_p^2 + \nu_c^2$. The coordinates x and z are given in units of the tunneling length L, and momenta p_x and p_z are given in units of $\gamma/2$. The tunneling trajectories then take the form:

$$
\begin{aligned}
x(\tau) = \; & -\frac{A_1}{\lambda_1}\sin\lambda_1\tau + \frac{A_2}{\lambda_1}\cos\lambda_1\tau - \frac{A_3}{\lambda_2}\sinh\lambda_2\tau - \frac{A_4}{\lambda_2}\cosh\lambda_2\tau; \\
p_z(\tau) = \; & \frac{\nu_p^2+\lambda_1^2}{\nu_c\lambda_1}(A_2\cos\lambda_1\tau - A_1\sin\lambda_1\tau) + \frac{\lambda_2^2-\nu_p^2}{\lambda_2\nu_c}(A_3\sinh\lambda_2\tau + A_4\cosh\lambda_2\tau); \\
z(\tau) = \; & \frac{\nu_p^2+\lambda_1^2}{\nu_c\lambda_1^2}(A_1\cos\lambda_1\tau + A_2\sin\lambda_1\tau) \\
& + \frac{\lambda_2^2-\nu_p^2}{\nu_c\lambda_2^2}(A_3\cosh\lambda_2\tau + A_4\sinh\lambda_2\tau) - \bar{\nu}^{-2}; \\
p_x(\tau) = \; & A_1\cos\lambda_1\tau + A_2\sin\lambda_1\tau + A_3\cosh\lambda_2\tau + A_4\sinh\lambda_2\tau - \nu_c z(\tau). \qquad (6.7)
\end{aligned}
$$

Here, the eigenvalues $\lambda_{1,2}$ of the matrix derived from the equations of motion are given by:

$$
\begin{aligned}
\lambda_1^2 &= \frac{1}{2}\left[2\bar{\nu}^2 - \nu^2 + \sqrt{(2\bar{\nu}^2-\nu^2)^2 + 8\bar{\nu}^2\nu_p^2}\right], \\
\lambda_2^2 &= \frac{1}{2}\left[\nu^2 - 2\bar{\nu}^2 + \sqrt{(2\bar{\nu}^2-\nu^2)^2 + 8\bar{\nu}^2\nu_p^2}\right].
\end{aligned}
$$

The constants A_i, $i = 1, 2, 3, 4$ are determined from the initial conditions (4.16,4.18):

$$A_1 = \frac{2\nu_c + \nu_p x(0)(\nu^2 - \lambda_2^2)\coth[\omega_p\beta/2 - \nu_p\tau_{\rm rd}]}{\lambda_1^2 + \lambda_2^2}$$
$$A_2 = \frac{4\bar{\nu}^2\nu_c - (\nu^2 - \lambda_2^2)(2\nu_c - \nu_p^2 x(0))}{\lambda_1(\lambda_1^2 + \lambda_2^2)}$$
$$A_3 = -\frac{2\nu_c + \nu_p x(0)(\nu^2 + \lambda_1^2)\coth[\omega_p\beta/2 - \nu_p\tau_{\rm rd}]}{\lambda_1^2 + \lambda_2^2}$$
$$A_4 = \frac{-4\bar{\nu}^2\nu_c + (\nu^2 + \lambda_1^2)(2\nu_c - \nu_p^2 x(0))}{\lambda_2(\lambda_1^2 + \lambda_2^2)}$$

According to the boundary condition (4.12), at the exit point $x(\tau_{\rm rd}) = p_z(\tau_{\rm rd}) = 0$, which allows to find $\tau_{\rm rd}$ and $x(0)$. In particular, as it follows from expressions for $x(\tau)$ and $p_z(\tau)$ on the tunneling trajectory (6.7), this is equivalent to requiring that $A_1 \sin\lambda_1\tau_{\rm rd} = A_2\cos\lambda_1\tau_{\rm rd}$ and $A_3\sinh\lambda_2\tau_{\rm rd} = -A_4\cosh\lambda_2\tau_{\rm rd}$.

The tunneling exponent is then given by:

$$R = \gamma L\left[2\tau_{\rm rd} + \frac{\tau_{\rm rd}}{\bar{\nu}^2} - \left(1 + \frac{\nu_p^2}{\lambda_1^2}\right)\frac{A_2}{\lambda_1\nu_c} + \left(1 - \frac{\nu_p^2}{\lambda_2^2}\right)\frac{A_4}{\nu_c\lambda_2}\right] \tag{6.8}$$

Expression (6.8) is plotted in Fig. 6.1 for the quantity W(B)/W(0). The correction to $R(B) - R(0)$ from the image potential and other terms of $U_1(z)$ in Eq. (6.6) is $\sim 1/\gamma L$. This results in changes to the theoretical curves that are smaller than the uncertainty in $R(B) - R(0)$ due to the uncertainties in n and $\mathcal{E}_\perp$ in the experiment [34]. Note, however, that the potential $U_1(z)$ has to be taken into account when comparing the tunneling rate W itself with experiment.

As seen from Figs. 6.1, 6.2 the dynamical many-electron theory is in good qualitative and quantitative agreement with the experiment, without any adjustable parameters. At low temperatures ($T = 0.04$ K), the many-electron tunneling rate is bigger than the single-electron estimate [34] by a factor of 10^2 for $B = 0.25$ T, see Fig.6.2.

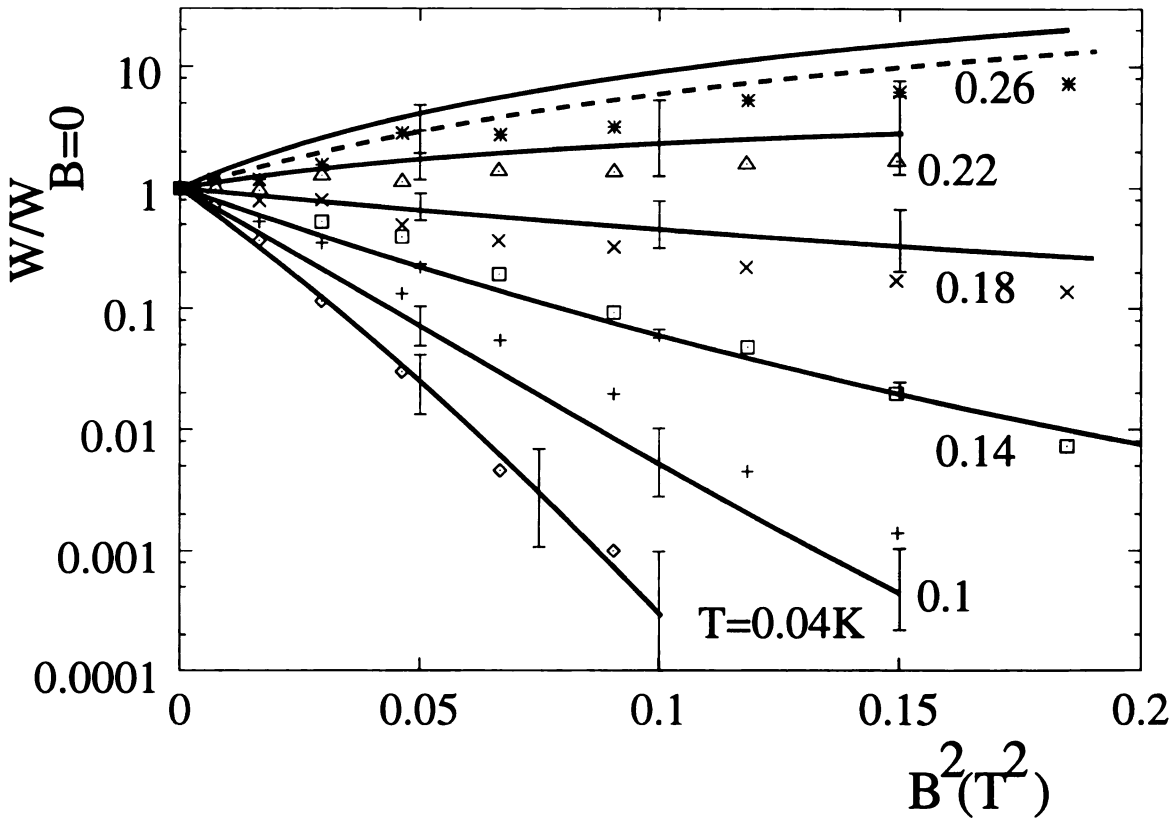

Figure 6.1: The relative rate of electron tunneling from helium surface $W(B)/W(0)$ as a function of the magnetic field B for the electron density $n = 0.8 \times 10^8 cm^{-2}$ and the calculated pulling field $\mathcal{E}_\perp = 24.7$ V/cm (solid curve). Solid lines show how the theory compares to the experimental data [34]. The errorbars show the uncertainty in the theoretical values due to the uncertainty in the parameters of the experiment.

For this temperature, the tunneling rate is well described by the $T \to 0$ limit, cf [56]. The B-dependence of the tunneling rate is very sensitive to temperature. It becomes less pronounced for higher T, and the role of dynamical many-electron effects becomes less important, too. Interestingly, the theoretical data on the *ratio* of $W(B)/W(0)$ become less sensitive to the experimental uncertainties in the cell geometry (which determines $\mathcal{E}_\perp$) and the electron density n for intermediate temperatures $T \sim 0.14$ K. This is because the corresponding errors in $W(B)$ and $W(0)$ compensate each other for such temperatures.

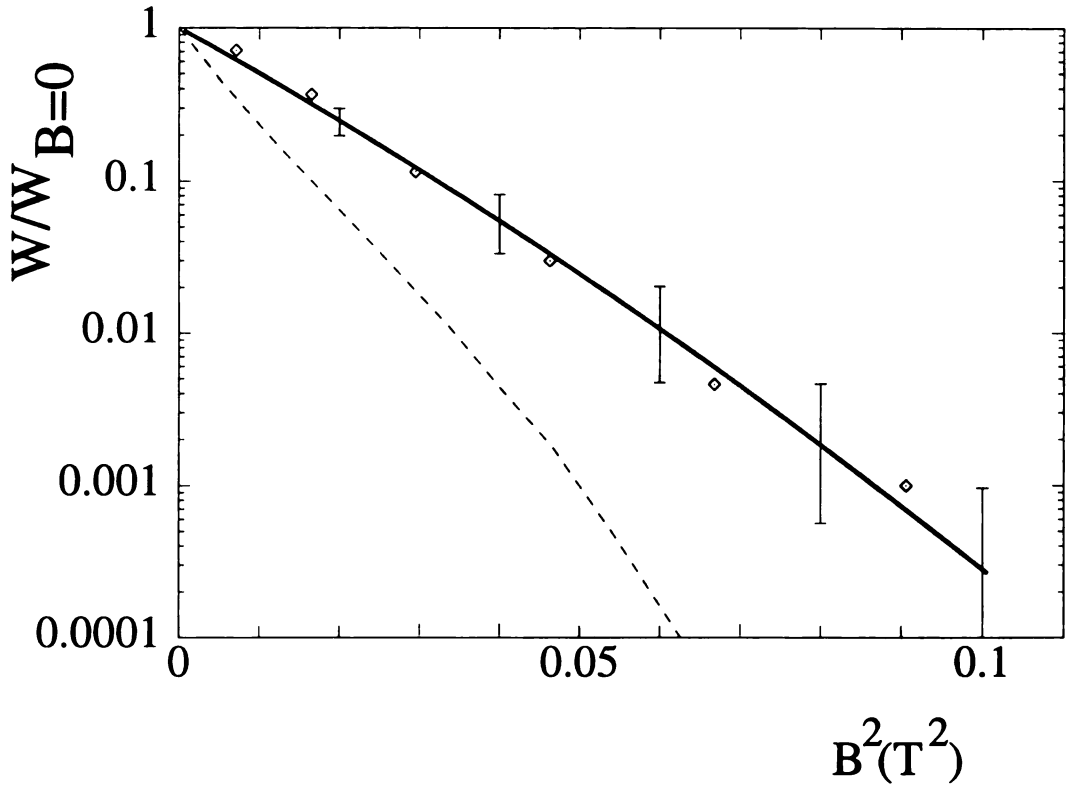

Figure 6.2: The rate of electron tunneling from helium surface $W(B)$ as a function of the magnetic field B for the electron density $n = 0.8 \times 10^8 cm^{-2}$ and the calculated pulling field $\mathcal{E}_\perp = 24.7$ V/cm (solid curve). Solid line is the theoretical calculation for $T = 0$. The experimental data are taken from [34] for $T = 0.04$ K. For such low temperature, predictions of finite and zero temperature theory are very close to each other, as can be noted by comparing with Fig. 6.1, where the finite-temperature curve is given. The error bars show the uncertainty in the theoretical values due to the uncertainty in the parameters of the experiment. The dashed curve is the calculation [34] for $T = 0.04$ K without inter-electron momentum exchange.

The crossover to magnetic-field enhanced tunneling occurs for temperature $T_c \approx 0.19K$, for the parameters in Fig. 6.1. The expected increase of the tunneling rate with B for $T > T_c$ is shown in Fig. 6.1. It has indeed been observed in the experiment [34]. The analysis of the experiment requires to establish whether, for temperatures of interest, escape actually occurs via tunneling. To that end we note first that, as it follows from a direct variational calculation, the potential $U(z)$ (6.4), with the

parameter values specified in Fig. 6.1, has only one metastable intrawell state.

If the intrawell relaxation were fast enough, the temperature of the crossover from tunneling to activation T_a for $B = 0$ would be given by the condition that the tunneling exponent R_g be equal to the activation exponent $(U_{\max} - E_g)/T$ [here, $U_{\max}$ is the maximal value of the potential $U(z)$]. This would give $T_a \approx 0.15$ K. However, activated escape requires that the in-plane thermal energy of an electron be transformed into the energy of its out-of-plane motion. This involves a large transfer of the in-plane momentum $\sim [2m(U_{\max} - E_g)]^{1/2}$. The electron-electron interaction does not give rise to such a transfer in a strongly correlated system, since the reciprocal inter-electron distance is $n^{1/2} \ll [2m(U_{\max} - E_g)]^{1/2}$.

The major process which gives rise to the momentum transfer is scattering by capillary waves on the helium surface, ripplons [53]. Electron-ripplon coupling is weak [77]. As a result, the prefactor in the activation rate, which is quadratic in the coupling constant, is small. For $B = 0$ it is $\sim \gamma^2 T^2/\hbar\sigma$ [78], where σ is the surface tension of liquid helium. For temperatures $T < 0.25$ K this prefactor is less than the prefactor in the tunneling rate $(\hbar\gamma^2/m)\exp(-2)$ by a factor $< \times 10^{-5}$. Therefore the crossover from tunneling to activation occurs for higher temperatures than it would follow from the condition of equal tunneling and activation exponents.

For the parameters in Fig. 6.1, the rates of activation and tunneling escape become equal for temperatures slightly higher than 0.26 K (for $B = 0$). Therefore the experimentally observed increase of the escape rate with B is indeed due to the discussed mechanism of B-enhanced tunneling. The smaller experimental values of the relative escape rate $W(B)/W(0)$ for $T = 0.26$ K can be understood by noticing that

the activation rate is close to the tunneling rate for such T, and since it presumably only weakly depends on B, the overall slope of $\ln[W(B)/W(0)]$ should be smaller than that of the theoretical curve which ignores activation (approximately, by a factor of two).

To include the activation processes in the overall escape probability, $W = W_{\rm tunn} + W_{\rm act}$, the probability of the over-barrier escape was calculated following the logic of the paper [78]:

$$W_{\rm act} = C\frac{m}{\hbar^3\sigma}(k_BT)^2E_a\left(1+3\frac{k_BT}{E_a}\right)e^{-E_a/k_BT}, \tag{6.9}$$

where the numerical factor $C = 1.42$ differs by a factor of 4 from those in Ref. [78]. The barrier height gives the activation exponent $E_a = U_{\rm max} - E_g$. The result for the escape rate for $T = 0.26$ K is shown by the dashed line in Fig. 6.1. This calculation neglects the change in the probability of over-barrier escape with magnetic field. Although the rate of activation escape indeed only weakly depends on B, there are several factors that could affect the over-barrier escape in a magnetic field. First, the field may "push" the ground state upward in energy, by $m\omega_c^2[\langle z^2\rangle - \langle z\rangle^2]/2$, for a weak field (the averaging is performed for the ground state). A second factor is the change, by the magnetic field, of the wave functions with energies close to the barrier top. For $B = 0.4$ T the magnetic length $l = (\hbar c/eB)^{1/2}$ is ~ 0.6 of the distance from the helium surface to the barrier top position $(\Lambda/|e\mathcal{E}_\perp|)^{1/2}$. Both factors decrease the activation energy for over-barrier escape.

6.3 The prefactor

The dependence of the potential $U(z)$ (6.4) on n gives rise to the density dependence of the tunneling rate $W(B)$ even for $B = 0$. We can calculate the exponent and the prefactor in $W(0)$ by matching the WKB wave function under the barrier for $1/\gamma \ll z \ll L$ with the tail of the non-WKB intrawell solution (here, $L = \hbar^2\gamma^2/2m|e\mathcal{E}_\perp|$ is the characteristic barrier width). In the spirit of the logarithmic perturbation theory (LPT) [79], the wave function of the ground state inside the well and not too far from it can be sought in the form

$$\psi_g(z) = \text{const} \times z \exp[-A(z)] \tag{6.10}$$

[we explicitly take into account that the function $\psi_g(z)$ has a zero in the ground state].

Near the well ($z \ll L$) the first term in (6.6) provides the major contribution to the potential. The solution can be found by considering the last two terms in the potential $U_0(z)$ (6.5) as a perturbation $\delta U(z)$, which is polynomial in z. Using the anzats (6.10 for the wave function, one gets a Riccati equation for the function $f(z) \equiv dA/dz$:

$$\frac{df}{dz} + \frac{2}{z}(f - \gamma) - f^2 + \gamma^2 = 2m(E - \delta U). \tag{6.11}$$

The function f has to equal to γ for $z = 0$. The general solution has the form:

$$f = \gamma + \int_C^z dz_1 2m(E - \delta U(z_1))\frac{z_1^2}{z^2}\exp[-2\gamma(z - z_1)] + Bz^{-2}\exp[2\gamma z]. \tag{6.12}$$

Since we are looking for the localized state wave function, f has to go to zero as $z \to \infty$. Therefore, coefficient $B = 0$ and integration constant $C = \infty$. The energy

E can be found from the condition that function f remains finite as $z \to 0$:

$$E = \frac{\int_0^\infty dz z^2 \delta U(z) e^{-2\gamma z}}{\int_0^\infty dz z^2 e^{-2\gamma z}}. \tag{6.13}$$

From expression (6.13), it si clear that the contribution to the energy E from different orders in z of potential δU are independent and additive, so that for the perturbation $\delta U(z) = Cz^\mu$, the energy is given by

$$E = (2\gamma)^\mu (\mu + 2)!/2, \tag{6.14}$$

and the function f has the form

$$f(z) = \gamma + 2mC \sum_{i=0}^{\mu-1} (2\gamma)^{-(i+1)} z^{\mu-i} \frac{(\mu+2)!}{(\mu+2-i)!}. \tag{6.15}$$

Near the well, the linear term $\propto \mathcal{E}_\perp$ dominates the quadratic one in (6.5). To the first order in $\mathcal{E}_\perp$, the exponent $A(z)$ of the wave function can be obtained by integrating over z the function f from (6.15), with $\mu = 1$ and $C = -|e\mathcal{E}_\perp| \equiv -\gamma^2/2mL$:

$$A(z) \approx \gamma z \left(1 - \frac{z}{4L}\right). \tag{6.16}$$

The correction to A (6.16) is small for z small compared to the barrier width L. We note that the exponent $A(z)$ has an overall functional form which differs from that of the commonly used [53] variational wave function $\psi(z) \propto z \exp(-\tilde{\gamma} z)$, with $\tilde{\gamma}$ being the variational parameter.

The expression for A (6.16) matches the small-z/L expansion of the action S of the WKB wave function under the barrier for $L \gg z \gg \gamma^{-1}$. This allowed us to find the prefactor in the WKB wave function and in the tunneling rate. The resulting tunneling rate is shown in Fig. 6.3. It fully agrees with the experiment (see also

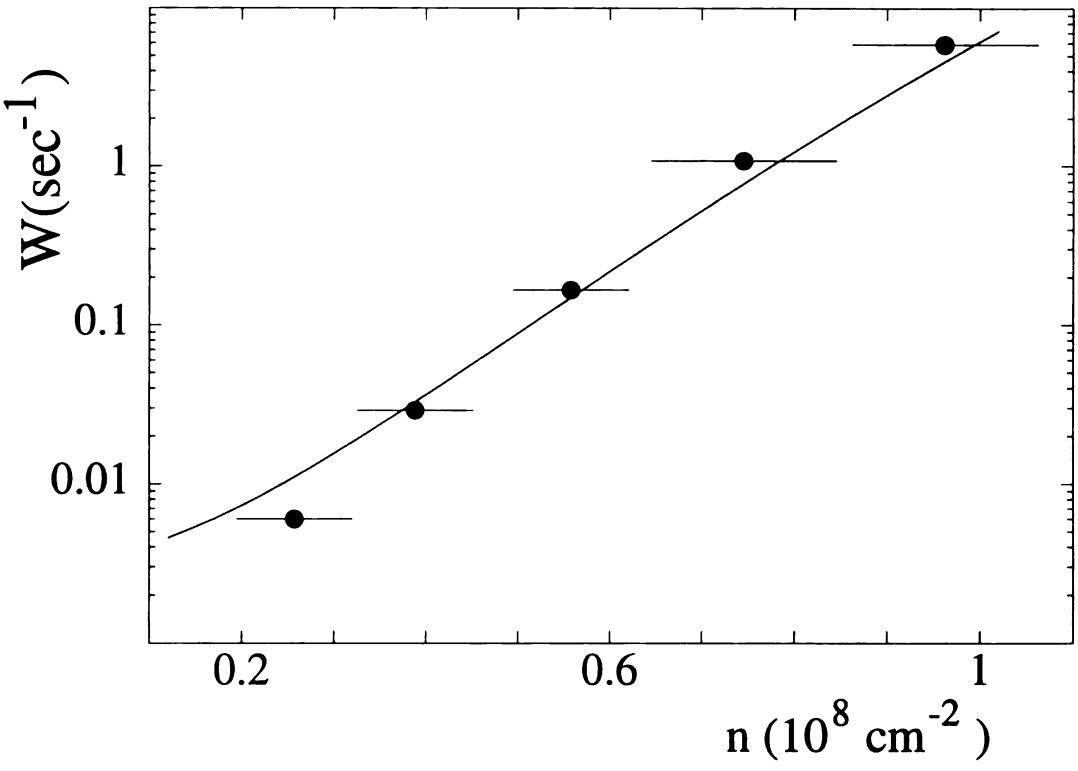

Figure 6.3: The rate of electron tunneling from the helium surface $W(0)$ for $B = 0$ as a function of the electron density. The dots show the experimental data [34]. The pulling field $\mathcal{E}_\perp$ for $n \to 0$ is calculated for the parameters used in the experiment to be 26.7V/cm.

Ref. [80], where a good agreement was obtained between measured and numerically calculated tunneling rates without magnetic field for electrons on helium).

Chapter 7

Conclusions

We have developed a semiclassical theory of tunneling decay in a magnetic field. We show that, as in the case without the magnetic field, the tunneling exponent can be found from the classical equations of motion. However, in contrast to the $B = 0$-case, decay of the wave function under the barrier is accompanied by oscillations. Related to this is the conclusion that the particle appears from under the barrier with finite real velocity, and behind the boundary $U(\mathbf{r}) = E$ of the classically allowed region. In the presence of a magnetic field it is no longer sufficient to find the wave function just at the boundary of a classically allowed region: it is necessary to find both the exit point (or any point on the trajectory of the escaped particle), and the absolute value of the wave function along it.

From the technical point of view, the semiclassical solution of the tunneling problem in a magnetic field is based on the analytic continuation of the wave function to complex space. In the semiclassical approximation this corresponds to considering trajectories with complex coordinates, momenta and time. The action $S(\mathbf{r})$ calcu-

lated along such tunneling trajectories will have both real and imaginary part, and this would describe both decay and oscillations of the wave function. The condition for the particle to become classically observable is that its coordinate and momentum become real, i.e. Im $\mathbf{r}$=Im $\mathbf{p}$=$\mathbf{0}$. The real part of momentum (or velocity) is not necessarily equal to zero, and gives the initial momentum of the escaped particle. This momentum was accumulated due to the magnetic field during motion under the barrier. As we show, the set of complex under barrier trajectories has caustics. The semiclassical approximation breaks down at the caustics. Different branches that correspond to decaying and increasing solutions, and to incident and outgoing waves match at the caustic, and we show how to choose the appropriate solutions to account for the boundary conditions.

We have also analyzed the single-particle decay problem in a magnetic field for finite temperatures. We have modified the known bounce technique for the problem of decay from a parabolic metastable potential well. In the presence of a magnetic field, the bounce trajectory becomes complex. However, as we show, the corresponding action remains real, and the prefactor in the partition function is purely imaginary, although the structure of the related eigenvalue problem is totally different (the eigenvalues become complex).

If the tunneling potential cannot be approximated as parabolic near its minimum, at least in one direction, the "bounce" technique no longer works regardless of the presence of a magnetic field. Such a situation is relevant in tunneling from 2DES, where the out-of-plane motion is quantized and the tunneling potential is strongly non-parabolic in the out-of-plane direction (either singular, as it is in the case of

electrons on helium, or discontinuous, as in the case of 2DES in semiconductor heterostructures).

Of central interest for 2D science are the effects of electron correlations. We show that tunneling in a magnetic field provides a unique tool for revealing and investigating these effects. They lead to an exponential increase of the tunneling rate as compared to the predictions of the non-interacting electrons picture. The mechanism responsible for such an increase is similar to a Mössbauer effect, where a gamma quantum can transfer its momentum to the crystal as a whole. In our case the momentum that is transfered to the electron system as a whole is an in-plane Hall momentum acquired by the tunneling electron during its motion out of the layer. In the non-interacting picture it is this in-plane Hall momentum that leads to an exponential suppression of the tunneling rate in a parallel to the layer field. However, complete transfer of this momentum almost never occurs, as it requires that the rate of inter-electron momentum exchange (plasma frequency) be much larger than the inverse characteristic imaginary time of motion on the tunneling trajectory. When these two quantities are of the same order, only a part of the Hall momentum is transfered in the "recoil-free" way, which results in a partial, yet very substantial compensation of the suppression to the escape rate introduced by the parallel field. Similarly to a Mössbauer effect, there is no need for a long-range order in an electron system for our mechanism to work. The effect should be seen even if electrons form a strongly correlated fluid without the long-range order.

At high temperatures the tunneling rate is expected to exhibit a number of new unusual features. One of the most interesting of them is that a parallel magnetic field

may *enhance*, rather than suppress the tunneling rate. Such B-enhanced tunneling does not happen in all systems. Competing processes, such as tunneling from higher in energy intra-well states or activation, limit the range of temperatures where B-enhanced tunneling can be observed. On the other hand, sufficiently strong magnetic fields will always suppress the tunneling rate, which set the limits on magnetic fields that enhance tunneling. Nevertheless, the possibility to increase the tunneling rate without changing parameters of the tunneling barrier is not only unexpected, but also very useful. For example, in the development of quantum cascade lasers, high tunneling rates are necessary to achieve an inverted level occupation, meanwhile the parameters of the tunneling barriers are essentially fixed by other requirements.

The B-enhanced tunneling leads in turn to several types of switching effects, such as switching between tunneling from different intra-well states, and from over-barrier activation to tunneling, and vice versa. These switching processes may differ qualitatively for barriers, where the tunneling length changes with intra-well energy, as opposed to barriers, where the length does not depend on the energy. Both cases have been analyzed in detail using simple models of a triangular and a square potential in order to describe the first and second situation, respectively.

The results have been compared to the tunneling data from experiments on strongly correlated electron systems formed on liquid helium surface [34]. The analytically calculated tunneling rate and its evolution with field and temperature are in full qualitative and quantitative agreement with the experimental data, with no adjustable parameters. This proves that tunneling experiments with a magnetic field parallel to the layer can be used in order to reveal strong electron correlations and in-

vestigate in-plane electron dynamics in a 2DES. The measurable quantity is the auto-correlation function of the in-plane momentum of an electron in a strongly correlated 2DES. Of particular interest are low-density 2DESs in semiconductor heterostructures. Until now correlated systems in semiconductors have been investigated by tunneling mostly for the magnetic field **B** perpendicular or nearly perpendicular to the electron layer. We show that for typical densities used in low-density systems, and with barriers grown with standard techniques tunneling experiments designed to probe in-plane correlations would require easily attainable values for magnetic field and temperature.

Appendices

Appendix A

The instanton method in a magnetic field: analysis of the prefactor

To find the prefactor in Z, we consider paths that are close to the extremal trajectory $\bar{\mathbf{r}}(\tau) + \delta\mathbf{r}(\tau)$, and show that the integral (3.23) provides an imaginary contribution to Z. The action S_E along these paths can be expanded as:

$$S_E \approx S_E[\bar{\mathbf{r}}(\tau)] + \frac{1}{2}\int\int d\tau d\tau' \frac{\delta^2 S_E}{\delta \mathbf{r}_i(\tau)\delta \mathbf{r}_j(\tau')}\delta\mathbf{r}_i(\tau)\delta\mathbf{r}_j(\tau') \tag{A.1}$$

To evaluate the integral (3.23), we would like to diagonalize the operator for $\delta^2 S_E$, and therefore have to look at the eigenvalue problem:

$$\int_{-\frac{1}{2T}}^{\frac{1}{2T}} d\tau' \frac{\delta^2 S_E}{\delta \mathbf{r}_i(\tau)\delta \mathbf{r}_j(\tau')}\boldsymbol{\psi}_{nj}(\tau') = \lambda_n \boldsymbol{\psi}_{ni}(\tau) \tag{A.2}$$

We need to investigate some properties of the eigenvectors $\boldsymbol{\psi}(\tau)$ before we could use them to expand the fluctuations $\delta\mathbf{r}(\tau)$ around the extremal trajectory $\bar{\mathbf{r}}(\tau)$. In the

presence of a magnetic field the operator itself in (A.2) becomes non-Hermitian. For example, in the case of a uniform $\mathbf{B}$ it may written as $F(\tau)\ \psi_n(\tau) = \lambda_n\ \psi_n(\tau)$ with

$$F_{ij}(\tau) = -m\frac{d^2}{d\tau^2}\delta_{ij} + \frac{\partial^2 U}{\partial r_i \partial r_j} + im\omega_c \epsilon_{ijk}\hat{B}_l \frac{d}{d\tau} \tag{A.3}$$

The eigenvectors of the problem (A.2) form a biorthogonal set, meaning that eigenvectors $\{\psi_n\}$ are orthogonal to eigenvectors $\{\phi_n\}$ of the Hermitian conjugate operator: $F^\dagger \phi_n = \lambda_n^* \phi_n$. Taking into account the symmetry (3.26) of the extremal trajectory $\bar{\mathbf{r}}(\tau)$, and counting the imaginary time from the middle point $\beta/2$, we find that the operator F belongs to the class of $\mathcal{PT}$-symmetric non-Hermitian Hamiltonians:

$$F^\dagger(\tau) = F(-\tau) = F^*(\tau). \tag{A.4}$$

In our case, variable τ is a space coordinate, so that inversion $\mathcal{P}$ corresponds to $\tau \to -\tau$, while time reversal $\mathcal{T}$ is a complex conjugation. Therefore we have come upon yet another example of $\mathcal{PT}$-symmetric Hamiltonian. Recent physical applications of non-Hermitian Hamiltonians include depinning of vortices in type-II superconductors [81] and growth of populations [82]. Bifurcation of the initially real eigenvalues [83] into the complex plane with increasing of an imaginary external field (in our case - magnetic field) indicates the delocalization transition.

The symmetry (A.4) is a strong property, and in particular it shows that $\psi_n(\tau) = \phi_n^*(\tau)$. Then the orthogonality relation reads:

$$\int_{-\beta 2}^{\beta/2} d\tau \psi_m(\tau)\psi_n(\tau) = A_n \delta_{mn}, \tag{A.5}$$

where A_n is a normalization factor.

Because the operator F is non-Hermitian, some of the eigenvalues λ_n will be complex. Let us compare the spectra of operators F and $F^\dagger$. In general, they are not the same, but in our case it will be true. We start with the eigenvalue equation for operator $F^\dagger$:

$$F^\dagger(\tau)\psi_n^*(\tau) = \lambda_n^*\psi_n^*(\tau),$$

perform the time inversion, and then use the symmetry (A.4) to get

$$F(\tau)\psi^*(-\tau) = \lambda_n^*\psi^*(-\tau).$$

The last equation does not mean that all eigenvalues λ_n are real. Instead, it shows that the spectrum of operators F is identical to that of operator $F^\dagger$. The eigenvalues λ_n are either real, or are present in pairs of complex conjugated numbers.

We are now in position to expand the fluctuations around the extremal trajectory $\mathbf{r}(\tau) - \bar{\mathbf{r}}(\tau)$ in terms of eigenvectors $\psi_n(\tau)$:

$$\delta\mathbf{r}(\tau) = A_n^{-1/2}\sum c_n\psi_n(\tau), \quad c_n = A_n^{-1/2}\int_{-\beta/2}^{\beta/2} d\tau\delta\mathbf{r}(\tau)\psi_n(\tau), \tag{A.6}$$

Note that by multiplying an eigenvector ψ_n by a phase factor $e^{i\alpha}$ does change the phase of the normalization factor A_n by 2α. However the coefficients of expansion $\{c_n\}$ remain unchanged. The second-order correction to the action is diagonal in c_n variables,

$$S_E \approx S_E[\bar{\mathbf{r}}(\tau)] + \sum_n \lambda_n c_n^2/2. \tag{A.7}$$

The statistical sum is therefore given by a Gaussian integral in variables $\{c_n\}$. One

could formally rewrite (3.23) as

$$Z = \left[\int_{\mathbf{r}(-\beta/2)=\mathbf{r}(\beta/2)} \int_{\mathbf{r}^*(-\beta/2)=\mathbf{r}^*(\beta/2)} \mathcal{D}\mathbf{r}(\tau)\mathcal{D}\mathbf{r}^*(\tau) e^{-S_E[\mathbf{r}(\tau)]-S_E[\mathbf{r}^*(\tau)]}\right]^{-1/2}$$
$$\propto e^{-S_E[\bar{\mathbf{r}}(\tau)]} \prod_n \left[\int dc_n \int dc_n^* \exp[-\lambda_n c_n^2 - \lambda_n c_n^{*2}]\right]^{-1/2} \tag{A.8}$$

The integration over variables c_n is easy to perform, the prefactor will be proportional to

$$Z \propto \prod_n \lambda_n^{-1/2} e^{-S_E[\bar{\mathbf{r}}(\tau)]}, \quad \text{for } \lambda_n \neq 0. \tag{A.9}$$

Integration in (A.8) over variable c_i that corresponds to $\lambda_i = 0$ will be done below. Since the spectrum of operator F contains complex eigenvalues in pairs, they provide positive contribution to the prefactor. We now turn our attention to the real part of the spectrum of operator F. The real negative eigenvalues are of utmost importance, and there should be an odd number of them, in order for $S_E[\bar{\mathbf{r}}(\tau)]$ to determine the exponent of the imaginary part of statistical sum Z.

First of all, one of the eigenvectors is known - it is $\boldsymbol{\psi}_1 = d\bar{\mathbf{r}}/d\tau$. This can be checked by a direct substitution to the eigenvalue equation (A.2):

$$\int_{-\frac{1}{2T}}^{\frac{1}{2T}} d\tau' \frac{\delta^2 S_E}{\delta \mathbf{r}_i(\tau)\delta \mathbf{r}_j(\tau')} \frac{d\bar{\mathbf{r}}_j}{d\tau'} = \frac{\delta S_E}{\delta \mathbf{r}_i(\tau)} = 0. \tag{A.10}$$

Therefore, $\boldsymbol{\psi}_1$ corresponds to $\lambda_1 = 0$. In the integral (3.23) we integrate over various paths $\delta\mathbf{r}(\tau)$. According to transformation (A.6), the shift in $\delta\mathbf{r}(\tau)$ due to a change in coefficient c_1 is given by

$$\Delta\mathbf{r}(\tau) = A_1^{-1/2} \Delta c_1 \boldsymbol{\psi}_1(\tau)$$

On the other hand, the shift of the middle point of the "bounce" may be regarded as

one of the possible fluctuations around $\bar{\mathbf{r}}(\tau)$

$$\Delta\mathbf{r}(\tau) = \frac{d\bar{\mathbf{r}}(\tau - \tau_0)}{d\tau_0}\Delta\tau_0 = -A_1^{-1/2}\boldsymbol{\psi}_1(\tau)\Delta\tau_0$$

Assuming that $\beta \gg 1$ (we consider the limit of low temperatures), the position of the middle point can be anywhere in the interval $(-\beta/2, \beta/2)$. A shift in the middle point results only in an exponentially small change of initial values. By comparing the last two formulas, we find that $\Delta c_1 = \Delta\tau_0$, and therefore

$$\int dc_1 \Rightarrow \int_{-\beta/2}^{\beta/2} d\tau_0 = \beta.$$

The integration over c_1 that correspond to $\lambda_1 = 0$ has thus been performed. No divergence occur in the prefactor (A.9) due to the presence of the zero eigenvalue. It is to be excluded from the product in (A.9) Instead, we obtain a very natural factor of $\beta = T^{-1}$, which eliminates a linear dependence of the tunneling rate (3.22) on temperature.

Presence of a zero eigenvalue is not related to magnetic field, and occurs without the magnetic field as well [9, 10]. For $B = 0$, the first eigenvector $\boldsymbol{\psi}_1(\tau) = d\mathbf{r}_{\rm cl}(\tau)/d\tau$, where the path $\mathbf{r}_{\rm cl}(\tau)$ is real and corresponds to a classical trajectory in the inverted potential $-U(\mathbf{r})$. The fact that the eigenvector $\boldsymbol{\psi}_1(\tau)$ gives the first excited state can be seen by noting that it has one, and only one, zero at the middle point of motion along the "bounce" trajectory: $\dot{\mathbf{r}}_{\rm cl}(0) = 0$. Without a magnetic field, operator F is Hermitian, so that the oscillation theorem is valid, and number of zeros enumerates the eigenstates, with the ground state eigenvector not having any zeros. Therefore there is one and only one negative $\lambda_0 < 0$, which makes the prefactor imaginary.

Let us follow the evolution of eigenvalues λ_n as we turn on the magnetic field. As we know the eigenvalue $\lambda_1 = 0$ is not shifted, other eigenvalues, however, will change. We also know that complex eigenvalues are present in complex conjugate pairs, and therefore have the same real part. Because the overall number of eigenstates remains unchanged with increasing of magnetic field, pairs of real eigenvalues first have to merge together. Only when their real parts are equal, the imaginary part may appear.

The state with $\lambda = 0$ does not mix with any other solutions. Suppose the opposite were true, so that two different states $\boldsymbol{\psi}_1 = d\bar{\mathbf{r}}/d\tau$ and $\boldsymbol{\psi}_2$ satisfy the condition $F\boldsymbol{\psi}_{1,2} = 0$. We can subtract these two equations from each other to obtain that

$$\frac{d}{d\tau}\left[-\boldsymbol{\psi}_2\dot{\boldsymbol{\psi}}_1 + \boldsymbol{\psi}_1\dot{\boldsymbol{\psi}}_2 - i\omega_c\hat{B}[\boldsymbol{\psi}_1 \times \boldsymbol{\psi}_2]\right] = 0.$$

Because the eigenvectors are zero at boundaries at $\pm\beta/2$, the following is true as well

$$-\boldsymbol{\psi}_2\dot{\boldsymbol{\psi}}_1 + \boldsymbol{\psi}_1\dot{\boldsymbol{\psi}}_2 + i\omega_c\boldsymbol{\psi}_2[\boldsymbol{\psi}_1 \times \hat{B}] = 0.$$

Remembering that $\boldsymbol{\psi}_1 = d\bar{\mathbf{r}}/d\tau$ and using the equations of motion (3.25) for $\bar{\mathbf{r}}$ we find that $\boldsymbol{\psi}_1\dot{\boldsymbol{\psi}}_2 - \nabla U\boldsymbol{\psi}_2 = 0$. This is a first order equation, and one solution is known to be $d\bar{\mathbf{r}}/d\tau$. It is also possible to show that the components of $\boldsymbol{\psi}_2$ which are perpendicular to $\boldsymbol{\psi}_1$ are equal to zero. The eigenvectors $\boldsymbol{\psi}_1$ and $\boldsymbol{\psi}_2$ differ only by a constant.

We have just shown that state of the zero eigenvalue $\lambda_1 = 0$ remains non-degenerate. Therefore, it separates the negative eigenvalue λ_0, which corresponds to the ground state, from the rest of positive eigenvalues, and prevents the ground state from mixing with higher levels.

After complex conjugate pairs have formed, they could, upon further increase of a magnetic field, change the sign of their real part from positive to negative, while having non-zero imaginary part. Then it is possible for the imaginary part to become zero again with increasing of the field. However, even if this were to happen, it would add an extra pair of real negative eigenvalues, and therefore the overall number of real negative eigenvalues would remain odd.

To summarize, we know that integration over paths close to the extremal path $\bar{\mathbf{r}}(\tau)$ provides an exponentially small imaginary part to the statistical sum Z. The exponent of the tunneling rate $W = 2T\text{Im } Z/\text{Re } Z$ is given by the Euclidean action S_E calculated along the extremal trajectory $\bar{\mathbf{r}}(\tau)$ that satisfies the equations of motion (3.25).

Appendix B

Many-electron influence functional $\mathcal{R}_{\rm ee}[z]$ at zero temperature

The scaling behavior of the tunneling exponent given by Eqs. (4.27) and (4.28) is quite general and takes place for all tunneling potentials provided characteristic frequency $\omega_p > \tau_f$. Below, the derivation is presented for a square barrier. Such potential is special because the velocity $\dot{z}(\tau_f)$ at the final point along the tunneling trajectory is not zero. The symmetry (4.13) is imposed. Under these circumstances it is easier rewrite the original retarded kernel $\mathcal{R}_{\rm ee}[z]$ as an integral from 0 to τ_f:

$$\mathcal{R}_{\rm ee}[z] = -\omega_c^2 \int_0^{\tau_f} \int_0^{\tau_1} d\tau_1 d\tau_2 z(\tau_1) z(\tau_2) [\chi(\tau_1 - \tau_2) + \chi(2\tau_f - \tau_1 - \tau_2)] \qquad \text{(B.1)}$$

At zero temperature, the kernel $\chi(\tau) = m(2N)^{-1} \sum \omega_{\mathbf{k}j} \exp[-\omega_{\mathbf{k}j}\tau]$. It is clear that different frequencies component are independent, therefore let us examine a kernel $\chi(\tau) = m\omega \exp[-\omega\tau]$.

Because of the exponential dependence of the kernel $\chi(\tau)$, the major contribution

comes from $\tau = 0$. For the first term in (B.1), this corresponds to $\tau_1 - \tau_2 \ll \omega^{-1}$, and we can use the expansion (4.26) as before [for convenience I rewrite it here]:

$$z(\tau_2) \approx z(\tau_1) + \dot{z}(\tau_1)(\tau_2 - \tau_1) + \frac{1}{2}\ddot{z}(\tau_1)(\tau_2 - \tau_1)^2$$

For the second term in (B.1), both τ_1 and τ_2 have to be close to τ_f. Therefore both $z(\tau_1)$ and $z(\tau_2)$ have to be expanded near τ_f:

$$z(\tau_{1,2}) \approx z(\tau_f) + \dot{z}(\tau_f)(\tau_{1,2} - \tau_f) + \frac{1}{2}\ddot{z}(\tau_f)(\tau_{1,2} - \tau_f)^2 \tag{B.2}$$

A straightforward integration gives the following answer for the influence functional:

$$\mathcal{R}_{\rm ee}[z] = -\frac{m\omega_c^2}{2N}\sum_{\mathbf{k}j}\left[\int_0^{\tau_f} d\tau z^2(\tau) + \omega_{\mathbf{k}j}^{-2} z(\tau)\ddot{z}(\tau) - z(\tau_f)\dot{z}(\tau_f)\omega_{\mathbf{k}j}^{-2}\right] \tag{B.3}$$

As for a smooth tunneling barrier, the term $\propto z^2(\tau)$ cancels the single-electron magnetic barrier in (4.23). If potential is purely square, then $\ddot{z}(\tau) \equiv 0$ [hard to imagine, but to just to show that the scaling results (4.27), (4.28) hold in this case]. Mass renormalization is then due to the boundary term $\propto z(\tau_f)\dot{z}(\tau_f)$, since for constant $\dot{z}$, we can always write it as an integral

$$\mathcal{R}_{\rm ee}[z] = -m\omega_c^2 \int_0^{\tau_f} d\tau \left[z^2(\tau) - (2N)^{-1}\sum_{\mathbf{k}j}\omega_{\mathbf{k}j}^{-2}\dot{z}^2(\tau)\right] \tag{B.4}$$

On the other hand, if $\ddot{z}$ is not identically zero on the optimal trajectory, then the same answer (B.4) is achieved by one integration by parts.

Frequency-dependence of the influence functional is studied next. It is shown below the larger the phonon frequency $\omega_{\mathbf{k}j}$, the larger is the absolute value of the contribution from this mode to the many-electron influence functional $\mathcal{R}_{\rm ee}[z]$. For $T = 0$, the function that we sum over phonon frequencies in $\mathcal{R}_{\rm ee}[z]$ is given by:

$$f(\omega, \tau_f) = \int_0^{2\tau_f} d\tau_1 \int_0^{\tau_1} d\tau_2 z(\tau_1) z(\tau_2) \omega e^{-\omega(\tau_1 - \tau_2)} \tag{B.5}$$

We will show now that this function is monotonic in terms of the frequency parameter ω. Indeed, its derivative with respect to ω is:

$$f'_\omega(\omega,\tau_f)=\int_0^{2\tau_f}d\tau_1 z(\tau_1)\int_0^{\tau_1}d\tau_2 z(\tau_2)(1-\omega(\tau_1-\tau_2))e^{-\omega(\tau_1-\tau_2)}$$

Using the symmetry $z(2\tau_f-\tau)=z(\tau)$ of the tunneling trajectory, we can change the upper integration limit from $2\tau_f$ to τ_f. Because for $\tau_2\le\tau_1\le\tau_f$, tunneling trajectory $z(\tau)$ monotonically increases with τ, we have $z(\tau_2)<z(\tau_1)$. Therefore one can substitute $z(\tau_1)$ by a smaller quantity $z(\tau_2)$:

$$\begin{aligned}f'_\omega(\omega,\tau_f)> \; 2\int_0^{\tau_f}d\tau_1\int_0^{\tau_1}d\tau_2 z^2(\tau_2)\left[(1-\omega(\tau_1-\tau_2))e^{-\omega(\tau_1-\tau_2)}\right.\\ \left.+(1-\omega(2\tau_f-\tau_1-\tau_2))e^{-\omega(2\tau_f-\tau_1-\tau_2)}\right] \qquad \text{(B.6)}\end{aligned}$$

Changing the order of integrations in order to integrate over τ_1, we get:

$$f'_\omega(\omega,\tau_f)=4\int_0^{\tau_f}d\tau_2 z^2(\tau_2)(\tau_f-\tau_2)e^{-2\omega(\tau_f-\tau_2)}>0$$

In this way, we know that terms corresponding to higher phonon frequencies provide larger contribution to $\mathcal{R}_{\rm ee}[z]$. In addition, the density of phonon states also favors larger $\omega_{\mathbf{k}j}$. To summarize we can conclude that at least for $T=0$, the tunneling rate is determined by high-frequency phonons, which in the case of Wigner crystal correspond to short-range vibrations. The out-of-plane tunneling probes the short-range order in a 2DES.

Appendix C

Square barrier: calculation of the tunneling exponent.

In the Einstein approximation of a Wigner crystal, the tunneling problem is formulated for one-particle with an effective tunneling potential:

$$H = \frac{1}{2m}(p_x + \omega_c z)^2 + \frac{p_z^2}{2m} + \frac{\hbar^2\gamma^2}{2m} + \frac{1}{2}m\omega_0^2 x^2 - m\omega_0^2 z^2 \qquad \text{(C.1)}$$

In what follows, we will scale the coordinates by the tunneling length L, meanwhile the momenta will be scaled by $\hbar\gamma/2$. This results in the scaling of the energy by $\hbar^2\gamma^2/(4m)$, and the action S by $\hbar\gamma L/2$. The frequencies found in the Hamiltonian (C.1) will be scaled by combination $\hbar\gamma/(2mL)$, which indeed has the appropriate dimension of s^{-1}, and is half the imaginary tunneling time for $B = 0$. The dimensionless frequencies are therefore defined as $\nu_{p,c} = 2mL\omega_{p,c}/\hbar\gamma$ and $\bar{\nu} = 2mL\bar{\omega}/\hbar\gamma$. The Hamiltonian in these dimensionless variables takes the form:

$$H = \frac{1}{2}(p_x + \nu_c z)^2 + \frac{p_z^2}{2} + 2 + \frac{1}{2}\nu_p^2 x^2 - \bar{\nu}^2 z^2$$

The corresponding equations of motion are linear:

$$\frac{dp_z}{d\tau} = -2\bar{\nu}^2 z - \nu_c \frac{dx}{d\tau}; \quad \frac{dp_x}{d\tau} = -\nu_p^2 x; \quad \frac{dz}{d\tau} = p_z; \quad \frac{dx}{d\tau} = -p_x - \nu_c z \tag{C.2}$$

and have real and imaginary eigenfrequency of vibrations:

$$\lambda_2^2 = \left[\nu^2 - 2\bar{\nu}^2 + \sqrt{(\nu^2 - 2\bar{\nu}^2)^2 + 8\bar{\nu}^2\nu_p^2}\right]/2$$

$$\lambda_1^2 = \left[-\nu^2 + 2\bar{\nu}^2 + \sqrt{(\nu^2 - 2\bar{\nu}^2)^2 + 8\bar{\nu}^2\nu_p^2}\right]/2$$

Using the initial conditions for the trajectories (4.16), the tunneling trajectories can be found to be:

$$\begin{aligned}
x(\tau) &= -\frac{A_1}{\lambda_1}\cos\lambda_1\tau + \frac{A_2}{\lambda_1}\sin\lambda_1\tau + \frac{A_3}{\lambda_2}\cosh\lambda_2\tau + \frac{A_4}{\lambda_2}\sinh\lambda_2\tau; \\
p_z(\tau) &= \frac{\nu_p^2 - \lambda_2^2}{\nu_c\lambda_2}\left[A_3\cosh\lambda_2\tau + A_4\sinh\lambda_2\tau\right] + \frac{\nu_p^2 + \lambda_1^2}{\lambda_1\nu_c}\left[-A_1\cos\lambda_1\tau + A_2\sin\lambda_1\tau\right] \\
z(\tau) &= -\frac{\nu^2 + \lambda_1^2}{2\bar{\nu}^2\nu_c}\left[A_1\sin\lambda_1\tau + A_2\cos\lambda_1\tau\right] + \frac{\lambda_2^2 - \nu^2}{2\bar{\nu}^2\nu_c}\left[A_3\sinh\lambda_2\tau + A_4\cosh\lambda_2\tau\right] \\
p_x(\tau) &= -\nu_c z(\tau) - \left[A_1\sin\lambda_1\tau + A_2\cos\lambda_1\tau + A_3\sinh\nu_2\tau + A_4\cosh\lambda_2\tau\right]
\end{aligned}$$

where constants A_i, $i = 1, 2, 3, 4$ are given by:

$$\begin{aligned}
A_1 &= \frac{\nu_p^2(\lambda_2^2 - \nu^2)x_0 - 2\omega_c\lambda_1^2}{\lambda_1(\lambda_1^2 + \lambda_2^2)}; \quad A_2 = \frac{\nu_p x_0(\lambda_2^2 - \nu^2)}{(\lambda_1^2 + \lambda_2^2)}\coth[\omega_p(\beta/2) - \nu_p\tau_{\rm rd}]; \\
A_3 &= \frac{\nu_p^2 x_0(\nu^2 + \lambda_1^2) - 2\omega_c\lambda_2^2}{\lambda_2(\lambda_1^2 + \lambda_2^2)}; \quad A_4 = \frac{\nu_p x_0(\nu^2 + \lambda_1^2)}{(\lambda_1^2 + \lambda_2^2)}\coth[\omega_p(\beta/2) - \nu_p\tau_{\rm rd}].
\end{aligned}$$

Here, $\tau_{\rm rd} = \tau_f/(2mL/\hbar\gamma)$.

Until now, the boundary conditions at the exit point have not yet been taken into account. The tunneling potential (C.1) is special in that respect that there a two possible boundary conditions depending on the parameters of the Hamiltonian. For $\bar{\nu} > 1$ and $B = 0$, the boundary condition is

$$p_z(\tau_{\rm rd}^{(1)}) = x(\tau_{\rm rd}^{(1)}) = 0, \tag{C.3}$$

where the superscript denotes that the imaginary tunneling time was found using condition (C.3), or equivalently from:

$$\frac{\lambda_1}{\lambda_2}\frac{\nu^2+\lambda_1^2}{\nu^2-\lambda_2^2}\left[\frac{\nu_p}{\lambda_2}\cosh\lambda_2\tau_{\rm rd}^{(1)}+\coth[\omega_p(\beta/2)-\nu_p\tau_{\rm rd}^{(1)}]\sinh\lambda_2\tau_{\rm rd}^{(1)}\right]\cos\lambda_1\tau_{\rm rd}^{(1)}$$
$$=\left[\frac{\nu_p}{\lambda_1}\cos\lambda_1\tau_{\rm rd}^{(1)}-\coth[\omega_p(\beta/2)-\nu_p\tau_{\rm rd}^{(1)}]\sin\lambda_1\tau_{\rm rd}^{(1)}\right]\cosh\lambda_2\tau_{\rm rd}^{(1)} \qquad \text{(C.4)}$$

The corresponding tunneling exponent is given by $S_E^{(1)}=2\tau_{\rm rd}^{(1)}$.

Upon either increasing of the magnetic field or decreasing Ω, there appears another tunneling trajectory, which satisfies the condition:

$$z(\tau_{rd}^{(2)})=1,\ x(\tau_{\rm rd}^{(2)})=0, \qquad \text{(C.5)}$$

In the explicit form, the equation for $\tau_{\rm rd}^{(2)}$ is

$$2\bar{\nu}^2\nu_p^2\nu_c(\cosh\lambda_2\tau_{\rm rd}^{(2)}-\cos\lambda_1\tau_{\rm rd}^{(2)})\left[\lambda_1\sinh\lambda_2\tau_{\rm rd}^{(2)}-\lambda_2\sin\lambda_1\tau_{\rm rd}^{(2)}\right.$$
$$\left.-\sqrt{2}\bar{\nu}\coth[\nu_p(\beta/2-\tau_{\rm rd}^{(2)})](\cos\lambda_1\tau_{\rm rd}^{(2)}-\cosh\lambda_2\tau_{\rm rd}^{(2)})\right]$$
$$=\left[(\nu^2+\lambda_1^2)\lambda_1\left(\sinh\lambda_2\tau_{\rm rd}^{(2)}\coth[\nu_p(\beta/2-\tau_{\rm rd}^{(2)})]+\frac{\nu_p}{\lambda_2}\cosh\lambda_2\tau_{\rm rd}^{(2)}\right)\right.$$
$$\left.+\lambda_2(\lambda_2^2-\nu^2)\left(\sin\lambda_1\tau_{\rm rd}^{(2)}\coth[\nu_p(\beta/2-\tau_{\rm rd}^{(2)})]-\frac{\nu_p}{\lambda_1}\cos\lambda_1\tau_{\rm rd}^{(2)}\right)\right]$$
$$\times\left[\lambda_1(\nu^2+\lambda_1^2)\sin\lambda_1\tau_{\rm rd}^{(2)}-\lambda_2(\lambda_2^2-\nu^2)\sinh\lambda_2\tau_{\rm rd}^{(2)}-\bar{\nu}^2(\lambda_1^2+\lambda_2^2)\right] \qquad \text{(C.6)}$$

The tunneling exponent calculated along the trajectory with boundary condition (C.5) is given by

$$S_E^{(2)}=2\tau_{\rm rd}^{(2)}+p_z(\tau_{\rm rd}^{(2)})/2. \qquad \text{(C.7)}$$

In the range of parameters where both trajectories exist, then the exponent of the escape rate will be given by the smaller of $S_E^{(1)}$ and $S_E^{(2)}$. Switching between the regimes where the tunneling exponent is determined by one or the other boundary

conditions leads to singularity in the derivative of tunneling exponent, as can be seen in Fig. 4.4.

In summary, tunneling through a square barrier have been analyzed taking into account the "correlation-hole" potential from the electrons remaining in the layer. The tunneling exponent have been found exactly by solving the equations of motion (C.2). The result describes tunneling at finite temperatures, including the $T = 0$ case as an appropriate limit.

Bibliography

[1] G. Gamow, Z. Phys. **51**, 204 (1928).

[2] R. W. Gurney and E. U. Condon, Nature **122**, 439 (1928).

[3] J. R. Oppenheimer, Phys. Rev. **13**, pp. 66-81 (1928).

[4] F. Hund, Z. Phys. **43**, pp. 805-26 (1927).

[5] R. H. Fowler and L. Nordheim, Proc. R. Soc. London A **119**, pp. 173-81 (1928).

[6] J. E. Lilienfeld, Z. Phys. **23**, 506 (1922).

[7] L. D. Landau and E. M. Lifshitz, *Quantum mechanics: non-relativistic theory* (Pergamon, NY 1977).

[8] G. Wentzel, Zeits. f. Phys. **38**, pp. 518-29 (1926); H. A. Kramers, Zeits. f. Phys. **39**, pp. 828-40 (1926); L. Brillouin, Comptes Rendus, **183**, 24 (1926).

[9] J. S. Langer, Ann. Phys. **41**, pp. 108-57 (1967).

[10] S. Coleman, Phys. Rev. D **15**, pp. 2929-36 (1977); C. G. Callan and S. Coleman, Phys. Rev. D **16**, pp. 1762-8 (1977).

[11] M. V. Berry and K. E. Mount, Rep. Progr. Phys. **35**, pp. 315-97 (1972).

[12] *Quantum Tunneling in Condensed Matter*, eds. Yu. Kagan and A. J. Leggett (Elsevier, NY 1992).

[13] A. Auerbach and S. Kivelson, Nucl. Phys. **B257**, pp. 799-858 (1985).

[14] Z. H. Huang, T. E. Feuchtwang, P. H. Cutler, and E. Kazes, Phys. Rev. A **41**, pp. 32-41 (1990).

[15] U. Eckern and A. Schmid, in *Quantum Tunnelling in Condensed Matter*, eds. Yu. Kagan and A. J. Leggett (Elsevier, NY 1992), pp. 145-228.

[16] A. O. Caldeira and A. J. Leggett, Ann. Phys. **149**, pp. 374-455 (1983).

[17] E. J. Heller, Phys. Rev. Lett. **53**, pp. 1515-8 (1984); in *Quantum Chaos and Statistical Nuclear Physics*, ed. by T. H. Seligman and H. Nishioka, pp. 162-81 (1986).

[18] M.C. Gutzwiller, *Chaos in Classical and Quantum Mechanics* (Springer-Verlag, NY, 1990).

[19] S. Tomsovic and E. J. Heller, Phys. Rev. E **47**, pp. 282-299 (1993).

[20] M. V. Berry, Proc. R. Soc. Lond. A **423**, pp. 219-31 (1989).

[21] S. C. Creagh and N. D. Whelan, Phys. Rev. Lett. **84**, pp. 4084-4087 (2000); Phys. Rev. Lett. **82**, pp. 5237-40 (1999); Ann. Phys **272**, pp. 196-242 (1999).

[22] R. J. Sladek, J. Phy. Chem. Solids, **5**, pp. 157-70 (1958); L. Halbo and R. J. Sladek, Phys. Rev. **173**, pp. 794-802 (1968).

[23] J. Smoliner, W. Demmerle, G. Berthold, E. Gornik, and G. Weiman, Phys. Rev. Lett. **63**, pp. 2116-9 (1989); G. Rainer, J. Smoliner, and E. Gornik, Phys. Rev. B **51**, pp. 17642-7 (1995).

[24] J. P. Eisenstein, T. J. Gramila, L. N. Pfeiffer, and K. W. West, Phys. Rev. B **44**, pp. 6511-4 (1991); S. Q. Murphy, J. P. Eisenstein, L. N. Pfeiffer, and K. W. West, Phys. Rev. B **52**, pp. 14825-8 (1995).

[25] L. Zheng and A. H. MacDonald, Phys. Rev. B **47**, pp. 10619-24 (1993).

[26] J. A. Simmons, S. K. Lyo, N. E. Harff, and J. F. Klem, Phys. Rev. Lett. **73**, pp. 2256-9 (1994).

[27] S. K. Lyo, Phys. Rev. B **50**, pp. R4965-8 (1994).

[28] J. A. Simmons, S. K. Lyo, J. F. Klem, M. E. Sherwin, and J. R. Wendt, Phys. Rev. B **47**, pp. 15741-4 (1993).

[29] T. S. Lay, X. Ying, and M. Shayegan, Phys. Rev. B **52**, pp. R5511-4 (1995).

[30] T. Jungwirth, T. S. Lay, L. Smrčka, and M. Shayegan, Phys. Rev. B **56**, pp. 1029-32 (1997).

[31] T. Ihn, H. Carmona, P. C. Main, L. Eaves, and M. Henini, Phys. Rev. B **54**, pp. R2315-8 (1996).

[32] M. J. Yang, C. H. Yang, B. R. Bennett, and B. V. Shanabrook, Phys. Rev. Lett. **78**, pp. 4613-6 (1997).

[33] M. Lakrimi, S. Khym, R. J. Nicholas, D. M. Symons, F. M. Peeters, N. J. Mason, and P. J. Walker, Phys. Rev. Lett. **79**, pp. 3034-7 (1997).

[34] L. Menna, S. Yücel, and E. Y. Andrei, Phys. Rev. Lett. **70**, pp. 2154-7 (1993); S. Yücel, L. Menna, and E. Y. Andrei, Physica B **194 – 196**, pp. 1223-4 (1994); E. Y. Andrei, in Ref. [53].

[35] H. A. Fertig and B. I. Halperin, Phys. Rev. B **36**, pp. 7969-76 (1987).

[36] V. S. Popov, B. M. Karnokov, and V. D. Mur, Sov. Phys. JETP **86**, pp. 860-74 (1998) [Zh. Eksp. Teor. Fiz. **113**, pp. 1579-1605 (1998)]; A. M. Perelomov and V. S. Popov, Sov. Phys. JETP **25**, pp. 336-43 (1967) [Zh. Eksp. Teor. Fiz. **52**, pp. 514-26 (1967)]; V. S. Popov, V. P. Kuznetsov, and A. M. Perelomov Sov. Phys. JETP **26**, pp. 222-32 (1968)[Zh. Eksp. Teor. Fiz. **53**, pp. 331-47 (1967)]; L. P. Kotova, A. M. Perelomov, and V. S. Popov, Sov. Phys. JETP **27**, pp. 616-21 (1968) [Zh. Eksp. Teor. Fiz. **54**, pp. 1151-61 (1968)].

[37] P. Ao, Phys. Rev. Lett. **72**, pp. 1898-1901 (1994); Phys. Scripta **T69**, pp. 7-12 (1997).

[38] B. I. Shklovskii, JETP Lett. **36**, pp. 51-4 (1982).

[39] A. V. Khaetskii and B. I. Shklovskii, Sov. Phys. JETP **58** pp. 421-7, (1983) [Zh. Eksp. Teor. Fiz. **85**, pp. 721-34 (1983).

[40] B. I. Shklovskii and A. L. Efros, JETP **57**, pp. 470-6 (1983).

[41] Qin Li and D. J. Thouless, Phys. Rev. B **40**, pp. 9738-43 (1989).

[42] T. Martin and S. Feng, Phys. Rev. B **44**, pp. 9084-7 (1991).

[43] J. Haidu, M. E. Raikh, and T. V. Shahbazyan, Phys. Rev. B **50**, pp. 17625-7 (1994); M. E. Raikh and T. V. Shahbazyan, Phys. Rev. B **51**, pp. 9682-95 (1995)

[44] B. Hellfer and J. Sjöstrand, Ann. Scuola Norm. Sup. Pisa Cl. Sci. (4) **14**, pp. 625-57 (1988).

[45] S. Nakamura, Comm. Math. Phys. **200**, pp. 25-34 (1999) and references therein.

[46] T. Barabash-Sharpee, M. I. Dykman, P. M. Platzman, Phys. Rev. Lett. **84**, pp. 2227-30 (2000).

[47] M. I. Dykman, T. Sharpee, P. M. Platzman, in preparation.

[48] E. Abrahams, S. V. Kravchenko, and M. P. Sarachik, Rev. Mod. Phys. **73**, pp. 251-66 (2001); e-print: cond-mat/0006055.

[49] M. J. Lea and M. I. Dykman, Physica B **251**, pp. 628-35 (1998);

[50] E. Teske, Yu. P. Monarkha, M. Seck, and P. Wyder, Phys. Rev. Lett. **82**, pp. 2772-5 (1999).

[51] K. Shirahama, S. Ito, H. Suto, and K. Kono, J. Low Temp. Phys. **101**, pp. 439-44 (1995); K. Shirahama and K. Kono, Phys. Rev. Lett. **74**, pp. 781-4 (1995).

[52] M. I. Dykman and L. S. Khazan, JETP **50**, pp. 747-53 (1979); M. I. Dykman, M. J. Lea, P. Fozooni, and J. Frost, Phys. Rev. Lett. **70**, pp. 3975-8 (1993); M. I. Dykman, C. Fang-Yen, and M. J. Lea, Phys. Rev. B **55**, pp. 16249-72 (1997); M. I. Dykman and Yuri G. Rubo, Phys. Rev. Lett. **78**, pp. 4813-6 (1997).

[53] *Two-Dimensional Electron Systems on Helium and other Cryogenic Substrates*, ed. by E. Andrei (Kluwer, NY 1997).

[54] *Perspectives in Quantum Hall Effect*, ed. by S. Das Sarma and A. Pinczuk (Wiley, NY 1997).

[55] I. B. Spielman. J. P. Eisenstein, L. N. Pfeiffer, and K. W. West, Phys. Rev. Lett. **84**, pp. 5808-11 (2000).

[56] M. I. Dykman, T. Sharpee, and P. M. Platzman, Phys. Rev. Lett. **86**, pp. 2408-11 (2001).

[57] T. Sharpee, M. I. Dykman, P. M. Platzman, submitted for publication; cond-mat/0103151.

[58] I. Affleck, Phys. Rev. Lett. **46**, pp. 388-91 (1980).

[59] A. I. Larkin and Yu. N. Ovchinnikov, Pis'ma Zh. Eksp. Teor. Fiz. **37**, pp. 322-5 (1983) [JETP Lett. **37**, pp. 382-5 (1983)]; Zh. Eksp. Teor. Fiz. **86**, pp. 719-26 (1984) [JETP **59**, pp. 420-4 (1984)].

[60] M. V. Berry, Adv. Phys. **25**, pp. 1-26 (1976); Proc. R. Soc. Lond. A **427**, pp. 265-80 (1990); Proc. R. Soc. Lond. A **422**, pp. 7-21 (1989).

[61] J. Heading, *An Introduction to Phase-Integrals Methods* (London: Methuen, 1962).

[62] L. S. Schulman, *Techniques and Applications of Path Integration* (Wiley, New York, 1981).

[63] G. G. Stokes, Trans. Camb. Phil. Soc., **10**, pp. 106-128 (1857).

[64] M. I. Dykman, Lecture notes for the course "Theory of transport phenomena".

[65] P. M. Morse and H. Feshbach, *Methods of Theretical Physics* (McGraw-Hill, NY 1953).

[66] J. Yoon, C. C. Li, D. Shahar, D. C. Tsui, and M. Shayegan, Phys. Rev. Lett. **82**, pp. 1744-7 (1999); Phys. Rev. Lett. **84**, pp. 4421-3 (2000).

[67] C. C. Grimes and G. Adams, Phys. Rev. Lett. **42**, pp. 795-798 (1979).

[68] D. S. Fisher, B. I. Halperin, and P. M. Platzman, Phys. Rev. Lett. **42**, pp. 798-801 (1979).

[69] M. Ya. Azbel, Phys. Rev. Lett. **64**, pp. 1553-6 (1990); M. Ya. Azbel and P. M. Platzman, Phys. Rev. Lett. **65**, pp. 1376-9 (1990).

[70] R. P. Feynman and A. R. Hibbs, *Quantum Mechanics and Path Integrals* (McGraw-Hill, New York, 1965).

[71] R. Landauer and Th. Martin, Rev. Mod. Phys. **66**, pp. 217-28 (1994).

[72] Y. Iye, K. Kono, K. Kajita, and W. Sasaki, J. Low Temp. Phys. **38**, pp. 293-309 (1980).

[73] M. I. Dykman, J. Phys. C **15**, pp. 7397-416 (1982).

[74] M. W. Cole, Phys. Rev B **2**, pp. 4239-51 (1970); M.W. Cole and M.H. Cohen, Phys. Rev. Lett. **23**, pp. 280-3 (1974).

[75] V. B. Shikin, JETP **31**, 936 (1970); V. N. Shikin and Yu. P. Monarkha, Sov. J. Low Temp. Phys. **1** pp. 459-72 (1975).

[76] M. J. Lea, P. Fozooni, A. Kristensen, P. J. Richardson, K. Djerfi, M. I. Dykman, C. Fang-Yen, A. Blackburn, Phys. Rev. B **55**, pp. 16280-92 (1997).

[77] T. Barabash, M. I. Dykman, P. M. Platzman, V. N. Smelyanskiy, Phys. Rev. B **58**, R10214-7 (1998).

[78] S. Nagano, S. Ichimaru, H. Totsuji, and N. Itoh, Phys. Rev. B **19**, pp. 2449-56 (1979).

[79] R. J. Price, Proc. Phys. Soc. London **67**, pp. 383-5 (1954).

[80] G. F. Saville, J. M. Goodkind, and P. M. Platzman, Phys. Rev. Lett. **70**, pp. 1517-20 (1993).

[81] N. Hatano and D. R. Nelson, Phys. Rev. Lett. **77**, pp. 570-3 (1996); Phys. Rev B **56**, pp. 8651 (1997).

[82] D. R. Nelson and N. M. Shnerb, Phys. Rev. E **58**, 1383 (1998).

[83] C. M. Bender, M. Berry, P. N. Meisinger, van M Savage, and M. Simsek, J. Phys. A **34**, pp. L31-6 (2001); C. M. Bender, S. Boettcher, van M Savage, J. Math Phys **41**, pp. 6381-7 (200); C. M. Bender and S. Boettcher, Phys. Rev. Lett. **80**, pp. 5243-6 (1998); C. M. Bender, S. Boettcher, P. N. Meisinger, J. Math. Phys **40**, pp. 2201-2229 (1999).